Università degli Studi di Napoli

"Federico II"

Ph. D. in Chemical Sciences

XXX cycle

Increasing the Deposition Efficiency of Perfume Ingredients in Liquid Detergents

Preface

This Ph. D. thesis summarizes the work carried out during the last three years in the field of the industrial physical chemistry. The theoretical background was complemented by collecting experience in the characterization of both thermodynamic and structural properties of the investigated colloidal systems through light and neutron scattering techniques. At the same time, the knowledge and the application of different chromatographic techniques allowed gaining expertise also in the field of the analytical chemistry.

The Ph. D. project was funded by Procter & Gamble (P&G) and Consorzio interuniversitario per lo Sviluppo dei Sistemi a Grande Interfase (CSGI), Sesto Fiorentino, Italy and supported by the Julich Center for Neutron Science (JCNS) and ISIS at the STFC Rutherford Appleton Laboratory, providing beam times for the experiments involving neutrons. Moreover, further experiments were performed in the department of Strategic Innovation & Technology located at P&G Brussels Innovation Center, located in Strombeek-Bever, Belgium.

Contents

Introduction

The aim of this project is the development of perfume deposition technologies for use in liquid detergents, which represent very complex mixtures of natural and synthetic molecules. Current fragrance carriers (such as melamine formaldehyde-based polymer capsules) present a good compatibility with the laundry detergent components and a high perfume loading efficiency. However, not all the perfume raw materials can be stably incorporated into the capsules because some of them (mainly the hydrophilic ones) easily leak out of the capsules by breakage and diffusion before the capsules deposit on the fabrics during the wash. Therefore, these perfume ingredients are not deposited effectively on the fabrics.

On these basis, our aim is the design of innovative perfume carriers with i) excellent stability in liquid detergent formulation and ii) improved deposition during product application. Among the possible candidates for the development of such a technology, vinyl alcohol-based copolymers, currently referred to as PVA (poly vinyl alcohol) or EVOH (poly ethylene-co-vinyl alcohol), represent a suitable tool to obtain a carrier system, which can be used for the purpose of this project thanks to the great stability of their aggregates in water. Moreover, particles formed by these copolymers are characterized by excellent transport properties: indeed, diverse vinyl alcohol-based systems have been already proposed as carriers in biomedical applications or environmental science for pollutant removal. An efficient procedure to obtain PVA or EVOH-based particles consists in promoting the aggregation of the chains by preparing a polymer solution and adding a certain quantity of a salt (i.e. NaCl) that is able to favor the salting-out process: this effect was already tested for another common water soluble polymer like PEG (polyethylene glycol).

In the following section (chapter 1) we present different examples of polymer particle-based technologies and their preparation protocols, giving more emphasis to the vinyl alcohol-based technologies and the salting-out method, which was

studied in this project. A detailed description of the materials and methods used for the preparation and the characterization of the investigated systems is given in the experimental section (chapter 2). The choice of the salt used to induce the salting-out process is presented (chapter 3). Consequently, the polymer aggregation process triggered by the presence of the salt and the structural properties of the obtained polymer particles are discussed (chapter 4 and chapter 5, respectively). A model compatibility study performed in the presence of polymer aggregates and two common surfactants employed in the final liquid detergent matrix is shown (chapter 6). The perfume segregation efficiency and the washing tests aimed at evaluating the technology efficiency are presented in chapter 7 and chapter 8, respectively. Finally, conclusions are summarized in chapter 9.

Chapter 1 – Polymer particle-based technologies

During the last years, an emerging interest has been devoted to the development of micro- and nano-structured materials for a wide range of applications in biomedicine, catalysis or environmental science. Specifically, soft polymer particles have been proposed as effective technologies to deliver target molecules with a precise function. Different protocols for the preparation of polymer-based delivery systems can be found in literature and the choice of a particular preparation method strictly depends on the final application of the developed technology. In this Ph. D. project, our attention was focused on the ion-specific effect on the macromolecule solubility, rationalized through the so-called Hofmeister series, which can be used as a tool to predict the polymer aggregation behavior in solution. In particular, the polymeric aggregates prepared through the addition of a salt to a polymer solution to be used as an effective carrier system for increasing the deposition of perfume ingredients on fabrics. In this chapter, we give an overview of the methods aimed at preparing polymer particles, as well as a focus on the technologies which are currently in use at industrial level for enhancing the deposition efficiency of active components in laundry products. Some examples of application of vinyl alcohol-based copolymers, which were investigated in this project, are also shown. Moreover, we present some general theories concerning the Hofmeister effect, as well as a description of the aggregation mechanisms that lead to the particle formation, in order to provide a theoretical basis to support this study.

1.1 – An overview of polymer particle preparation protocols

Polymer particles can be prepared through many different preparation protocols, which can be usually divided into two groups: those based on the polymerization of

monomers and those taking advantage of preformed polymers, as clearly summarized in fig. 1.1.1.[1]

At the same time, these two methods can be classified into two categories: i) two-steps procedures involving the preparation of an emulsification system followed by formation of particles in the second step of the process and ii) one-step procedures where emulsification is not required for the particle formation.[2] Other methods have also been reported recently and they are based on spray-drying strategies[3,4], supercritical fluid technologies[5,6] or piezoelectrical ways[7].

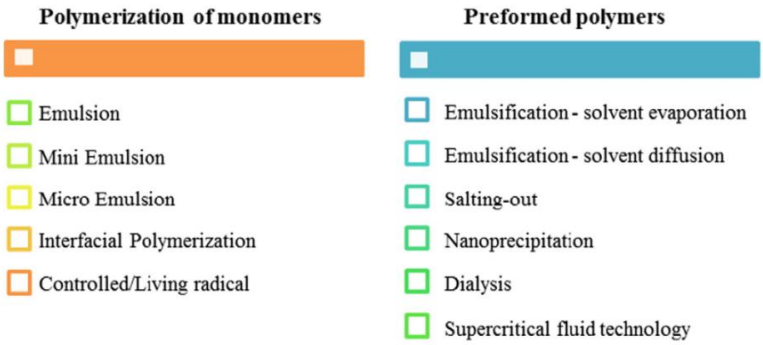

Figure 1.1.1 – Schematic representation of the preparation methods of polymer particles.

Concerning the first category, emulsions are defined as a mixing of two or more totally or partially immiscible liquids with or without a surface active agent. They are typically classified according to the size of the droplets: microemulsion, containing thermodynamically stable droplets with a diameter ranging from 10 to 100 nm and miniemulsion or macroemulsion, which are not stable and that contain droplets with a diameter ranging from 100 to 1000 nm and above 1000 nm, respectively.[8,9,10] Emulsions can be obtained through low-energy and high-energy emulsification techniques. Among the first ones, we can find the spontaneous emulsification[11,12], which consists in promoting the solubilization of the oily

component into a water-soluble solvent and then in adding the obtained solution into the aqueous phase. Such a technique is also described as solvent displacement method[13], well known as "Ouzo effect". Other routes are the emulsion inversion point[14] and the inversion temperature[15] methods. Among the second ones, we can find the emulsification with rotor-stator devices[16], sonication[17,18] and microfluidic techniques[19,20]. After the preparation of the emulsion, the formation of polymer particles can be carried out by following different protocols. The solvent evaporation method consists in dissolving the polymer into volatile solvent like dichloromethane, chloroform or ethyl acetate. In a second step, at least the 90% of solvent is removed through fast evaporation and then the residual solvent is evacuated through slow evaporation. Poly(lactic-co-glycolic acid) (PLGA)-, poly(lactic acid) (PLA)- and polyethylene glycol (PEG)-based particles were successfully prepared through this technique.[21,22,23] The solvent diffusion method consists in promoting the formation of a two-phase system, followed by emulsification and dilution with water with the consequent formation of polymeric particles from the emulsion. PLA, PLGA, but also gelatin or chitosan particles were synthesized through solvent diffusion[24,25,26], with poly-vinyl alcohol (PVA) typically employed as a steric stabilizer. Salting-out is another process that generally requires the use of a solvent miscible with water (usually acetone), whose solubility is modified by adding high amounts of salt or sucrose. The emulsion is formed with a polymer dissolved in the solvent droplets and particle precipitation is induced by adding a large quantity of water that drops the salt concentration. Typical salts used are magnesium chloride[27,28] or calcium chloride[29], even though salting-out can be exerted by preparing a saturated solution of PVA[30], which acts as thickener and emulsion stabilizer. A further process is the gelation of emulsion droplets, which is obtained by either cooling down the previously prepared nanoemulsion[31] or inducing ionic gelation[32] through the addition of divalent cations (like calcium). Conventional emulsion[33,34], surfactant-free emulsion[35,36], miniemulsion[37,38], microemulsion[39,40], interfacial[41] and controlled/living radical[42]

polymerization are other traditional protocols used for the preparation of polymer particles.

As regards the second category, nanoprecipitation is one of the easiest, most reproducible and economic routes to produce nanoparticles using preformed polymers. In this method only the polymer, the solvent and the non-solvent for the polymer are required: the polymer can be either synthetic or natural, typical polymer solvents are ethanol, acetone, hexane and a common non-solvent phase is either a single component or a mixture of non-solvents for the polymer, with or without surfactants. The mechanism of particle formation is similar to that one already described for the solvent displacement technique. Such a method can be chosen for a wide range of polymers[43,44] and also non-polymeric compounds[45]. Dialysis[46] is another common method very similar to the one previously described, with the presence of additional tools such as dialysis tubes or membranes provided with specific molecular weight cutoffs. Desolvation[47] is also very similar to nanoprecipitation and consists in promoting the precipitation of the polymer through addition of salts, alcohols or solvents in solution of macromolecules. Self-assembly and gelation are two other processes used to obtain polymer particles in an easy way. As an example, complexation of polyelectrolytes is a spontaneous association phenomenon involving charged macromolecules that are able to assemble themselves to form complexes which can be swollen by water. Nucleic acids[48], alginate[49] or chitosan[50] are commonly used.

1.2 – Increasing the deposition efficiency of active components: the current technologies at industrial level

From an industrial viewpoint, the choice of a proper technology implies considering different aspects like the cost of raw materials and process, the possibility to scale-up the preparation protocol and the compatibility with the other

components of the matrix where the technology is introduced. Therefore, a limited number of processes and materials can be taken into account.

Concerning the increase of deposition of active components like enzymes, perfumes, bleaching agents or antioxidants, many different technologies have been proposed and have been claimed. Generally, industrial technologies are designed to be the most versatile possible, covering a wide range of applications. However, in this paragraph we draw our attention on the delivery systems for perfume additives, since they represent the target molecules of this research project.

Stabilization and fragrance deposition increase can be achieved through the use of silicone pellets[51], perfume-impregned macroparticles[52] or powdery solids[53]. In most of these cases, it is possible to obtain a suspension rather than a homogeneous system. Alternatively, liquid formulations can be enclosed within pouches where the perfume is contained in the pouch core.[54,55] Also solid polymer matrices made of polypeptides or polyelectrolytes[56], as well as of silicone, silicon-wax or cellulose[57] have been claimed: in this case, the most hydrophobic and less volatile fragrances are dispersed within the matrix, that allows protecting the perfume from emulsification. Gel systems containing fragrances[58,59,60], able to release the active component upon external stimuli have also been proposed: natural polymers frequently used are carrageenan gum, gellan gum, Arabic gum, pectin, starch, whereas the most common synthetic polymers are poly(propylene glycol) esters, polyacrylates or poly-vinyl alcohol.

Even though some of the previous inventions can be used in liquid detergent matrices, the most successful technologies currently in use in laundry products are the polymer capsules, i.e. particles whose structure is usually characterized by a polymeric shell and a core containing perfume. Ethylene vinyl copolymers, as well as PVA, or poly-methyl methacrylates, polystyrene, ethyl cellulose, poly-vinyl pyrrolidones, poly-acrylic acid or starches have been used for designing the polymeric shell.[61,62,63,64,65,66]

Also in literature it is possible to find many different examples of fragrance containing capsules prepared by following distinct protocols. Peppermint oil was successfully encapsulated through preliminary emulsification and consequent *in situ* polymerization through the use of a melamine-formaldehyde polymer.[67] Optical and scanning electron micrographs of the obtained particles are shown in fig. 1.2.1. Vanillin was enclosed within polysulfone microcapsules prepared through the solvent displacement method.[68] Also α-pinene was encapsulated within acrylate-based polymers by miniemulsification through sonication followed by free radical polymerization of the monomers.[69] A blend of hydroxypropyl methylcellulose, PVA and ethylcellulose was used to prepare capsules in the presence of (1R)-camphor, (3R)-citronellal, eucalyptol, D-limonene, (1R, 2S, 5R)-menthol and 4-tert-butylcuclohexyl salicylate by following the solvent displacement method supported by dialysis.[70] Again, α-pinene was enclosed upon emulsification and encapsulation through the use of a glass capillary microfluidic device[71]: in particular, the photocurable oil in the middle phase was *in situ* polymerized by UV exposure, as shown in fig. 1.2.2.

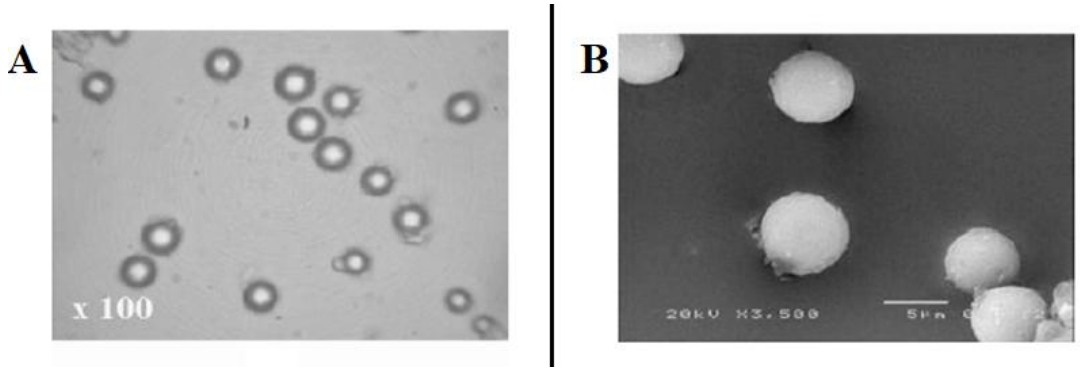

Figure 1.2.1 – Image photographs of melamine-formaldehyde resin microcapsules containing peppermint oil. Panel A: optical micrograph (× 100). Panel B: scanning electron micrograph (× 3500).[67]

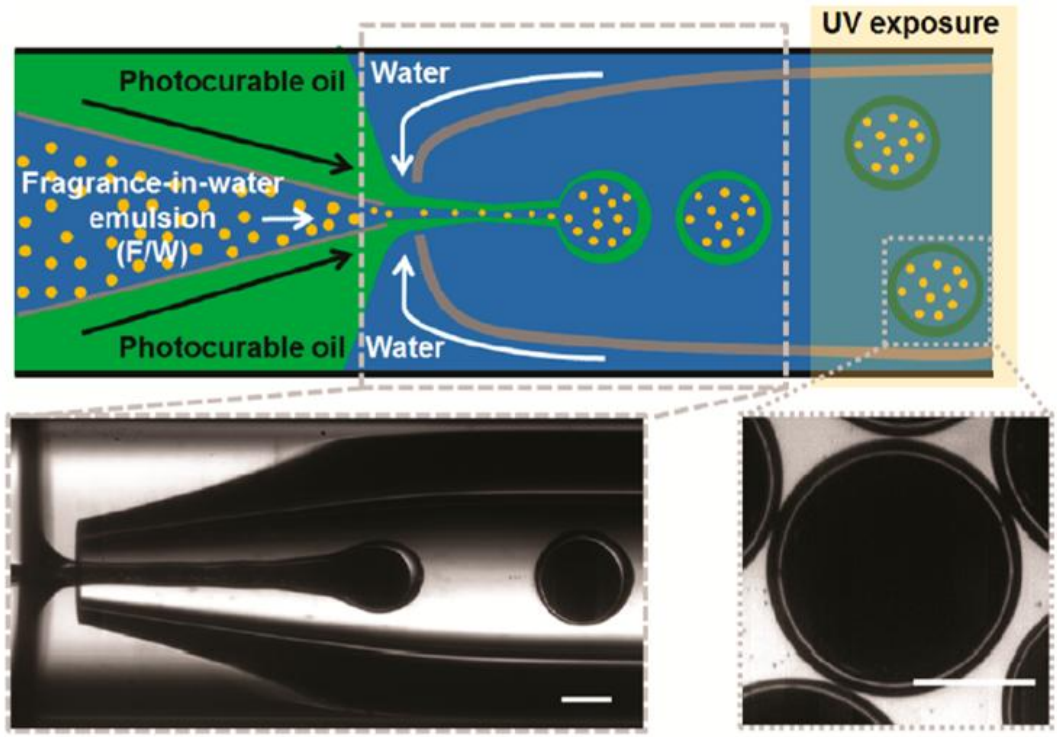

Figure 1.2.2 – Schematic illustration of the glass capillary microfluidic device for preparing polymer microcapsules enclosing a preformed fragrance-in-water (F/W) emulsion. Bottom optical microscope image shows the generation of triple emulsion drops containing multiple internal fragrance drops. Upon UV irradiation, the photocurable oil in the middle phase polymerizes to form a polymeric shell. Scale bar represents 200 μm.[71]

The main advantages of the polymer capsules are the high compatibility with the laundry detergent components and the high perfume loading efficiency (up to 30% w/w of active component). However, the main drawback of this technology is that not all perfume components remain within the capsules since they can leak out due to various mechanisms (such as diffusion or capsule breakage) before the product is used. Those perfume ingredients are then emulsified by the surfactants contained in the detergent matrix. A promising alternative to the rigid capsules are the soft capsules, whose structure is composed by a soft polymer matrix enclosing perfume

surrounded by the surfactants contained in the laundry detergent that are able to self-assemble to form spheroidal particles. In this case, the polymer matrix is not cross-linked and the mechanical resistance is higher. Therefore, soft particle-based technologies may represent a successful improvement of the current technologies.

1.3 – Vinyl alcohol-based technologies: an overview

As already shown in the previous paragraphs, vinyl alcohol-based copolymers, such as PVA or poly-ethylene-vinyl alcohol (EVOH) are among the most common species used for preparing polymer particles. This is thanks to their non-toxicity, non-carcinogenicity, good biocompatibility and desirable physical properties such as rubbery or elastic nature and high degree of swelling in aqueous solutions.[72,73] Moreover, these copolymers are commercially available and can be obtained at low cost, which are two important factors to consider from an industrial point of view.
It is possible to find many examples of vinyl alcohol-based technologies in literature and several preparation protocols. A model protein drug, bovine serum albumin (BSA), was successfully incorporated into injectable PVA hydrogel nanoparticles prepared by mixing a BSA and a PVA solution and by adding silicon oil to an aqueous BSA and PVA solution.[72] Then, the obtained mixture was homogenized in order to obtain a water-in-oil emulsion, which was frozen through multiple freeing-thawing cycles resulting in the conversion of the emulsion to a suspension of PVA hydrogel particles extracted by using acetone and separated by means of filtration. Fig. 1.3.1 shows a scanning electron micrograph of the obtained particles, with a radius of about 100 nm. Capillary electrophoresis was then used in order to check the release efficiency of BSA, which was found to be about 95% at 37 °C.

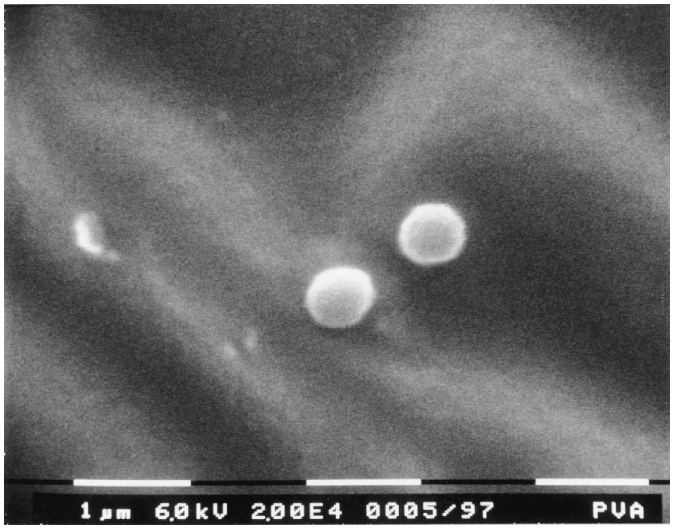

Figure 1.3.1 – A scanning electron micrograph of the PVA hydrogel nanoparticles showing the shape and the surface characteristics.[72]

Acrylamine-functionalized PVA particles for would healing application were prepared through UV cross-linking. The model drug used for this study was soybean trypsin inhibitor, whose maximum release was about 76% in optimized conditions.[74] PVA particles can be also prepared through chemical cross-linking. Glutaraldehyde is the most common molecule used for this purpose. As an example, PVA microspheres were prepared via inverse suspension-chemical cross-linking method.[75] In this study, the effect of stirring speed, cross-linker amount, hydrochloric acid concentration and oil-to-water volume ratio on microsphere diameter were taken into account. EVOH functional nanofibers for pollutant removal with an average radius of 260 nm were successfully synthesized through melt-blending extrusion of immiscible blends.[76] In a second step, layer deposition technology was used in order to obtain films formed by the previously prepared EVOH fibers. The resulting membranes were then tested for Cr(VI) adsorption. EVOH foams in the presence of propylene carbonate as a cross-linker were prepared by a high-temperature thermal treatment that allowed the formation of a gel phase.[77] In this case, among the different parameters considered, also the effect

of the propylene carbonate amount on the foam expansion ratio was taken into account and it was found that such a parameter reaches a maximum value at intermediate cross-linker concentration, as shown in fig. 1.3.2.

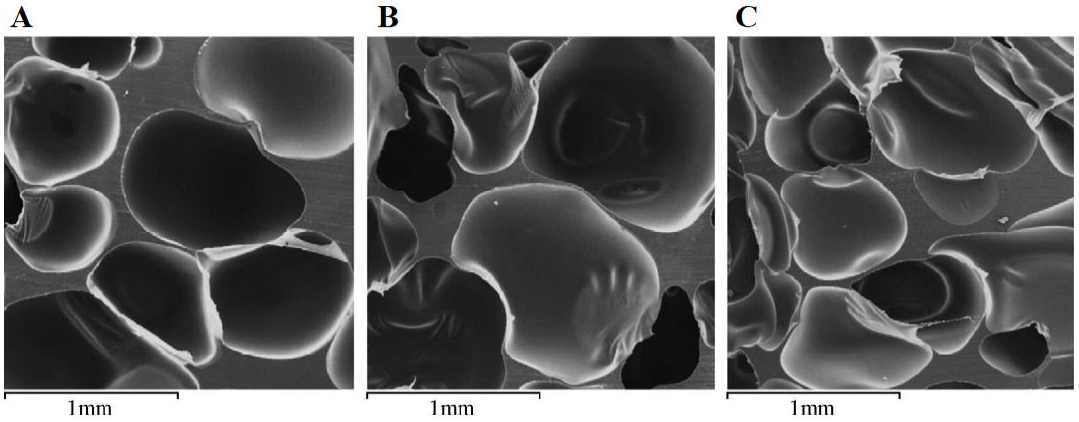

Figure 1.3.2 – Scanning electron micrographs of EVOH foams with different propylene carbonate contents. Image A: 2 parts per hundred resin (phr). Image B: 6 phr. Image C: 10 phr.[77]

In this Ph. D. project, we decided to investigate about an easy and cheap particle preparation protocol, which differs from the previous ones shown in this paragraph. This method is the salting-out, already described in paragraph 1.1. Such a protocol does not require the use of chemical cross-linkers and does not modify the structure of the vinyl alcohol-based copolymers, preserving their original properties of biocompatibility and biodegradability. The theoretical bases that support this preparation method are discussed in detail in the following paragraphs.

1.4 – The Hofmeister effect

The presence of different ions affects the solubility of macromolecules in solution.[78,79,80,81] In his first pioneering study[78] Franz Hofmeister rationalized the ion-specific effect on the protein solubility, demonstrating that the influence of the

salt on the protein conformation is strictly dependent on the nature of the ions. This phenomenon was rationalized through the so-called Hofmeister series[82,83,84], shown in fig. 1.4.1. Then, it was shown that this effect is more universal and the Hofmeister series was used to predict the physiochemical properties of many phenomena that occur in solution, like pH variation[85], protein crystallization[86], enzyme activities[87,88], optical rotation of aminoacids[89], emulsion stability[90], swelling and deswelling of hydrogels[91] and polymer solubility[92].

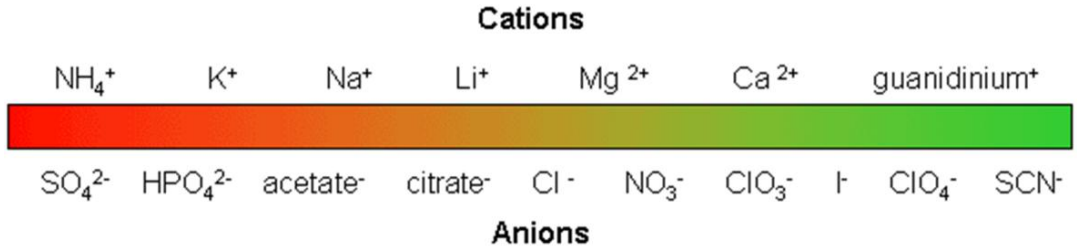

Figure 1.4.1 – Representation of the Hofmeister series. The species on the right are known as chaotropes and are able to increase the macromolecule solubility in water (salting-in effect), whereas the species on the left are known as kosmotropes and decrease the macromolecule solubility in water, leading to the salting-out phenomenon.

At the beginning, it was supposed that the ion specificity was intimately related to the specific interactions that ions have with water. This is reflected in different easily measurable physicochemical parameters of aqueous salt solutions, i.e. conductivity and viscosity.[93] As regards the conductivity in solution, it was originally hypothesized that the ionic electrochemical mobility in solution was high for small ions and low for big ions.[94] However, the trend was the opposite of what was expected, since the actual effective size of ions in water is very different for that in a crystal. This is due to the higher degree of hydration of the smaller ions (*e.g.* Li^+, F^-), which are highly polarizable and able to bear several water molecules while migrating in solution. As a consequence, they move slowly compared with

bigger and poorly hydrated ions. Concerning the viscosity of salt solutions, it was found that such a parameter is related to the nature of the salts according to the following equation[95]:

$$\frac{\eta}{\eta_0} = A\sqrt{c} + Bc \qquad \text{equation 1.4.1}$$

where η/η_0 is the relative viscosity, A is an electrostatic parameter about equal for all salts and B is an ion-specific parameter known as the Jones Dole viscosity coefficient. Therefore, it was supposed that the water structure, formed by a dynamic fluctuation of the hydrogen bond network, was affected by the ion nature, thus by the B value. The ions with a positive value of this parameter increased the viscosity of aqueous solutions, making order in the water structure, whereas those with a negative B value decreased the viscosity, breaking the water structure order. The former were called kosmotropes, the latter chaotropes. On the basis of this classification, the Hofmeister's experiment on salt induced protein precipitation can be clearly explained: kosmotropic anions withdraw the water molecules from the hydration shell of proteins, reducing their solubility and forcing the aggregation, i.e. the salting-out phenomenon, whereas chaotropic anions act with the opposite mechanism, leading to the salting-in phenomenon.[96]

However, there are several observations that demonstrate that the mechanism at work is more complicated than that one presented and there are still many open questions that are not solved. Firstly, whereas the kosmotropic behavior of anions can be clearly explained by the water withdrawing power mechanism previously discussed, the salting-out behavior of chaotropic cations still remains a doubt. Secondly, it was found in literature that the Hofmeister series was reversed in order.[97,98] This is due to the fact that both specific surface hydration–ion hydration interactions and hydrated ion–bulk water interactions are involved. Thirdly, it was originally thought that the Hofmeister effects occurred at high salt concentrations, typically from 0.5 to 3 M[99], but it was then shown that the ion-specific effect has a strong impact at definitely lower salt concentrations (from 0.1 to 0.15 M),

reflecting the key role of the ion specificity in most biochemical mechanisms.[100] Finally, some experiments have demonstrated that ions do not affect hydrogen bonding of water beyond their first solvation shells.[101] Therefore, ions do not affect the long-range water structure.

Many macromolecules show ion-specific aggregation and changes in phase transition temperature with ion types. Let us consider a model macromolecular surface, shown in fig. 1.4.2, and let us assume that the macromolecular surface does not undergo direct ion-induced structural changes.[102]

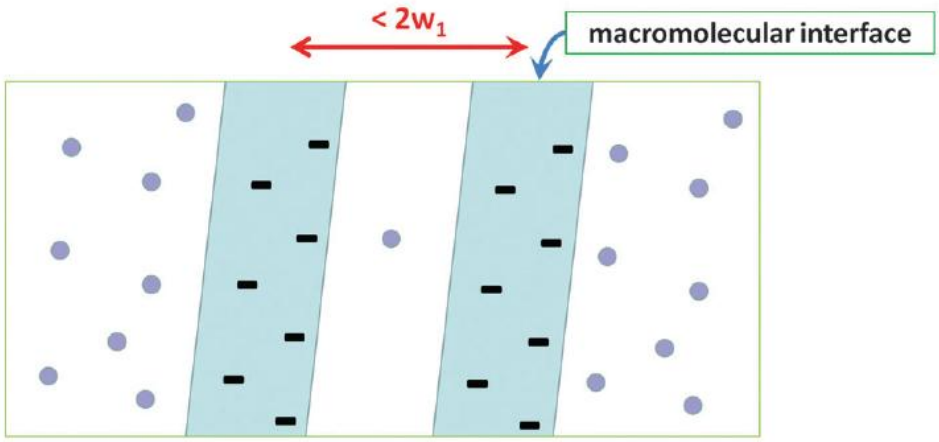

Figure 1.4.2 – Schematic representation of two macromolecules in ion solutions. Ions are drawn as spheres.

Instead, at the macromolecular surface, the surface ion concentration and the bulk ion concentration can be different, and there can be an excess charge density accumulated at the macromolecular surface. When two surfaces approach closer than the interfacial depth w_1, where the surface ion concentration deviates from the bulk ion concentration, this will induce depletion interaction, while at the same time any excess charge at one macromolecular surface will also interact with the excess charge at the other macromolecular surface electrostatically. As a consequence, the macromolecules feel the attractive force when ions are depleted

from the macromolecular surface, which is proportional to the concentration difference between the bulk ion concentration and the surface ion concentration. At the same time, when the surface ion concentration becomes significant, the excess charge density at the macromolecular surface induces electrostatic repulsion. Therefore, the aggregation phenomenon is governed by two opposite forces: the depletion attraction that favors the salting-out and the excess charge repulsion that favors the salting-in, i.e. the homogeneous distribution of the macromolecules in solution. The ions ranked higher in the Hofmeister series, such as Cl^-, have smaller ion concentrations at the surface compared with ions ranked lower, such as Br^- and I^-. As a consequence, both depletion attraction and excess charge repulsion act in a concerted way to favor macromolecular aggregation.[102]

1.5 – The salting-out behavior exerted by sodium chloride

As clearly shown in the previous paragraph, some salts are able to trigger the aggregation of macromolecules in solution. In particular, for the present study, sodium chloride was used in order to induce the formation of the EVOH and PVA-based particles. The reason will be explained in chapter 3, where experimental data supporting this choice are presented.

Furthermore, it has been already shown in literature that sodium chloride, whose position in the Hofmeister series is within the salting-out behavior, is able to favor the aggregation of many different hydrophilic polymers[103,104]. Indeed, the presence of NaCl above a threshold concentration which depends on the nature of the polymer may dramatically influence the interaction between the solvent and the solute, as shown for both natural (*e.g.* lysozyme[105]) and synthetic macromolecules (*e.g.* poly(styrene-b-sodium acrylate)[106]). From a thermodynamic point of view, this happens due to the change of two fundamental parameters that are involved in the aggregation process: the second virial coefficient[107] and the interaction

parameter[108] that describe the polymer-solvent and the polymer-polymer interaction, respectively. Light scattering techniques, i.e. Static Light Scattering and Dynamic Light Scattering, are the method of choice for the determination of these parameters. At the same time, the above-mentioned techniques can be used to determine fundamental structural parameters, like the radius of gyration or the molar weight of the scattering particles, whose knowledge allows shedding light on the kind of regime that governs the aggregation process.

1.6 – The aggregation mechanisms: a theoretical insight

The most widely considered form of colloid aggregation is that which begins with a suspension of monodisperse particles. Upon aggregation, these particles collide due to their Brownian motion and stick together irreversibly to form rigid clusters. The clusters themselves continue to diffuse, collide and form yet larger clusters, resulting in a polydisperse mass distribution. This process is called cluster-cluster aggregation, and is a non-equilibrium, kinetic growth process. Both the aggregation kinetics and the shape of the cluster mass distribution are intrinsically related to the structure of the clusters that are ultimately formed. A complete characterization of this aggregation process must include a full description of both the structure of the clusters, as well as the shape and time evolution of the cluster mass distribution.[109]
Two different regimes of colloid aggregation have been identified. The first occurs when the aggregation rate depends only on the time between the collisions of the particles due to their diffusion and is called diffusion limited aggregation (DLA).[109]
The second occurs when the reaction rate of two particles is much slower than the collision rate, so that a large number of collisions are necessary before two particles can stick together, and is called reaction limited aggregation (RLA).[110]
A kinetic study on the evolution of the cluster mass over time allows determining which regime governs the aggregation process. The time dependence of the cluster

mass can be determined by means of the Smoluchowski equations[111]. For a DLA process, a linear dependence is predicted and the relation between cluster mass and time can be represented as follows:

$$\overline{M} = \frac{t}{t_0} + 1 \qquad \text{equation 1.6.1}$$

where $t_0 = \frac{3\eta V}{8k_B T N_0}$ with $\overline{M}$ the average cluster mass, t the aggregation time, η the viscosity of the fluid, T the temperature and N_0/V the initial particle concentration.
For a RLA process, an exponential dependence is predicted:

$$\overline{M} \approx \exp\left(\frac{t}{t_0}\right) \qquad \text{equation 1.6.2}$$

From the analysis of Light Scattering data collected for three different colloidal systems (gold, silica and polystyrene latex nanoparticles) it was finely demonstrated that both kinds of regime are universal and independent on the nature of the cluster. This was clearly presented through the construction of master curves where the data from all investigated systems are reported, showing an excellent superposition of the different scaled datasets.[109,110]
An example of master curve obtained from Dynamic Light Scattering data is shown in fig. 1.6.1. In particular, experimental data from the three different colloidal systems were represented by scaling the average effective diffusion coefficient through the use of a constant, i.e. the value of diffusion coefficient at null scattering vector. Then, this ratio was plotted as a function of the product between the scattering vector and the hydrodynamic radius.

In the case of soft polymers, such as elastomers with glass-transition temperature significantly lower than room temperature, upon aggregation they may deform or even coalesce as a result of polymer chain inter-diffusion or viscous flow. Due to

the coalescence, the particle identity within a cluster is lost, that is, all of the spherical primary particles merge to form a larger spherical particle.

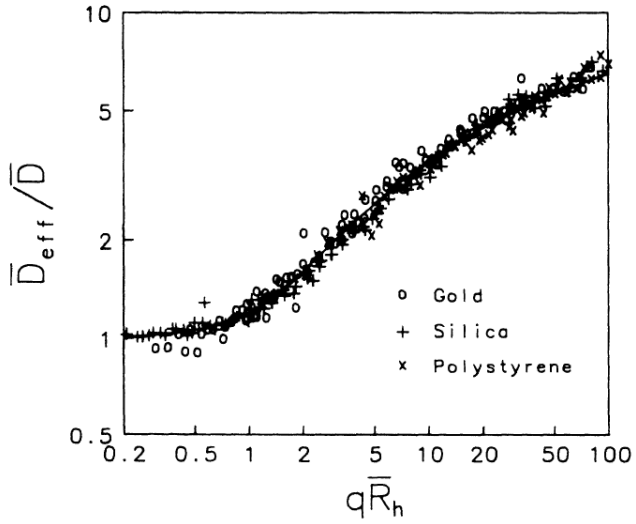

Figure 1.6.1 – Master curves obtained independently for gold, silica and polystyrene latex nanoparticles for RLA.[110]

Once coalescence occurs between two particles, even though it is a physical process owing to the inter-diffusion and anchoring of the polymer chains, the two particles can permanently stick together and are difficult to separate. If the coalescence of particles within a cluster can be controlled to a desired degree through physical gelation, a permanent gel can be directly obtained with desired structures.[112]

Chapter 2 – Experimental section

The design of a novel technology for applications in laundry products implies a deep study that starts from the choice of a proper preparation protocol. In this project, we drew our attention on the salting-out phenomenon, which may occur when either natural or synthetic macromolecules are present in solution together with salts. The polymer aggregation behavior depends on the nature of the kosmotropic species used in order to favor the aggregation process, on the polymer-polymer and the polymer-solvent interactions, as well as on the effect exerted by all the components present in complex mixtures like surfactants and additives (i.e. perfumes). We performed a study aimed at increasing the number of components of the investigated systems gradually, starting from a binary solution containing just polymer and water until reaching a complex mixture containing polymer, salt, surfactant, additives and solvents. In particular, in order to rationalize the role of each species, as a first step we needed to study the chemico-physical properties of many different systems containing a limited number of components. As a second step, we focused our attention on the synergic effect of all components shedding light on possible interactions among them. In this chapter, the materials and methods used for the preparation of all these solutions are reported, as well as the sample preparation procedure. Moreover, the protocols and the procedures followed to design the technology for the final application are described.

2.1 – Investigating the Hofmeister series: the choice of the salt

2.1.1 – Materials

Poly-vinyl alcohol (PVA) +99% hydrolyzed, mass average molecular weight 85000 ÷ 124000 g mol^{-1}, sodium chloride (NaCl, purity ≥ 99%, AR grade), sodium thiocyanate (NaSCN, purity ≥ 99.9%), potassium chloride (KCl, purity ≥ 99.0%)

and calcium chloride ($CaCl_2$, purity ≥ 96.0%) were purchased from Sigma Aldrich, Milano (Italy). All aqueous solutions were prepared by using twice distilled Milli-Q water.

2.1.2 – Sample preparation

A PVA stock solution was prepared by weighing the polymer and water into a glass vial. The vial was placed into a controlled temperature bath at 85 °C and the solution was kept under stirring at 700 rpm for 4 hours. The obtained solution was kept at room temperature (about 20°C) for 1 hour. Stock salt solutions at different concentrations were prepared by adding the proper quantities of salt and water into a vial. In order to avoid the presence of dust particles, all solvents were filtered by using 0.20 μm filters. PVA stock solution was filtered, since a small amount of polymer was not completely solubilized. About 2 g of solution were used for determining the PVA concentration through Total Organic Carbon (TOC) analysis. For Dynamic Light Scattering measurements, the samples were prepared by diluting a stock PVA 2% w/w solution with water and/or a stock salt 4.5 mol kg^{-1} solution.

2.1.3 – Characterization techniques

TOC analysis was performed by splitting the amount of PVA solution used for the analysis in two parts. A first aliquot of solution was treated with phosphoric acid so as to transform all the inorganic carbon into CO_2. A second aliquot of solution was injected into a combustion chamber at 700 °C in order to transform all the carbon (both inorganic and organic) into CO_2. An IR spectrophotometer was used for determining the concentration of carbon dioxide. Then, the TOC was determined by subtracting the carbon concentration obtained in the acidification step from the carbon concentration obtained in the combustion step.

Dynamic Light Scattering (DLS) measurements were carried out by using a home-made instrument composed by a Photocor compact goniometer, a SMD 6000 Laser Quantum 50 mW light source operating at 532.5 nm, a photomultiplier (PMT-120-OP/B) and a correlator (Flex02-01D) from *Correlator.com*. All measurements were performed at 25 °C with the temperature controlled through the use of a thermostat bath. We measured the scattering intensity at fixed scattering angle of 90°.

2.2 – Characterization of the aggregation process

2.2.1 – Materials

Poly-ethylene-vinyl alcohol (EVOH) HR-3010 resin (purity > 97%) was purchased from Kuraray, Chiyoda, Tokyo (Japan). Poly-vinyl alcohol (PVA) +99% hydrolyzed, mass average molecular weight 85000 ÷ 124000 g mol^{-1}, sodium chloride (NaCl, purity ≥ 99%, AR grade) and dideuterium water (D_2O, 99.9% atom D) were supplied by Sigma Aldrich, Milan (Italy). All aqueous solutions were prepared by using twice distilled Milli-Q water with the only exception of samples for neutron scattering experiment where D_2O was used.

2.2.2 – Sample preparation

Stock polymer and NaCl solutions were prepared as described above.
For Dynamic Light Scattering measurements on solutions containing EVOH, the samples were prepared by diluting a stock EVOH 2% w/w solution with water and/or a stock NaCl 2.3 mol kg^{-1} solution. We analyzed a 1% w/w salt-free polymer solution and 15 samples at 5 different EVOH concentrations (0.70% w/w, 0.85% w/w, 1.00% w/w, 1.15% w/w and 1.30% w/w) and 3 different NaCl concentrations (0.65 mol kg^{-1}, 0.75 mol kg^{-1} and 0.85 mol kg^{-1}). For PVA we followed the same protocol described for EVOH. The samples were prepared by

diluting a stock PVA 2% w/w solution with water and/or a stock NaCl 4.5 mol kg^{-1} solution. In this case, the polymer concentration was kept constant (1% w/w) and 5 different NaCl concentrations (1.500 mol kg^{-1}, 1.625 mol kg^{-1}, 1.750 mol kg^{-1}, 1.875 mol kg^{-1} and 2.00 mol kg^{-1}) were studied.

The samples prepared for Small Angle Neutron Scattering measurements on the EVOH solution were prepared by following the same procedure shown for the samples analyzed through Dynamic Light Scattering by using a mixed solvent, so as to obtain a final solvent weight ratio D_2O/H_2O of 80/20. Such ratio was chosen in order to obtain a good contrast between the polymer and the solvent keeping a reasonable EVOH solubility. We prepared a free-salt sample containing EVOH at 1% w/w. For PVA, D_2O was chosen as a solvent and a sample at PVA 1% w/w was prepared.

For Static Light Scattering measurements on solutions containing EVOH, the samples were prepared by diluting a stock EVOH 2% w/w solution with water and/or a stock NaCl 4.5 mol kg^{-1} solution. We studied 4 sets of samples at different NaCl concentrations: 0 mol kg^{-1} (i.e. salt-free samples), 0.25 mol kg^{-1}, 0.75 mol kg^{-1} and 1.50 mol kg^{-1}. For each set, 4 different EVOH concentrations were investigated (0.50% w/w, 0.75% w/w, 1.00% w/w and 1.50% w/w). For PVA the same procedure described for EVOH was followed, with the only exception that the investigated NaCl concentrations were 0 mol kg^{-1}, 0.50 mol kg^{-1}, 1.00 mol kg^{-1} and 2.00 mol kg^{-1}. For each set, 4 different PVA concentrations were investigated (0.25% w/w, 0.50% w/w, 0.75% w/w and 1.00% w/w).

2.2.3 – Characterization techniques

Static Light Scattering (SLS) and Dynamic Light Scattering (DLS) measurements were performed by using the same instrument described above. We measured the scattering intensity at fixed scattering angle of 90°.

The refractive indexes of all solutions studied through SLS were measured by using an Abbe refractometer (Atago® NAR-3T) operating at 25°C by dropping 100 μL of solution between the illuminating and the refracting prisms. Each measurement was repeated three times and the average value of refractive index was calculated.

Small Angle Neutron Scattering (SANS) measurements were performed at 25 °C with the KWS-2 diffractometer operated by Julich Centre for Neutron Science at the FRMII source located at the Heinz Maier Leibnitz Centre, Garching (Germany). For all the samples, neutrons with a wavelength of 5 Å and $\Delta\lambda/\lambda \leq 0.2$ were used. A two-dimensional array detector at two different wavelength (W)/collimation (C)/sample-to-detector (D) distance combinations (W 5 Å/C 8 m/D 2 m and W 5 Å/C 8 m/D 8 m) measured neutrons scattered from the samples. These configurations allowed collecting data in a range of the scattering vector modulus q between 0.08 $Å^{-1}$ and 0.4 $Å^{-1}$ for the salt-free samples containing only polymer at 1 % w/w.

2.3 – Structural characterization of polymer aggregates

2.3.1 – Materials and sample preparation

The same materials presented in paragraph 2.2.1 were used. Stock polymer and NaCl solutions were prepared as described above.

For Static Light Scattering measurements on EVOH aggregate solutions, 3 sets of 5 samples at constant NaCl concentration and different polymer concentrations were prepared by diluting a stock EVOH 1% w/w aggregate solution with a NaCl stock solution of the same concentration. We studied 3 different NaCl concentrations: 0.65 mol kg^{-1}, 0.75 mol kg^{-1} and 0.85 mol kg^{-1}. At each NaCl concentration, 5 different EVOH concentrations (0.20% w/w, 0.40% w/w, 0.60% w/w, 0.80% w/w and 1.00% w/w) were investigated. Samples containing PVA were prepared by

diluting a stock PVA 1% w/w aggregate solution with a NaCl stock solution of the same concentration. We studied 5 different NaCl concentrations: 1.500 mol kg^{-1}, 1.625 mol kg^{-1}, 1.750 mol kg^{-1}, 1.875 mol kg^{-1} and 2.000 mol kg^{-1}. At each NaCl concentration, 5 different PVA concentrations (0.20% w/w, 0.40% w/w, 0.60% w/w, 0.80% w/w and 1.00% w/w) were investigated.

For Small Angle Neutron Scattering measurements on EVOH solution, 3 samples at constant EVOH concentration (1% w/w) and 3 different NaCl concentrations (0.45 mol kg^{-1}, 0.55 mol kg^{-1} and 0.65 mol kg^{-1}) were prepared by using a mixed solvent so as to obtain a final solvent weight ratio D_2O/H_2O of 80/20. For PVA, 3 samples at constant PVA concentration (0.85% w/w) and at 3 different NaCl concentrations (1.50 mol kg^{-1}, 1.75 mol kg^{-1} and 2.00 mol kg^{-1}) were prepared by using D_2O as a solvent.

2.3.2 – Characterization techniques

Cryogenic Transmission Electron Microscopy (Cryo-TEM) was used to study the microstructure of the EVOH aggregates in the presence of NaCl. The EVOH samples were vitrified by using a standard vetrification robotic system (Vitrorobot™ Mark IV by FEI™) at 25 ^oC and 100% relative humidity. A sample drop of 1-2 μL was loaded on a carbon-coated film with a woven pattern supported on a copper grid (standard 200-mesh TEM grids by Electron Microscopy Science). Once the sample was loaded on the carbon grid, the drop was rapidly blotted in order to remove any sample excess from the grid. Following the loading and blotting, the grid was quenched into clean liquid ethane and as result a thin layer of vitrified EVOH sample was obtained. The samples were then rapidly placed into a cryogenic holder in the presence of liquid nitrogen (N_2) at a temperature below -170 ^oC to maintain the vetrification and avoid any structural change during data collection. The microscope used is the FEI™ Tecnai G2 Sphera, which was held with an accelerating voltage of 200 kV. The EVOH samples were observed in a

low-dose mode to minimize radiation damages. Sample images were taken with a digital camera and analyzed with Gatan Digital Micrograph software.

Transmission Electron Microscopy (TEM) images for PVA were collected by using a JEM-2100 Plus Transmission Electron Microscope located at the department of Chemistry of Texas Christian University.

Static Light Scattering (SLS) and Dynamic Light Scattering (DLS) measurements were carried out by using the same instrument described above. In the case of SLS, we measured the scattering intensity at different scattering angles: 60°, 75°, 90°, 105° and 120°, in the case of DLS, at fixed scattering angle of 90°.

The refractive indexes of all solutions studied through SLS were measured by using the instrument described above.

Small Angle Neutron Scattering (SANS) measurements were performed by using the same instrument described above. In this case, a two-dimensional array detector at three different wavelength (W)/collimation (C)/sample-to-detector (D) distance combinations (W 5 Å/C 8 m/D 2 m, W 5 Å/C 8 m/D 8 m, and W 5 Å/C 20 m/ D 20 m) measured neutrons scattered from the samples. These configurations allowed collecting data in a range of the scattering vector modulus q between 0.002 $Å^{-1}$ and 0.4 $Å^{-1}$. For the sample at higher NaCl concentration, we also used neutrons with a wavelength of 10 Å and $\Delta\lambda/\lambda \leq 0.2$ and the same wavelength (W)/collimation (C)/sample-to-detector (D) distance combination reported above, in order to extend the experimental profile at lower values of the scattering vector.

2.4 – Investigation on polymer-surfactant interaction

2.4.1 – Materials

EVOH, PVA, NaCl and D_2O, whose characteristics are reported in paragraph 2.2.1, were used. A mixture of non-ionic ethoxylated surfactants (Lorodac 7-24, traded as C12-C14 ethoxylated alcohols, 100% active component) was supplied by Sasol,

Antwerp, Belgium. Sodium Laureth Sulfate (SLES, 70% active component) was supplied by KLK Tensachem, Liège, Belgium.

2.4.2 – Sample preparation

Stock polymer and NaCl solutions were prepared as described above. Surfactant (C12-C14 ethoxylated alcohols or SLES) solutions were prepared by weighing a certain amount of surfactant into a glass vial and by adding either water, D_2O, a NaCl solution or a polymer solution according to the type of sample to prepare.

Samples for surface tension measurements on binary (surfactant + water) systems were obtained by preparing a stock solution at a surfactant concentration corresponding to about 10 times the expected critical micellization concentration. This solution was then gradually added to about 15 g of water. Samples for surface tension measurements on ternary (surfactant + polymer + water) systems were prepared by preparing a stock surfactant solution by using a polymer (EVOH or PVA) solution at 1% w/w as a solvent at a surfactant concentration corresponding to about 10 times the critical micellization concentration. This solution was then gradually added to about 15 g of polymer solution at 1% w/w. Samples for surface tension measurements on ternary (surfactant + NaCl + water) systems were obtained by preparing a stock surfactant solution by using a 2 mol kg^{-1} NaCl solution as a solvent at a surfactant concentration corresponding to about 5 times the critical micellization concentration. This solution was then gradually added to about 15 g of a 2 mol kg^{-1} NaCl solution.

DLS measurements on binary (surfactant + water) systems were carried out on 3% w/w surfactant solutions, whereas DLS measurements on quaternary (surfactant + polymer + NaCl + water) systems were performed at 1% w/w polymer (EVOH or PVA), 0.65 mol kg^{-1} or 1.50 mol kg^{-1} NaCl (for EVOH and PVA, respectively) and at a surfactant concentration corresponding to 5 times the critical micellization concentration determined in water.

SANS measurements on binary (surfactant + D_2O) systems were carried out on 5% w/w surfactant solutions, whereas SANS measurements on quaternary (surfactant + polymer + NaCl + solvent) systems were performed at 1% or 0.85% w/w polymer (for EVOH and PVA, respectively), 0.45 mol kg^{-1} or 1.50 mol kg^{-1} NaCl (for EVOH and PVA, respectively) and at a surfactant concentration corresponding to 5 times the critical micellization concentration determined in water.

2.4.3 – Characterization techniques

Surface tension measurements were carried out by using a Sigma 70 Force Tensiometer from Nordtest, equipped with an interface and a system unit and based on the du Noüy ring technique. This method allows measuring the force required to raise a platinum ring from the surface of the liquid, which is related to the surface tension.

Dynamic Light Scattering (DLS) measurements were performed by using the same instrument described above. We measured the scattering intensity at fixed scattering angle of 90°.

We carried out Small Angle Neutron Scattering (SANS) measurements with the same instrument and configuration described in paragraph 2.3.2.

2.5 – Fragrance segregation process

2.5.1 – Materials

EVOH, PVA and NaCl, whose characteristics are reported in paragraph 2.2.1, were used. A fragrance mixture of 10 different components (Decylaldheyde, p-Methylacetophenone, Methyl salicylate, Eugenol, Hexyl Acetate, Citral, Ethyl-2-Methyl Butyrate, Geraniol, Habanolide and PRM A) was supplied by Procter and Gamble. The exact composition of such mixture was determined through GC-FID

(Gas Chromatography with Flame Ionization Detection) by using the single components (all with purity ≥ 97%) supplied by Sigma Aldrich. Ethanol (purity ≥ 99.8%), hexane (purity ≥ 95%) and octane (purity ≥ 99%) were also purchased from Sigma Aldrich.

2.5.2 – Sample preparation

PRM stock solutions were prepared by solubilizing a certain amount of fragrance either in a mixture of hexane and octane 100:1 w/w or ethanol. Stock polymer and NaCl solutions were prepared as described above.

For GC-FID measurements on PRM solutions, 10 stock solutions of single fragrances at a concentration of 4% w/w were prepared by using as a solvent a mixture of hexane and octane 100:1 w/w. Then, 10 sets of samples at 2 more different PRM concentrations (1% w/w, 2% w/w) were obtained by diluting the stock 4% w/w solutions in the hexane and octane mixture, so as to have 3 PRM concentrations for each set of samples, which were used for building the calibration curves.

For the solubilization tests we prepared 11 samples at fixed fragrance concentration (1% w/w) and 11 different ratios of water and ethanol, ranging from 100/0 w/w to 0/100 w/w with a step of 10% w/w.

For Dynamic Light Scattering measurements the samples were prepared by diluting a stock EVOH 2% w/w solution with a stock PRM solution and ethanol. We analyzed 2 solutions containing fragrance at 0.5% w/w and polymer at 1% w/w solubilized in a mixture of ethanol and water 30/70 w/w.

For GC-FID measurements on the hexane extracts, firstly a solution containing polymer particles was prepared, by choosing a final EVOH or PVA concentration of 1% w/w and a final NaCl concentration of 0.85 mol kg^{-1} and 2.00 mol kg^{-1} for the samples containing EVOH and PVA, respectively. Then, a stock fragrance solution in ethanol was added, in order to have a final PRM concentration of 0.5%

w/w and a final ethanol concentration of about 30% w/w. The final concentrations here reported are related to the final solutions obtained by mixing the aggregate solution with the PRM solution. Reference solutions without polymer and at comparable PRM concentrations were prepared. Finally, about 1 g of solutions containing polymer, NaCl, PRM, water and ethanol was filtered by using 0.20 μm filters and the filtered solutions were treated with 2 g of hexane. The same procedure was followed for the reference samples without polymer.

For GC-MS measurements on the hexane extracts, the same preparation protocol described for GC-FID measurements was followed. In this case, we tested 3 different concentrations of PRM A (0.09% w/w, 0.12% w/w and 0.15% w/w) and polymer (0.51% w/w, 0.68% w/w and 0.85% w/w), instead of the mixture of 10 fragrances and the fixed 1% w/w polymer concentration used for GC-FID measurements. The ratio PRM A/polymer was kept constant for all samples. The final ethanol concentration was 30% w/w and the final NaCl concentration was of 0.85 mol kg^{-1} and 2.00 mol kg^{-1} for the samples containing EVOH and PVA, respectively.

2.5.3 – Characterization techniques

GC-FID measurements were carried out by using a FOCUS GC System from Thermo Electron Corporation equipped with an apolar DB-5 capillary column (30 m x 0.32 mm x 0.25 μm) and a Flame Ionization Detection system with an acquisition rate of 300 Hz. Liquid injection was performed into an oven at 260 °C with a 1:8 split ratio. Nitrogen was used as mobile phase. We operated by using a temperature-programmed analysis (from 40 °C for 2 min to 200 °C for 15 min with a heating rate of 30 °C/min).

Dynamic Light Scattering (DLS) measurements were performed by using the same instrument described above. We measured the scattering intensity at fixed scattering angle of 90°.

GC-MS (Gas Chromatography with Mass Spectrometry detection) measurements were carried out by using a Hewlett Packard G1530A GC System equipped with a DB-5MS apolar capillary column (30 m x 0.25 mm x 1 μm) and a Hewlett Packard 5973 MSD (Mass Spectrometric Detector). Hexane extracts were put into 2 mL glass vials and closed with a magnetic cap provided with a perforable silicon septum. Liquid injection was performed into an oven at 260 °C with a 1:8 split ratio. We operated at constant flow mode (1.5 mL/min at 113 kPa, with a total flow of 16.8 mL/min) by using a temperature-programmed analysis (from 40 °C for 1 min to 80 °C with a heating rate of 30 °C/min and from 80 °C to 250 °C with a heating rate of 8 °C/min). Finally, the analytes were detected by fast GC-MS in full scan mode. Perfume concentrations were subsequently quantified through the use of Chemstation Software.

2.6 – Washing tests

2.6.1 – Materials

EVOH, PVA and NaCl, whose characteristics are reported in paragraph 2.2.1, were used. Ethanol (purity ≥ 99.8%) and PRM A (purity ≥ 97%) were purchased from Sigma Aldrich. PRM B (purity ≥ 97%) was supplied by International Flavors & Fragrance, Benicarló (Spain). Unperfumed liquid detergent containing both anionic and non-ionic surfactants was used for the washing tests.

The exact composition of the unperfumed laundry product and the name of the fragrances tested (traded as PRM A and PRM B) cannot be disclosed due to confidentiality.

2.6.2 – Sample preparation

Technology (polymer + fragrance) and reference (free perfume) solutions were prepared by following two different protocols: the 5 steps in a row protocol and the 5 steps in 2 parts protocol.

According to the first protocol, solutions and solvents were added as follows:

1) Polymer stock solution;
2) Water (if needed);
3) Ethanol (if needed);
4) PRM stock solution in ethanol;
5) NaCl stock solution in water.

According to the second protocol, solutions and solvents were added as follows:

FIRST PART

1) Polymer stock solution;
2) Water (if needed);
3) NaCl stock solution in water;

SECOND PART

4) Ethanol (if needed);
5) PRM stock solution in ethanol.

For both protocols, calculated volumes of all solutions and solvents were added under stirring at 1200 rpm. Final concentrations of all components were the same, independently on the protocol followed. Reference solutions were prepared by adding water instead of the polymer solution.

Tab. 2.6.2.1 reports the concentrations of the stock solutions and the final polymer, NaCl, PRM, ethanol and water concentrations. As an example, tab. 2.6.2.2 summarizes the amounts used for preparing the technology solutions for a fixed quantity of final solution (about 10 g) at a final technology concentration of 1% w/w. Such amounts differ according to the polymer and the PRM used for the preparation. The same stock solutions were used for preparing the samples at lower

technology concentrations (0.6% w/w and 0.8% w/w): in this case, we used a lower quantity of polymer and PRM solutions and a higher amount of ethanol and water.

Table 2.6.2.1 – Concentrations of stock solutions and final concentrations of all components in the mixture.

Technology	Concentration [% w/w]							
	Polymer stock	**NaCl stock**	**PRM stock**	**Polymer final**	**NaCl final**	**PRM final**	**Ethanol final**	**Water final**
EVOH particles + PRM A	2.00	18.1	0.750	0.850	4.68	0.150	19.8	74.52
EVOH particles + PRM B	2.00	19.8	0.750	0.925	4.68	0.0750	30.0	64.32
PVA particles + PRM A	4.00	21.1	0.750	0.850	10.4	0.150	19.8	68.8
PVA particles + PRM B	4.00	21.1	0.750	0.925	7.98	0.0750	30.0	61.02

Table 2.6.2.2 – Volumes of solvents and stock solutions needed for preparing the technology solutions at a fixed amount of final solution (about 10 g) at a final technology concentration of 1% w/w.

Technology	Volume [µL]				
	Water	**Ethanol**	**Polymer solution**	**NaCl solution**	**PRM solution**
EVOH particles + PRM A	1176	0	4325	2284	2579
EVOH particles + PRM B	0	2589	4706	2084	1290
PVA particles + PRM A	978	0	2162	4326	2579
PVA particles + PRM B	912	2589	2353	3331	1290

For DLS measurements we prepared 4 different sets of samples at distinct technology concentrations (0.6% w/w, 0.8% w/w and 1% w/w). Such samples and their references were prepared by following the 5 steps in two parts protocol and by using water, ethanol and the stock solutions whose concentrations are reported above.

Washing tests were carried out by using a Launder-o-Meter. Cotton and polyester fabric tracers of 5 cm x 5 cm were used. The details of the washing procedure are reported below:

1) The fabric is weighed and put into the metal Launder-o-Meter jar;
2) 10 metal spheres are added into the jar;
3) 200 mL of demineralized water are poured;
4) About 1 g of unperfumed detergent are added into the jar;
5) Either the free perfume reference solution or the technology solution (about 5.0 g) are poured into the jar;
6) The jars are closed and placed into the Lauder-o-Meter;
7) The temperature is set to be between 35 °C and 40 °C (37-38 °C);
8) After 1 hour, the jars are removed from the Launder-o-Meter;
9) The fabrics are squeezed by applying the same pressure;
10) The jars and the metal spheres are rinsed;
11) The washed fabric is put into the jar again together with the metal spheres;
12) 200 mL of demineralized water are poured;
13) The jars are closed and placed into the Lauder-o-Meter;
14) The temperature is set to be between 35 °C and 40 °C (37-38 °C);
15) After 5 minutes, the jars are removed from the Launder-o-Meter;
16) The fabrics are squeezed by applying the same pressure;
17) Finally, according to the test, the fabrics are treated as follows:
    a. for deposition: each fabric is placed into a tray on an aluminum foil and dried at room temperature for one night;

b. for dry release: each fabric is placed into a tray on an aluminum foil and dried at room temperature for one night;
c. for wet release: each fabric is placed into a vial for GC-MS head-space analysis and the vial is closed.

The samples for release tests were prepared by using glass vials of 20 mL equipped with a magnetic cap and a plastic septum.

The samples for deposition tests were prepared as follows:

1) Each dried fabric is put into a 20 mL vial;
2) 12 mL of ethanol are poured into each vial containing the fabrics;
3) 12 mL of ethanol are also poured into 3 vials for the preparation of the standards (at 3 different perfume levels);
4) All the vials containing the fabrics are placed into an oven with orbital shaking at 60 °C for 1 hour;
5) All the vials are transferred into an ultrasonic bath and left under sonication for 15 minutes;
6) The vials are shaken and each ethanol solution is poured into a different vial (containing the extracts);
7) A stock PRM solution (about 0.5% w/w of PRM in ethanol) is prepared. This solution is used to prepare a work solution with a concentration of 0.008% w/w of PRM in ethanol; 3 different amounts or work solutions are added to the vials containing 12 mL of ethanol, previously prepared;
8) 4.5 mL of a 20% w/w solution of NaCl are transferred into a vial for GC-MS head-space analysis. This procedure is repeated for each extract and standard solution. Each sample is replicated;
9) 0.5 mL of PRM solutions in ethanol (extracts and standards) are poured into the vials containing the NaCl solution;
10) The vials are closed and the GC-MS analysis is started.

2.6.3 – Characterization techniques

Dynamic Light Scattering (DLS) measurements were performed by using the same instrument described above. We measured the scattering intensity at fixed scattering angle of 90°.

GC-MS head-space analysis was carried out by using an Agilent Technologies 7890B GC System equipped with a DB-5UI apolar capillary column (30 m x 0.25 mm x 0.25 μm) and an Agilent Technologies 5977A MSD (Mass Spectrometric Detector). Either ethanol extracts or fabrics were put into 20 mL glass vials and closed with a magnetic cap provided with a perforable silicon septum. Samples were equilibrated for 10 minutes at 65 °C. Then, the head-space above the samples was sampled via Solid Phase Micro Extraction (SPME) by using a fiber made of Divinylbenzene (DVB), Carboxen and Polydimethylsiloxane (PDMS). The compounds adsorbed on the fiber were then desorbed into the GC by using a temperature-programmed analysis (from 40 °C for 0.5 min to 270 °C for 0.25 min with a heating rate of 17 °C/min). Finally, the analytes were detected by fast GC-MS in full scan mode. Perfume head-space concentrations were subsequently quantified through the use of Chemstation Software.

Chapter 3 – A preliminary screening of the Hofmeister series: a model study

The ion-specific effect on the solubility of macromolecules in water, rationalized through the Hofmeister series, can be used as an effective method to obtain polymer particles with desired microstructural properties thanks to the salting-out effect. By choosing the proper salt and optimizing the polymer and the salt concentration, it is possible to tailor the particle structural features like the radius and the degree of compactness and to speed up the aggregation process until complete conversion from free chains to aggregates. In this chapter, we present a model study concerning a screening of different salts belonging to the Hofmeister series with the aim of finding the best kosmotropic species to use in order to induce the aggregation process.

3.1 – Screening of different salts

We started to study the aggregation behavior of a highly hydrolyzed (+99%) PVA, chosen as a model polymer, in the presence of different salts whose anions and cations belong to the Hofmeister series. Fig. 3.1.1 reports the species investigated in this first preliminary screening. The anions and cations reported in the left side are well known salting-out agents, i.e. they favor the aggregation, whereas the species reported in the right side are salting-in agents, i.e. they increase the macromolecule solubility.[113,114,115] Therefore, we chose NaSCN, $CaCl_2$, KCl and NaCl, whose anions and cations belong to very distinct positions of the Hofmeister series.

DLS allowed us to study the aggregation process over time: fig. 3.1.2 shows the results related to the reference sample (free-salt) and the samples at the highest salt concentrations and at the highest polymer concentration (1% w/w) tested.

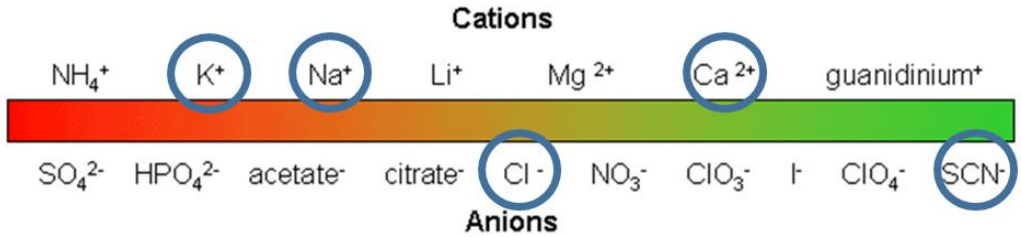

Figure 3.1.1 – Common cations and anions belonging to the Hofemeister series. Blue circles indicate the investigated species.

In the case of the salt-free sample, we can observe a population at about 20 nm, whose dimensions do not change over the 6 days of measurements. A similar behavior was found for the sample in the presence of NaSCN and for the sample in the presence of $CaCl_2$. In these three cases no aggregation was observed. Thus we can infer that the salting-in behavior induced by SCN^- and $Ca2^+$, predicted by the Hofmeister series, is followed for the investigated PVA. In the case of the sample in the presence of KCl, we observe the presence of a single and broad population just after the sample preparation and after 1 day, whereas after 3 days a second population appears. After 6 days the system reaches the equilibrium and no further evolution in terms of hydrodynamic radius distribution can be observed. For KCl concentrations higher than 1 mol kg^{-1} (1.25 mol kg^{-1} was tested) massive precipitation of the polymer occurs. In the case of the sample in the presence of NaCl, a second population appears after 1 day from preparation and a single population at about 200 nm can be observed after 3 days. Thus, we can infer that also for KCl and NaCl the salting-out behavior predicted by the Hofmeister series is followed. However, for the samples in the presence of KCl and NaCl salt concentration plays a key role in the aggregation process: whereas for KCl 1 mol kg^{-1} no further aggregation is observed, for NaCl 2 mol kg^{-1} the aggregation occurs in a very short time, even though the position of K^+ in the Hofmeister series is closer to the salting-out behavior with respect to Na^+.

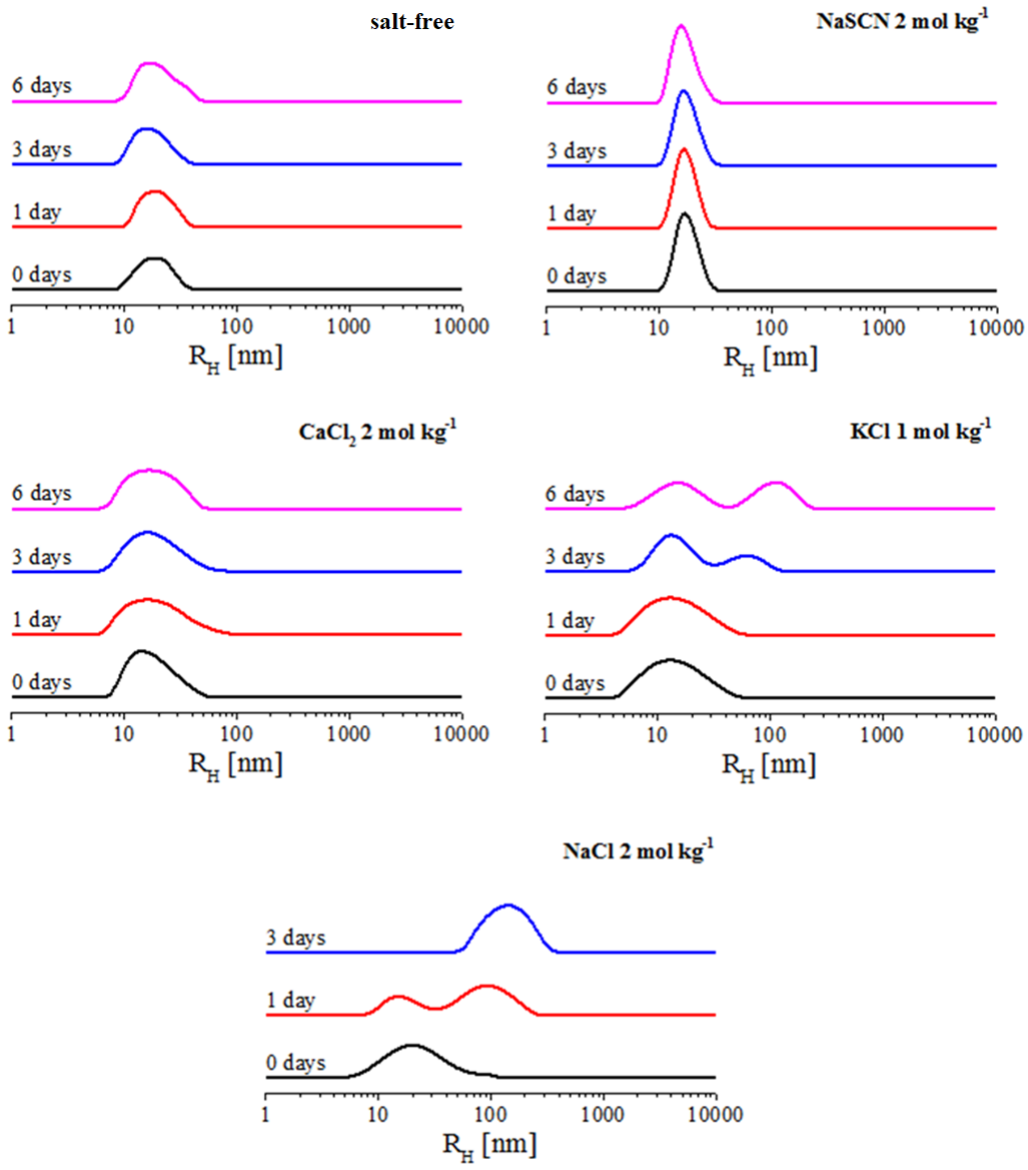

Figure 3.1.2 – Evolution of hydrodynamic radius distributions over time for the salt-free sample and for the samples in the presence of NaSCN 2 mol kg^{-1}, $CaCl_2$ 2 mol kg^{-1}, KCl 1 mol kg^{-1} and NaCl 2 mol kg^{-1} at constant PVA concentration (1% w/w).

3.2 – The choice of the salt

The preliminary results reported in the previous paragraph show that both KCl and NaCl are species that induce PVA aggregation over time. However, the aggregation in the presence of KCl is very sensitive to salt concentration, since a slight change of this parameter leads to massive precipitation of the polymer, whereas in the case of NaCl the aggregation process can be controlled more easily. Therefore, by taking into account the final aim of this project, which is finding a new technology for delivering active components in liquid detergent formulations, we decided to draw our attention to the polymer aggregation process in the presence of NaCl. Indeed, the aggregates obtained through the salting-out induced by NaCl could be used as an effective delivery system in laundry products.

When designing a process aimed at obtaining a carrier system, different parameters have to be considered. In our case, the most critical ones are the salt concentration and the polymer concentration: such parameters may have a strong impact on the particle size and morphology. Another important parameter is the time needed for the aggregation: this is an indirect parameter which is reasonably influenced by both salt and polymer concentration and it has to be considered in order to build-up a process which is compatible with the industrial timings.

Therefore, a complete rationalization of the polymer aggregation process in the presence of NaCl is fundamental. Two different polymers were chosen: a fully hydrolyzed (+99%) PVA, considered in this preliminary study as a model, and a super-hydrolyzed (+99.9%) EVOH. Once performed this basic research, an optimization of the critical parameters is needed in order to develop a process that occurs over a reasonable time scale.

Chapter 4 – Rationalization of the polymer aggregation process in the presence of sodium chloride

From the results shown in the previous chapter, we observe that NaCl is the best kosmotropic species to use in order to favor the aggregation process of PVA, chosen as a model polymer. In this chapter, we present a detailed study concerning the characterization of the aggregation process of two polymers (EVOH and PVA) in the presence of NaCl. Kinetic and thermodynamic aspects are discussed.

4.1 – The choice of the polymers

Among the possible candidates for the design of the target delivery technology, vinyl alcohol-based copolymers, currently referred to as PVA (poly vinyl alcohol) or EVOH (poly ethylene-co-vinyl alcohol), represent a suitable tool to obtain a carrier system characterized by a great stability of their aggregates in water. At the same time, EVOH and PVA are considered to be biocompatible, thanks to their low toxicity. Moreover, particles formed by such copolymers have excellent transport properties: indeed, different vinyl alcohol-based systems have been already proposed as carriers in biomedical applications or environmental science.[72,116,117] The structures of both copolymers are shown in fig. 4.1.1.

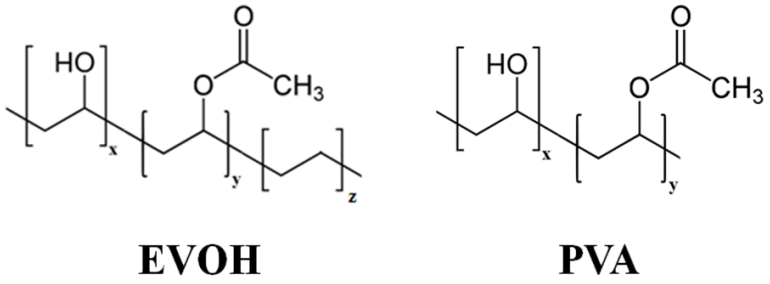

Figure 4.1.1 – EVOH (left) and PVA (right) structures: *x*, *y* and *z* represent the number of vinyl alcohol, vinyl acetate and ethylene units, respectively.

Both copolymers can be easily synthesized through radical polymerization using either vinyl acetate and ethylene (for EVOH) or just vinyl acetate (for PVA) as monomers. In a second step, the acetate groups are hydrolyzed in order to increase the polymer solubility in water. In the present study, we chose two super-hydrolyzed copolymers, containing more than 99% of vinyl alcohol. However, PVA is a polymer containing mainly vinyl alcohol units, whereas EVOH is a more hydrophobic polymer containing mainly both vinyl alcohol (about 60% mol) and ethylene (about 40% mol) units. Therefore, we are aware that the different chemical composition of the investigated species may have a deep influence on the aggregation properties in the presence of NaCl. Thus, we needed to rationalize the aggregation process for both copolymers, in order to optimize the polymer and the salt concentrations for the final application.

4.2 – Aggregation properties of aqueous polymer solutions

EVOH and PVA well dissolve in water up to 4% w/w and 10% w/w respectively, the maximum concentrations here tested. Fig. 4.2.1 shows the evolution of R_H over time obtained by DLS measurements for a 1% w/w EVOH and a 1% w/w PVA solution in water. For both systems, the results show the presence of a single population whose hydrodynamic radius is centered at 16 ± 1 nm for EVOH and at 18 ± 1 nm for PVA. Neither variation of R_H or additional populations were observed over time. The constancy of R_H and the lack of new populations with time seem to indicate that no aggregation occurs over the 21 days of measurements.

In order to shed light on the nature of such population, we performed SANS measurements on the polymer solutions at a concentration of 1% w/w. Fig. 4.2.2 and fig. 4.2.3 show the neutron scattering intensity profiles for EVOH and PVA obtained after 2 days from the preparation.

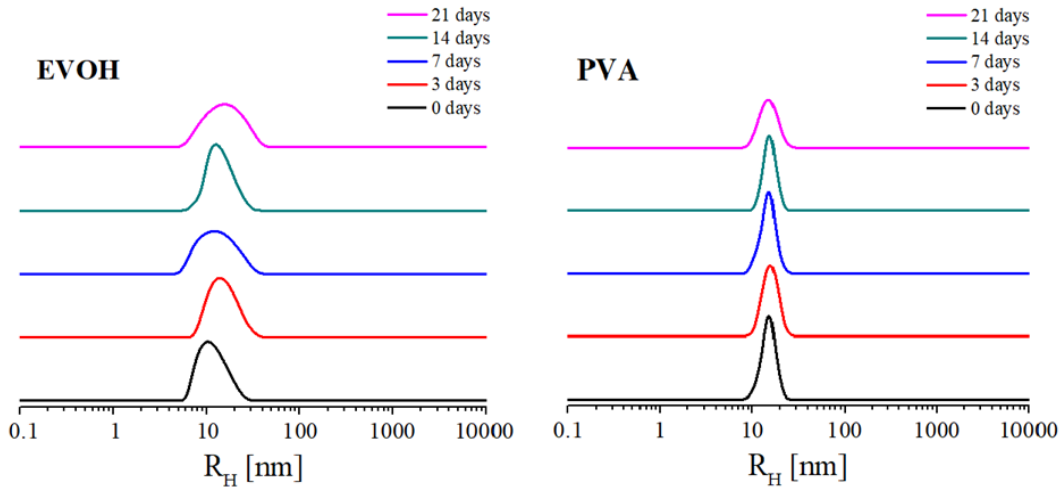

Figure 4.2.1 – Distribution curves of hydrodynamic radii for EVOH (left) and PVA (right) in water at different times from the preparation of the polymer solution at a concentration of 1% w/w.

In the case of solutions containing single polymer chains, two models are commonly used: the Debye Model[118] and the Polydispersed Gaussian Coil (PGC) model[118]. The former is used for gaussian polymer chains in theta solvent condition, i.e. when the polymer coils do not show either attractive or repulsive forces towards the solvent. The latter is used for gaussian polymer chains in good solvent condition, i.e. when the polymer coils show high affinity towards the solvent. Although both models were tested, the best result was obtained by using the PGC model, represented by the following equation:

$$\frac{d\Sigma}{d\Omega} = scale\frac{2\left[(1+Ux)^{-1/U} + x - 1\right]}{(1+U)x^2} + bkg \qquad \text{equation 4.2.1}$$

where $x = \frac{R_g^2 q^2}{1+2U}$ is the dimensionless chain dimension, depending on both the radius of gyration R_g and the polydispersity index $U = \frac{M_w}{M_n} - 1$.

This model calculates an empirical functional form for the scattering from a polydisperse polymer chain assuming a Schulz-Zimm type molecular weight distribution.[118]

From the Porod analysis performed in the high-*q* region (insets of fig. 4.2.2 and fig 4.2.3) we obtained a slope of -1.51 ± 0.02 for EVOH, and a slope of -1.48 ± 0.01 for PVA, close to the theoretical value of 5/3 = 1.667, which is the signature for fully swollen coils[119]. The fully swollen state is related to the high hydration of the chains. Therefore, by taking into account the high affinity of both polymers towards the solvent, the low polymer concentration and the absence of other populations from DLS measurements, the experimental curve was fitted by the Polydispersed Gaussian Coil (PGC) model, as represented by equation 4.2.1.

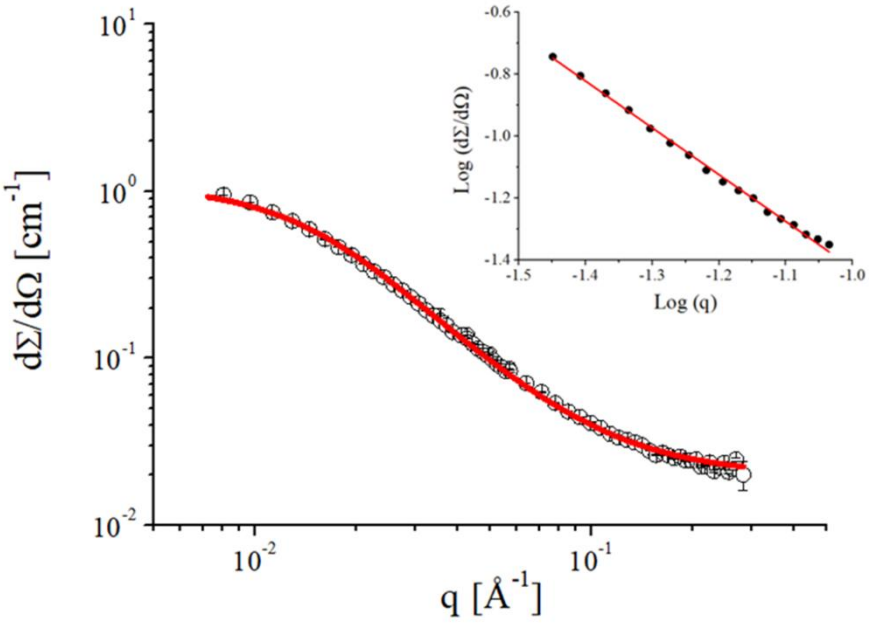

Figure 4.2.2 – Neutron scattering intensity profile for EVOH after 2 days from the preparation at a concentration of 1% w/w: experimental data are represented by circles and the fittings by straight lines. Inset: Porod analysis performed in the high-*q* region.

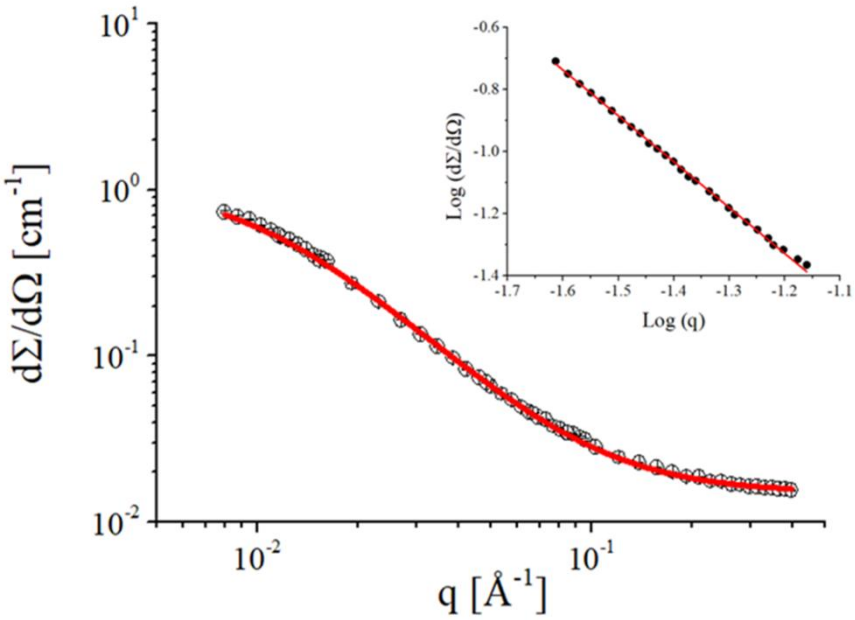

Figure 4.2.3 – Neutron scattering intensity profile for PVA after 2 days from the preparation at a concentration of 1% w/w: experimental data are represented by circles and the fittings by straight lines. Inset: Porod analysis performed in the high-*q* region.

The morphological parameters obtained from fitting are the radius of gyration of the free polymer chain and the polydispersity (M_w/M_n). For EVOH such values were found to be 13.8 ± 0.2 nm and 3.9 ± 0.1, respectively, whereas for PVA we obtained 16.5 ± 0.2 nm and 3.6 ± 0.1, respectively. R_H values well agree with the DLS result, if we consider that the hydrodynamic radius is slightly higher due to the contribution of the solvent hydration shell. As a consequence, we can assume that the single population observed corresponds to the free polymer chain.

4.3 – Sodium chloride effect on polymer behavior in solution

In order to study the effect of NaCl on the aggregation properties of EVOH, we performed a SLS study. The measurements were carried out in a NaCl concentration range 0 ÷ 1.5 mol kg^{-1}, so as to find the appropriate salt concentration at which the aggregation process is favored. Preliminarily, we analyzed 4 different sets of samples, characterized by the same concentration of salt and different concentrations of polymer at constant scattering angle (90°). Each dataset was fitted by using the equation A.1.4, according to a procedure widely diffused in literature[120,121], which allowed the Debye plot to be obtained. From the intercept of the fitting lines the polymer average molecular weight M_w was calculated whereas from their slope the second virial coefficient A_2 was obtained. Experimental data, linear fits and fitting parameters are shown in fig. 4.3.1 and tab. 4.3.1, respectively.

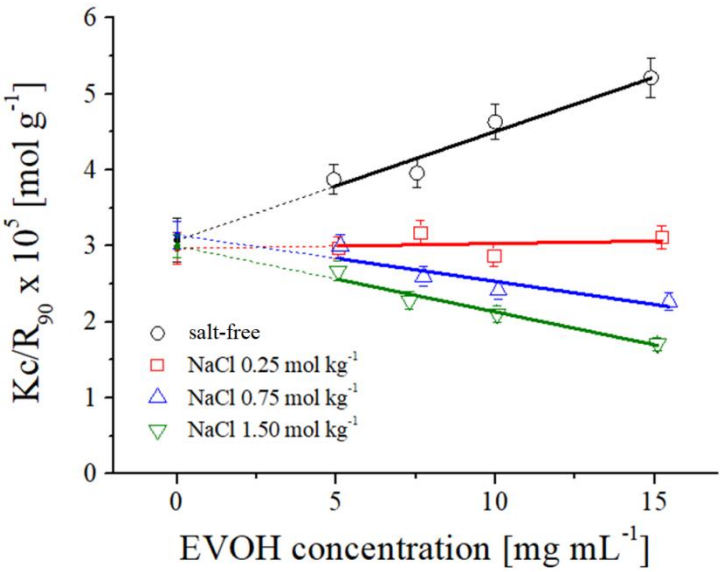

Figure 4.3.1 – Linear fits obtained from equation A.1.4 by SLS at 4 distinct salt concentrations. Error bars were calculated by considering the standard deviation on the average intensity value and the propagation of the relative error.

The values of M_w are the same at each NaCl concentration: this clearly indicates that no aggregates are present at time = 0, i.e. when the aqueous polymer and salt mixtures were prepared. The dependence of A_2 on salt concentration is reported in fig. 4.3.2.

Table 4.3.1 – Molecular weight M_w and second virial coefficient A_2 obtained from the fittings shown in fig. 4.3.1.

NaCl concentration [mol kg^{-1}]	**M_w [g mol^{-1}]**	**A_2 x 10^4 [mol mL g^{-2}]**
salt-free	32000 ± 3000	7.2 ± 1.6
0.25	34000 ± 2000	0.3 ± 1.0
0.75	32000 ± 2000	-3.0 ± 0.8
1.50	33000 ± 2000	-4.3 ± 0.7

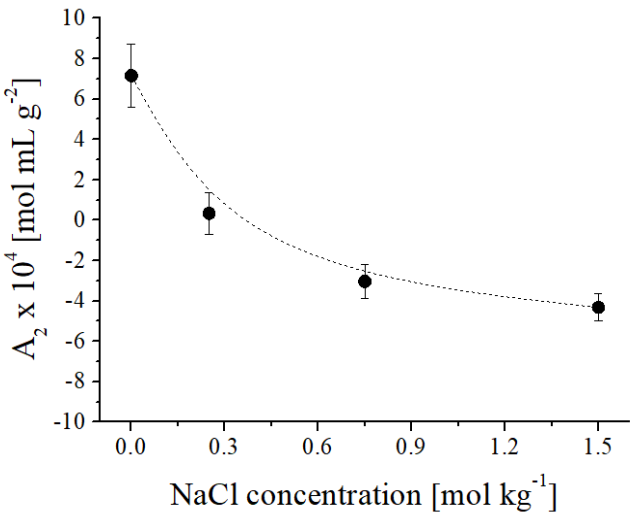

Figure 4.3.2 – Dependence of the second virial coefficient A_2 on the salt concentration. The dotted line is a guide to the eye.

Positive values of the second virial coefficient indicate a good solvent condition, i.e. polymer-solvent interactions are favored, whereas negative values indicate a bad solvent condition, i.e. such interactions are not favored and aggregation may

easily occur.[122] Therefore, we are able to predict the phase behavior of EVOH in solution. In the absence of the electrolyte (salt-free) the polymer is well hydrated and aggregation does not occur. For NaCl 0.25 mol kg^{-1}, A_2 is almost null and we are approaching the theta solvent condition, corresponding to an unperturbed state, for which the polymer-solvent and the polymer-polymer interactions are totally compensated. In this case, even slight temperature or concentration fluctuations may influence the equilibrium, easily leading to positive or negative values of A_2. For NaCl 0.75 mol kg^{-1} and NaCl 1.5 mol kg^{-1} A_2 is negative, indicating a bad solvent condition. In this case, the polymer is less hydrated due to the high salt concentration and, consequently, interactions between polymer and solvent are weak. Therefore, NaCl exerts a salting out effect promoting the polymer aggregation, which is thermodynamically favored.[123]

An identical SLS study was carried out also for PVA. In this case, the measurements were carried out in a wider NaCl concentration range (0 ÷ 2.0 mol kg^{-1}), since we had previously observed in the preliminary study shown in chapter 3 that a higher NaCl concentration is needed in order to favor PVA aggregation. Data analysis was performed as described above for EVOH solutions. Experimental data, linear fits and fitting parameters are shown in fig. 4.3.3 and tab. 4.3.2, respectively.

We can observe that the values of M_w are very similar among the samples at different NaCl concentration: this clearly indicates that no aggregates are present at time = 0, i.e. when the aqueous polymer and salt mixtures were prepared. The dependence of A_2 on salt concentration is reported in fig. 4.3.4. Also for PVA, we can notice a decreasing trend of A_2 with NaCl concentration, as already observed for EVOH, but in this case the value of the second virial coefficient does not become negative even at the highest NaCl concentration tested. Such a trend is similar to that one found in literature for lactoferrin[124]. Thus, we can infer that PVA has a stronger affinity for the solvent than EVOH.

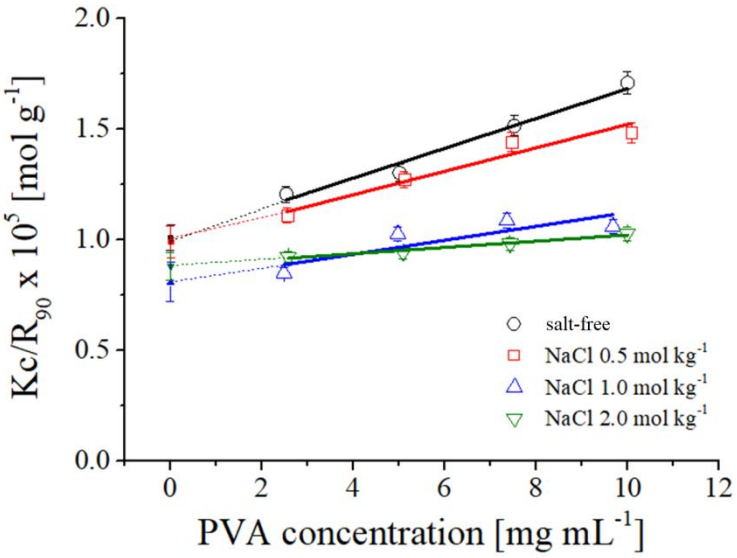

Figure 4.3.3 – Linear fits obtained from equation A.1.4 by SLS at 4 different salt concentrations. Error bars were calculated by considering the standard deviation on the average intensity value and the propagation of the relative error.

Table 4.3.2 – Molecular weight M_w and second virial coefficient A_2 obtained from the fittings shown in fig. 4.3.3.

NaCl concentration [mol kg^{-1}]	**M_w [g mol^{-1}]**	**A_2 x 10^4 [mol mL g^{-2}]**
salt-free	99000 ± 5000	3.4 ± 0.4
0.5	101000 ± 5000	2.7 ± 0.4
1.0	120000 ± 10000	1.6 ± 0.6
2.0	114000 ± 7000	0.7 ± 0.1

However, even though a NaCl concentration of 2 mol kg^{-1} is high enough to trigger PVA aggregation (as shown in the DLS study reported in chapter 3), the absence of a negative value of A_2 at any NaCl concentration does not explain the experimental evidence given by the previous DLS measurements. Therefore, we might assume that PVA aggregation is a kinetically controlled process, whose behavior cannot be easily predicted by the value of A_2. We can also hypothesize that the estimation of

the second virial coefficient for PVA in sodium chloride solutions should not be carried out on fresh polymer solutions, but after a certain time from preparation. However, we are aware that the presence of a monomodal hydrodynamic radius distribution is necessary in order to obtain reliable results from SLS analysis. Since a second aggregate population is observed after 24 hours from preparation for the sample at 2 mol kg^{-1} NaCl, we were not able to repeat this analysis at a different time.

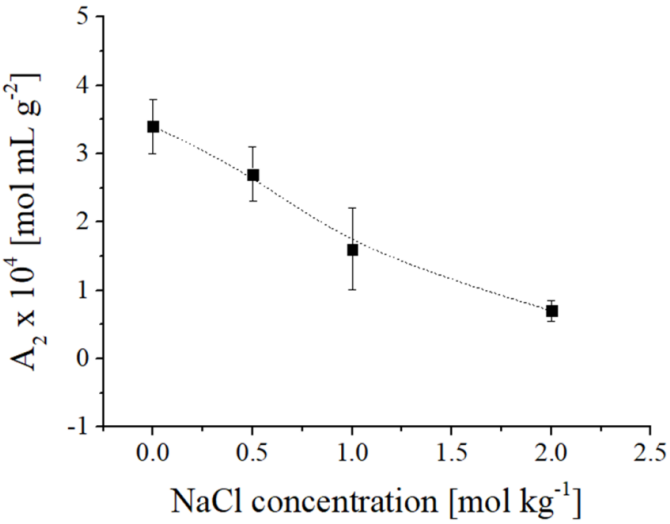

Figure 4.3.4 – Dependence of the second virial coefficient A_2 on the salt concentration. The dotted line is a guide to the eye.

4.4 – Aggregation process in the presence of sodium chloride

4.4.1 – EVOH aggregation process

SLS results clearly show that at NaCl concentrations above 0.25 mol kg^{-1} EVOH aggregation is promoted. Hence, aiming at rationalizing the aggregation process, we carried out DLS experiments by varying both salt and polymer concentration. We investigated the growth of the aggregates at NaCl concentrations corresponding to negative values of A_2, between 0.65 mol kg^{-1} and 0.85 mol kg^{-1}. We also studied

the effect of polymer concentration on the aggregation process, by varying it within the range 0.7% ÷ 1.3% w/w at constant salt concentration. Incubation of EVOH in the presence of NaCl eventually results in polymer precipitation and precipitation time depends on salt concentration. In particular it was observed at shorter times for higher salt concentrations: 15 days later at 0.65 mol kg^{-1} NaCl, 11 days later at 0.75 mol kg^{-1} NaCl and 8 days later at 0.85 mol kg^{-1} NaCl. DLS measurements were performed every day until precipitation occurred. Fig. 4.4.1.1 shows the evolution of the hydrodynamic radii over time for the samples at 1% w/w of polymer at 3 different NaCl concentrations. A similar trend was observed for other EVOH concentrations. All distribution curves indicate the presence of both a first population at about 15 nm and a second one, which appears at earlier times for higher NaCl concentrations. After a certain number of days, depending on salt content, the first population at lower R_H values disappears, indicating a complete conversion of the free chains to aggregates. This is achieved in 14 days at 0.65 mol kg^{-1} NaCl, in 10 days at 0.75 mol kg^{-1} NaCl and in 5 days at 0.85 mol kg^{-1} NaCl. Thus, at all salt and polymer concentrations aggregation is observed, at shorter times for higher NaCl concentrations, agreeing with the prediction based on the SLS results.

By plotting the evolution of hydrodynamic radii of the aggregates *vs* time it is possible to get further insights into the aggregation process of EVOH in the presence of NaCl. Fig. 4.4.1.2 reports the trend of the aggregate hydrodynamic radii over time at different polymer and salt concentrations. For all the samples we observe an increase of R_H over the days of measurements. However, the slopes of the curves reported in fig. 4.4.1.2 change when varying NaCl concentration: in particular, we can notice an increase of such slope with NaCl concentration. Therefore, it is possible to assume that aggregation is slower at 0.65 mol kg^{-1} NaCl and faster at 0.85 mol kg^{-1} NaCl.

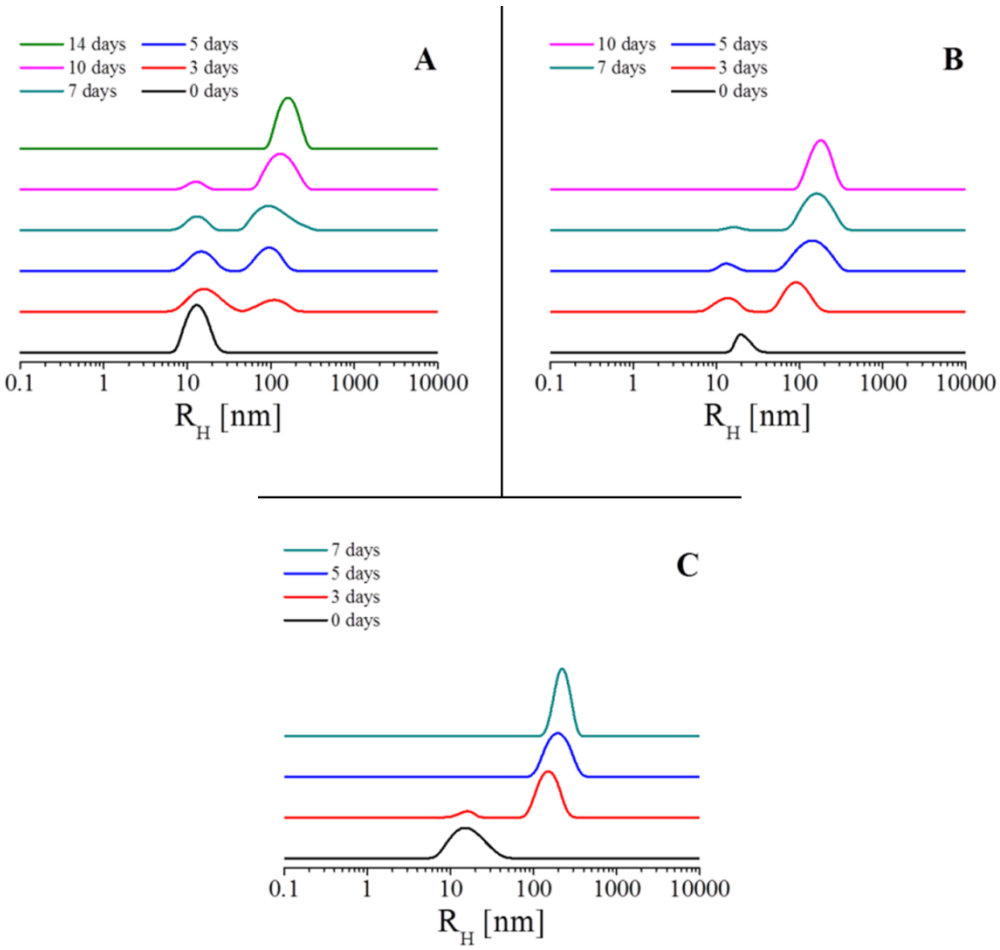

Figure 4.4.1.1 – Evolution of hydrodynamic radii distributions over time by DLS for a polymer concentration of 1% w/w and for NaCl concentrations of 0.65 mol kg^{-1} (panel A), 0.75 mol kg^{-1} (panel B) and 0.85 mol kg^{-1} (panel C).

DLS results clearly highlight that both salt concentration and polymer concentration influence the EVOH aggregation. Concerning the salt effect, from fig. 4.4.1.1 we observe that the increase of R_H is faster at higher NaCl concentrations. As regards the role of the polymer concentration (fig. 4.4.1.2), such parameter does not substantially influence the aggregation rate, since the slopes of the hydrodynamic radius curves versus time are similar at the same NaCl concentration, while it clearly affects the size of the aggregates. This effect is

particularly strong at 0.85 mol kg^{-1} NaCl, for which the hydrodynamic radius is twice bigger if we compare the datasets at the lowest and the highest polymer concentration. Therefore, NaCl concentration plays a key role in the aggregation rate, whilst mainly polymer concentration affects the aggregate size.

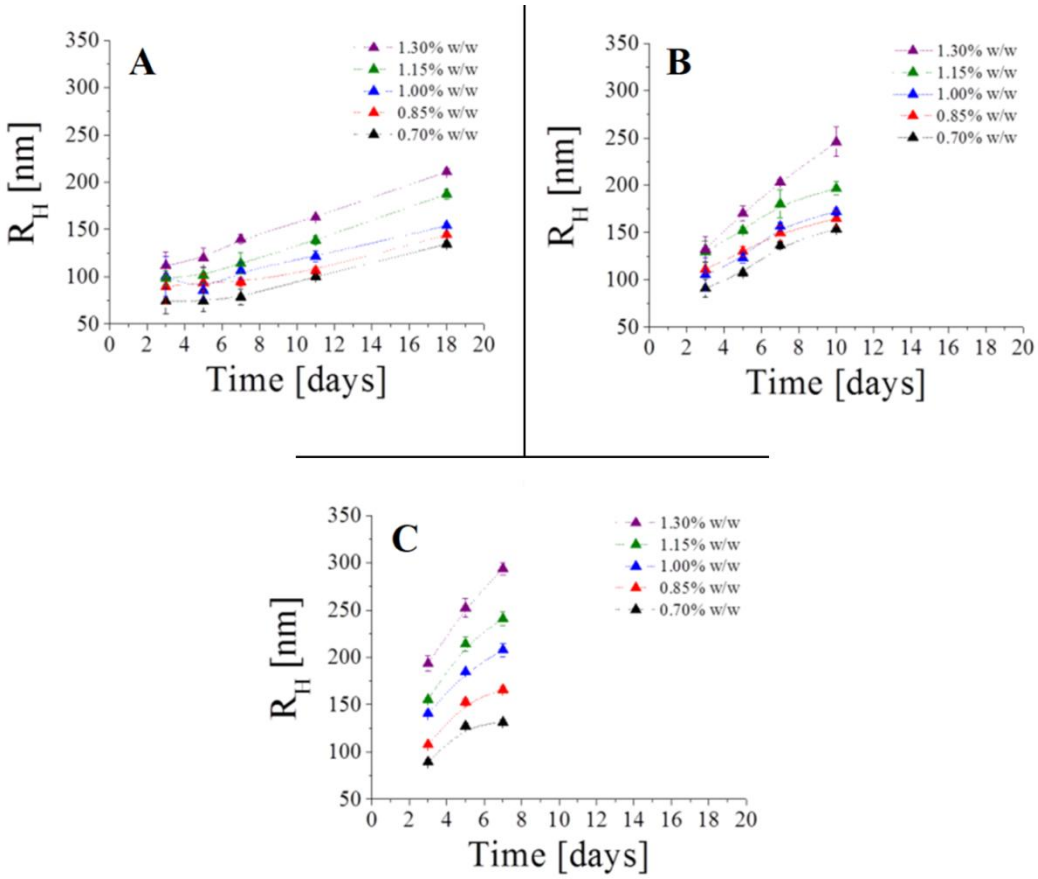

Figure 4.4.1.2 – Evolution of hydrodynamic radii of EVOH aggregates over time by DLS for 5 different polymer concentrations and 3 NaCl concentrations (0.65 mol kg^{-1}, panel A; 0.75 mol kg^{-1}, panel B; 0.85 mol kg^{-1}, panel C). Error bars were calculated by considering the standard deviation for 4 independent measurements. The dotted lines are guides to the eye.

An insight into the solute-solute interaction is given by the evaluation of the interaction parameter k_D in equation A.2.5. Diffusion coefficients as a function of polymer concentration were linearly fitted (fig. 4.4.1.3) and k_D values were calculated at different salt concentrations from DLS measurements carried out at time = 0. The interaction parameter (tab. 4.4.1.1) decreases with NaCl concentration, confirming the influence of salt concentration on the aggregation rate, earlier discussed. Furthermore, such results agree with those obtained from SLS measurements, which highlighted a progressive decrease of A_2 with salt concentration. A similar behavior was already shown elsewhere for lysozyme[105] and poly(styrene-b-sodium acrylate)[106].

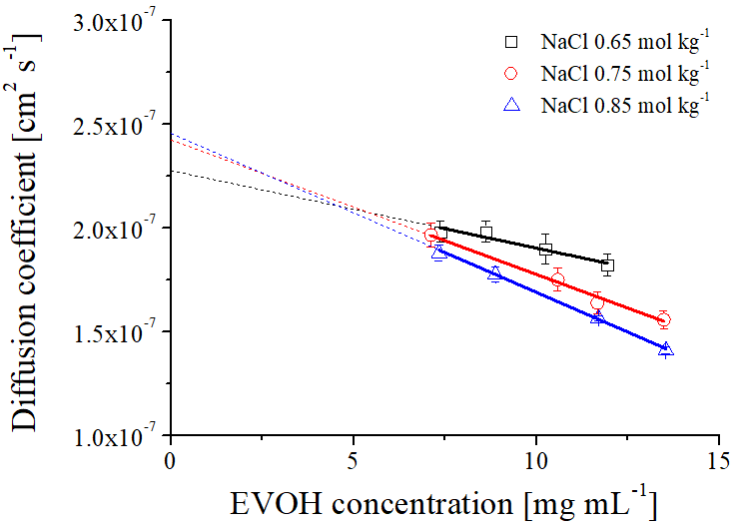

Figure 4.4.1.3 – Linear fits for free chains diffusion coefficient at 3 different NaCl concentrations from DLS measurements collected just after the preparation.

Table 4.4.1.1 – Interaction parameter k_D for free chains, calculated from equation A.2.5, at 3 different NaCl concentrations.

	NaCl 0.65 mol kg^{-1}	**NaCl 0.75 mol kg^{-1}**	**NaCl 0.85 mol kg^{-1}**
k_D	-0.19 ± 0.06	-0.31 ± 0.08	-0.44 ± 0.06

4.4.2 – PVA aggregation process

For PVA, since the effect of the polymer concentration was already studied for EVOH, we drew our attention on the effect of NaCl concentration on the aggregation process. Therefore, we investigated the growth of the aggregates at 5 different NaCl concentrations (1.500 mol kg^{-1}, 1.625 mol kg^{-1}, 1.750 mol kg^{-1}, 1.875 mol kg^{-1} and 2.000 mol kg^{-1}) and constant polymer concentration (1% w/w). Also for PVA, precipitation was observed at shorter times for higher salt concentrations: upon 46 days for 1.500 mol kg^{-1} NaCl, 26 days for 1.625 mol kg^{-1} NaCl, 15 days for 1.750 mol kg^{-1} NaCl, 9 days for 1.875 mol kg^{-1} NaCl, and 8 days for 2.000 mol kg^{-1} NaCl. Fig. 4.4.2.1 shows the evolution of the hydrodynamic radii over time for the samples at 1% w/w of polymer at 5 different NaCl concentrations. All curves indicate the presence of both a first population at about 18 nm and a second one, which appears at earlier times for higher NaCl concentrations.

The complete conversion from free chains to aggregates is achieved upon 15-16 days for 1.500 mol kg^{-1} NaCl, 7-8 days for 1.625 mol kg^{-1} NaCl, 3-4 days for 1.750 mol kg^{-1} NaCl, 3 days for 1.875 mol kg^{-1} NaCl and 2-3 days for 2.000 mol kg^{-1} NaCl. Therefore, also for PVA at all salt concentrations aggregation is observed and this process is faster at higher NaCl concentrations. Moreover, it is worth highlighting the presence of a further population that appears just before polymer precipitation, whose dimension ranges between 800 and 1200 nm. Only at NaCl 1.750 mol kg^{-1} this population is absent, but we can observe a single broad population. The presence of either this further population or a broad one is probably due to the coalescence of the aggregates, whose number becomes statistically relevant, leading to the formation of a third population of “aggregates of aggregates”. This phenomenon could explain the subsequent PVA precipitation, which is due to the increased aggregate size.

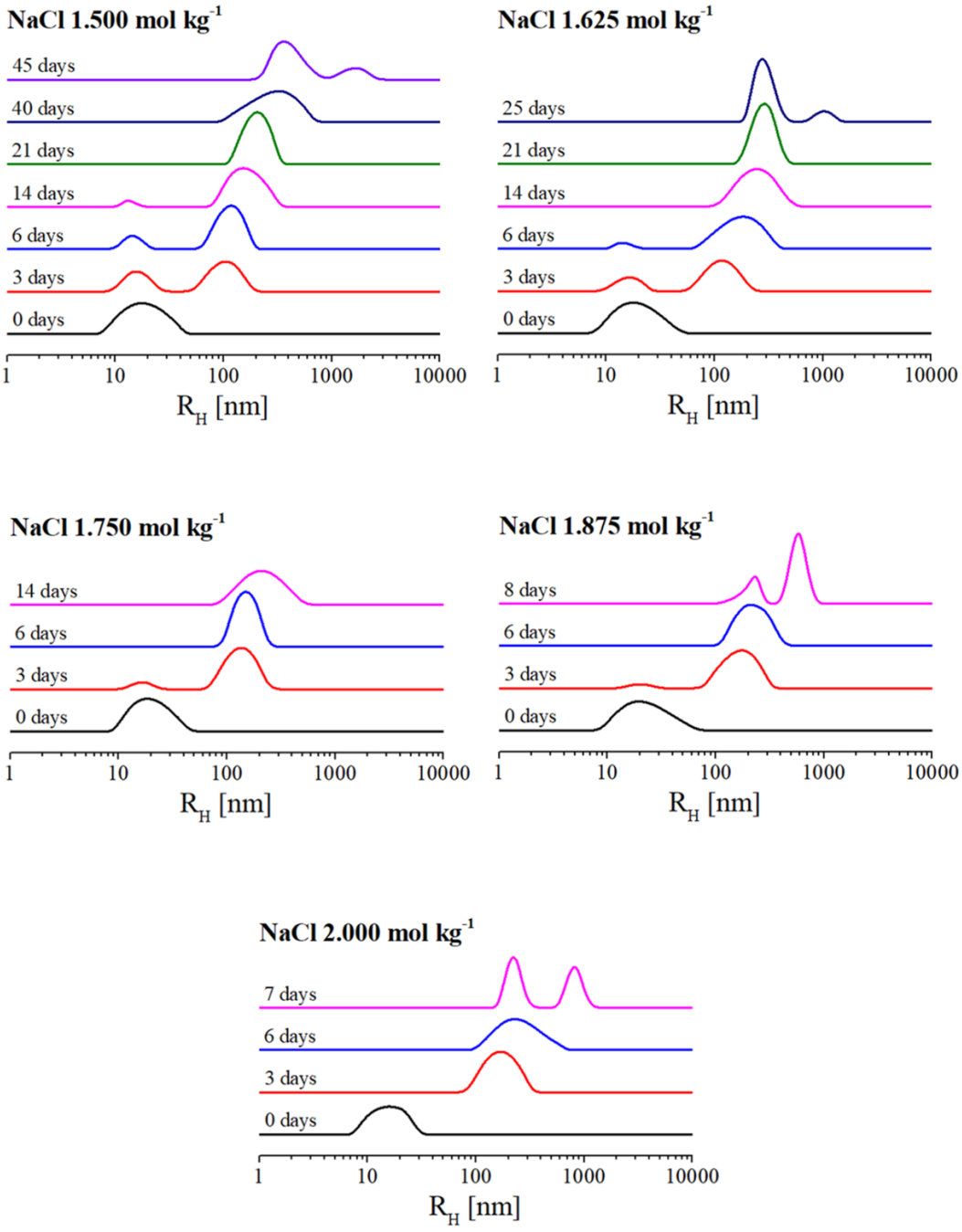

Figure 4.4.2.1 – Evolution of hydrodynamic radii distributions over time by DLS for a PVA concentration of 1% w/w and for 5 different NaCl concentrations.

4.4.3 – A picture of the aggregation process

From the previous results we can observe that both EVOH and PVA show a similar behavior in NaCl solutions. However, whereas for EVOH precipitation occurs just after the formation of a single aggregate population, for PVA this process is slower and a monomodal distribution is present for about 4 days at 2.0 mol kg^{-1} and for about 25 days at 1.5 mol kg^{-1}. As regards the conversion from free chains to aggregates, such a phenomenon seems to occur over similar times if compared the lowest and the highest NaCl concentrations tested for both polymers. For PVA particles, precipitation can be clearly explained by hypothesizing coalescence among aggregates, whereas for EVOH such process might be too fast to be monitored over time. However, due to the analogous aggregation behavior for both polymers, we can provide a general picture of the aggregation process, shown in fig. 4.4.3.1.

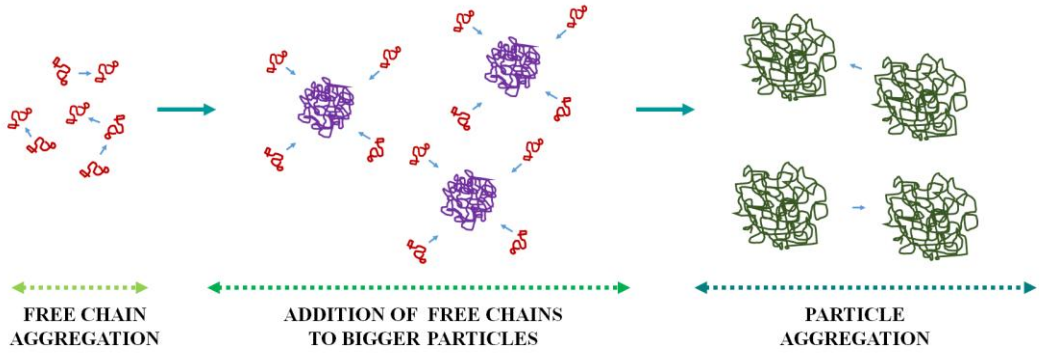

Figure 4.4.3.1 – Sketch representing a hypothetical mechanism of polymer aggregation for both EVOH and PVA: violet particles are the result from the free chain aggregation, whereas green particles come from the addition of free chains to the aggregates already formed.

In particular, free chain aggregation leads to the formation of bigger particles, whose dimensions grow over time by consecutive addition of free chains. At this step, both free chains and aggregates are present in solution and the scattering

contributions are relevant for both populations. Then, when free chains are not statistically significant, their scattering contribution is definitely lower and only the aggregate population appears from DLS data. At this stage, free chains are still present in solution and this explains, especially for PVA, why the growing process of the aggregates is still ongoing. Finally, when the aggregate number increases statistically, coalescence among bigger particles occurs, leading to polymer precipitation.

Chapter 5 – Structural characterization of polymer particles

In the previous chapter we observed that NaCl induces aggregation of both EVOH and PVA. In order to shed light on the structural properties of the aggregates obtained through salting-out, a combined microscopy and scattering study was performed. In this way, we were able to obtain a full picture of the investigated systems at different length scales.

5.1 – Determination of the aggregate structural parameters

5.1.1 – EVOH particles

In order to have structural information on EVOH aggregates, we performed Cryo-TEM measurements. Fig. 5.1.1.1 shows two Cryo-TEM images collected at 0.75 mol kg^{-1} NaCl and 1% w/w EVOH after 3 days from preparation. Such a time was chosen by taking into account the previous results from DLS, with the aim of obtaining a picture of the system during the aggregation process, when both free chains and aggregates are present in solutions. The polymer aggregates exhibit a "sponge-like" structure (fig. 5.1.1.1, panel A) where the free chains, which formed the aggregates, can be barely distinguished. Moreover, the images show the presence of particle whose radii are within the range of 70-100 nm, which is in good agreement with the DLS data. The image reported in fig. 5.1.1.1, panel B, clearly shows the presence of the primary particles (of radius ranging between 15 and 20 nm) composing the aggregate.

In order to obtain further information on the structural properties of these aggregates, we estimated their average molar weight through SLS. Such measurements were performed for 0.65 mol kg^{-1}, 0.75 mol kg^{-1} and 0.85 mol kg^{-1}

NaCl, once obtained a monomodal hydrodynamic radius distribution of polymer aggregates, as shown in fig. 4.4.1.1. Dilution of the stock 1% w/w EVOH aggregate solution, performed in order to have a set of samples at different polymer concentration, did not affect either the size or the particle radius distribution. Kc/R_θ values were plotted against $[hc + sin^2(\theta/2)]$, and each dataset was fitted at constant angle and constant concentration, as shown in equations A.1.5 and A.1.6. As an example, the Zimm plot obtained for EVOH aggregates at 0.75 mol kg^{-1} NaCl is shown in fig. 5.1.1.2. Parameters obtained from fittings are summarized in tab. 5.1.1.1. Once obtained the weight average molar weight of the particles, we also estimated the number of polymer chains N_{chains} within the aggregates, dividing the weight average molar weight of the particle by the weight average molecular weight of the free chain, previously obtained by SLS. Such results were combined with those from DLS measurements in order to estimate the chain density ρ_{chain}, expressed as number of polymer chains per unit of hydrodynamic volume. Results are shown in tab. 5.1.1.1.

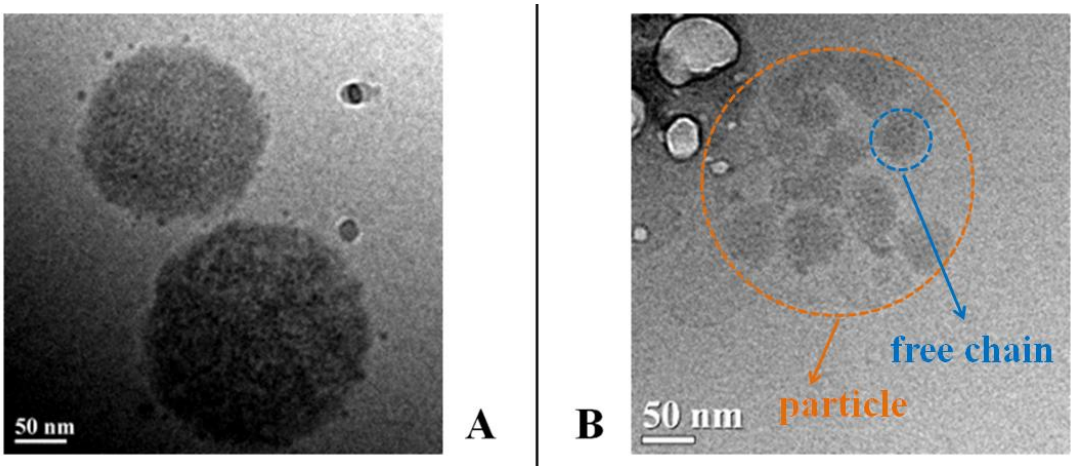

Figure 5.1.1.1 – Cryo-TEM images collected for EVOH aggregates at 0.75 mol kg^{-1}. The image in panel A well highlights the "sponge-like" structure of the polymer particle, whereas the image in panel B clearly shows the primary particles (free chains) approaching to form the aggregate.

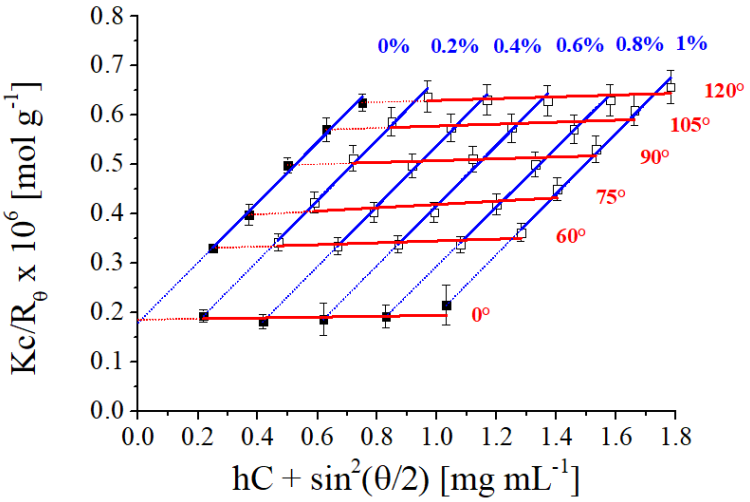

Figure 5.1.1.2 – Zimm plot for EVOH aggregates at 0.75 mol kg^{-1}. Open squares indicate experimental data, whereas straight blue lines and straight red lines represent the fitting curves at constant concentration and constant angle, respectively. Full squares indicate extrapolated points. Error bars were calculated as the standard deviation for 4 independent intensity measurements.

Table 5.1.1.1 – Aggregate structural parameters obtained by fitting data in fig. 5.1.1.2 and fig. 4.3.1 at different NaCl concentrations C_{NaCl}: weight average molar weight M_w; number of polymer chains within the aggregate N_{chains}; number of polymer chains per unit of hydrodynamic volume, i.e. chain density ρ_{chain}.

C_{NaCl} [mol kg^{-1}]	M_w [kg mol^{-1}]	N_{chains} [-]	ρ_{chain} x 10^5 [chains nm^{-3}]
0.65	1590 ± 20	48 ± 1	0.39 ± 0.01
0.75	5600 ± 300	170 ± 8	1.07 ± 0.07
0.85	19000 ± 400	580 ± 120	1.5 ± 0.3

By comparing the values of M_w, we can observe a progressive increase of molar weight of the aggregates with NaCl concentration. NaCl concentration directly affects the polymer density within the aggregate, since the value of ρ_{chain} increases

with salt concentration. Therefore, at higher NaCl concentrations the aggregate structure is more compact.

From DLS results, previously shown, we could observe an increasing tendency to the aggregation and a faster precipitation at higher salt concentrations. The knowledge of the aggregate molar weight allows the DLS measurements to be re-analyzed to estimate the value of the interaction parameter also for the aggregates. Indeed, the same procedure already shown for the free chains was repeated by taking into account the values of diffusion coefficients collected at a scattering angle of 90° on the same day of SLS measurements, once we observed the complete conversion of the free chains to aggregates. Linear fits and k_D values are shown in fig. 5.1.1.3 and tab. 5.1.1.2, respectively. The interaction parameter decreases with NaCl concentration, indicating a stronger tendency to the aggregation at higher salt concentrations. Differently from the data shown in fig. 4.4.1.3, related to the aggregation tendency for the free chains, in this case k_D reflects the aggregation tendency for the aggregates that leads to massive precipitation after a number of days that depends on salt concentration.

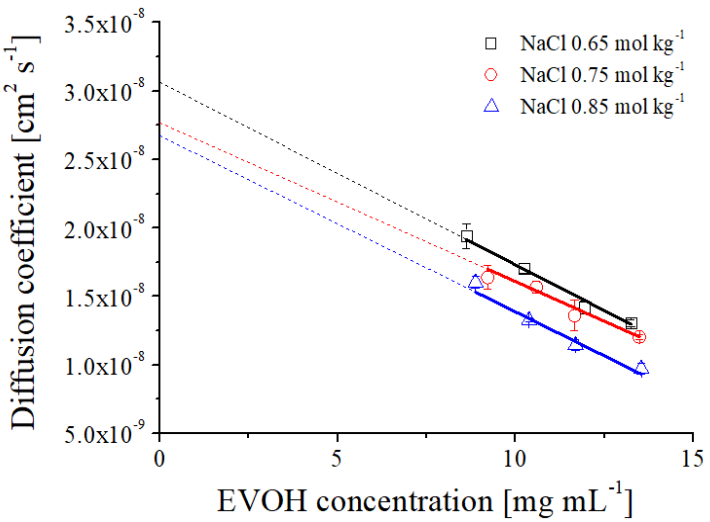

Figure 5.1.1.3 – Linear fits for polymer aggregates at 3 different NaCl concentrations from DLS measurements collected on the same day of SLS measurements.

Table 5.1.1.2 – Interaction parameter k_D for polymer aggregates, calculated from equation A.2.5, at 3 different NaCl concentrations.

	NaCl 0.65 mol kg^{-1}	**NaCl 0.75 mol kg^{-1}**	**NaCl 0.85 mol kg^{-1}**
k_D	-0.05 ± 0.01	-0.14 ± 0.03	-0.49 ± 0.07

5.1.2 – PVA particles

Also the structure of PVA aggregates was investigated through microscopy. However, differently from EVOH particle solutions, we were not able to use Cryo-TEM, due to the high concentration of NaCl in the investigated samples, that led to crystallization of NaCl during the freezing step. As a consequence, PVA particle structure was analyzed by means of TEM. Fig. 5.1.2.1 shows a TEM image collected at 1.75 mol kg^{-1} NaCl and 1% w/w PVA after 3 days from preparation.

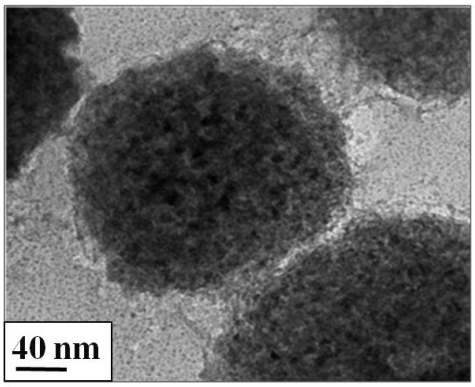

Figure 5.1.2.1 – TEM image collected for PVA particles at 1.75 mol kg^{-1}. The image well highlights the "sponge-like" structure of the aggregates.

The polymer aggregates exhibit a "sponge-like" structure, which looks very similar to that one already shown for EVOH particles. Therefore, irrespectively of the nature of the polymer, the aggregate structure is the same. Moreover, the image shows the presence of a spherical particle whose radius is about 90 nm, which is in good agreement with the DLS data.

In order to obtain further information on the structural properties of these aggregates, we estimated their average molar weight through SLS. Such measurements were performed for 1.500 mol kg^{-1}, 1.625 mol kg^{-1}, 1.750 mol kg^{-1} 1.875 mol kg^{-1} and 2.000 mol kg^{-1} NaCl, once obtained a monomodal hydrodynamic radius distribution of polymer aggregates, as shown in fig. 4.4.2.1. Also in this case, dilution of the stock 1% w/w PVA aggregate solution, performed in order to have a set of samples at different polymer concentration, did not affect either the size or the particle radius distribution. Since PVA aggregation occurs over a wider time scale, we were able to study the evolution of both the particle molar masses and structural parameters over time, by repeating the SLS measurements every day until polymer precipitation. Kc/R_θ values were plotted against $[hc + sin^2(\theta/2)]$, and each dataset was fitted at constant angle and constant concentration, as shown in equations A.1.5 and A.1.6. As an example, the Zimm plots obtained for PVA particles at 5 different NaCl concentrations at a specific time from the preparation (27 days, 19 days, 12 days, 6 days and 4 days for 1.500 mol kg^{-1}, 1.625 mol kg^{-1}, 1.750 mol kg^{-1} 1.875 mol kg^{-1} and 2.000 mol kg^{-1} NaCl, respectively) are shown in fig. 5.1.2.2. The evolutions of the aggregates molar weights and the hydrodynamic radii (from DLS measurements carried out on the same day of SLS measurements) over time are reported in fig. 5.1.2.3 and fig. 5.1.2.4, respectively. Moreover, from the values of R_H we estimated the evolution of the chain density over time, expressed as number of polymer chains per unit of hydrodynamic volume. Results are shown in fig. 5.1.2.5.

As regards the data reported in fig. 5.1.2.3, it is clear that at every NaCl concentration the aggregate molar weight shows an exponential dependence on the aggregation time. In particular, the growth is faster at higher NaCl concentrations, as already confirmed by DLS data, for which we can observe a linear dependence of R_H on time.

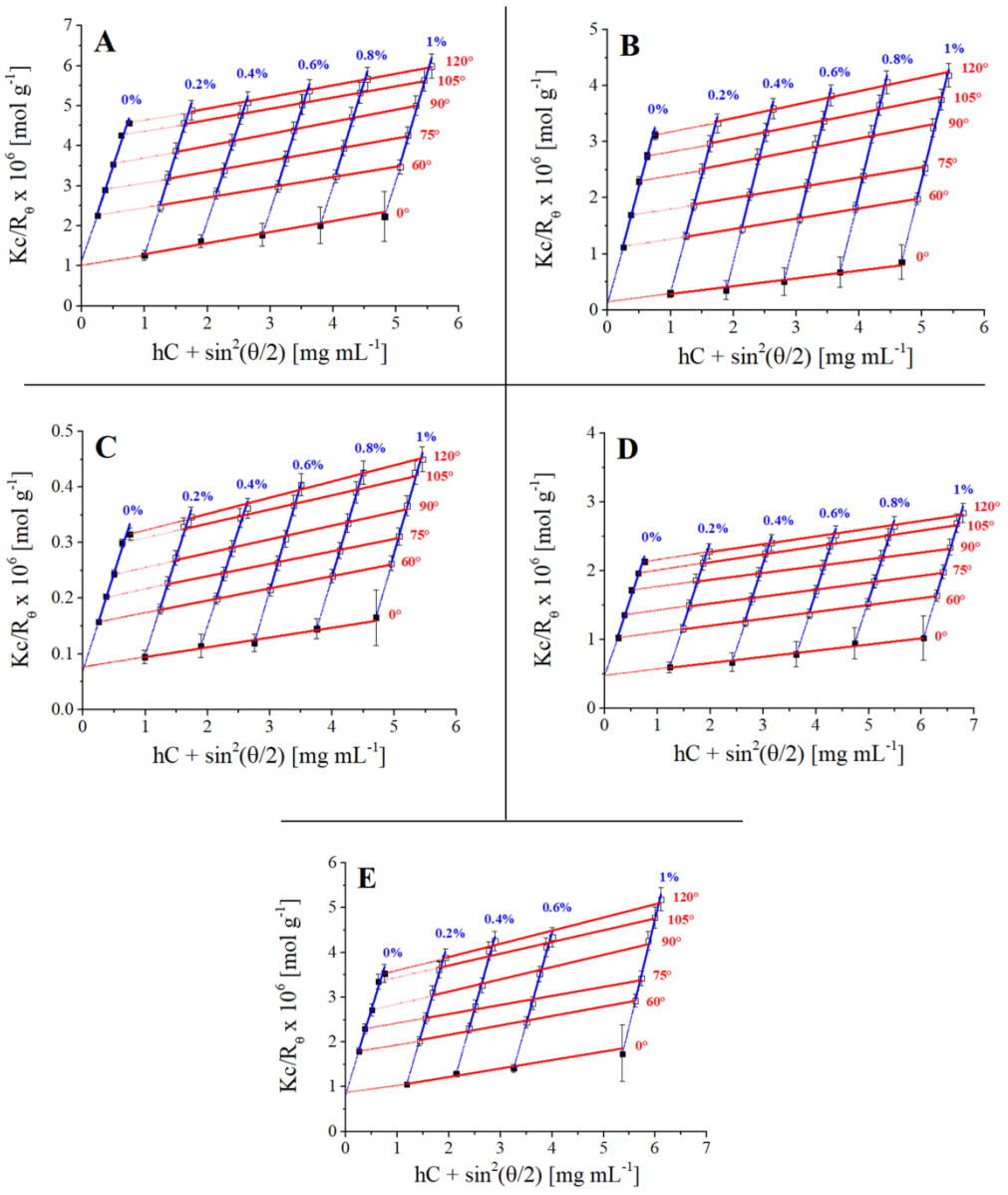

Figure 5.1.2.2 – Zimm plots for PVA aggregates at 1.500 mol kg^{-1}, 1.625 mol kg^{-1}, 1.750 mol kg^{-1} 1.875 mol kg^{-1} and 2.000 mol kg^{-1} NaCl (panel A, B, C, D and E, respectively). Open squares indicate experimental data, whereas straight blue lines and straight red lines represent the fitting curves at constant concentration and constant angle, respectively. Full squares indicate extrapolated points. Error bars were calculated as the standard deviation for 4 independent intensity measurements.

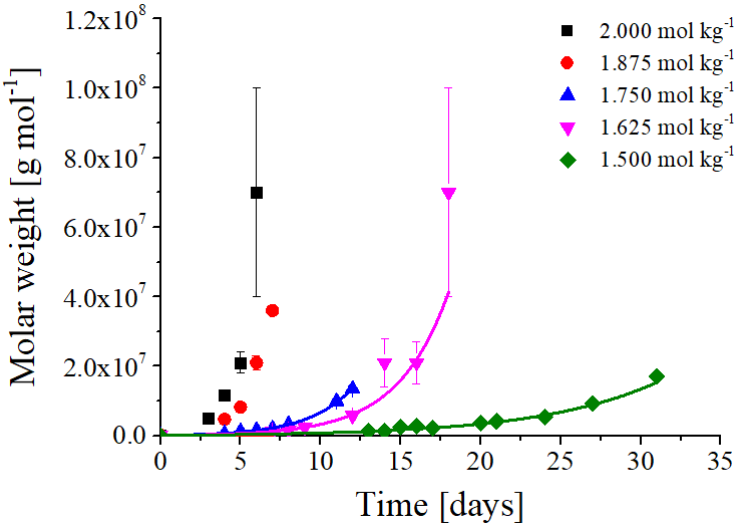

Figure 5.1.2.3 – Evolution of aggregate molar weights (obtained from SLS measurements) over time at 5 different NaCl concentrations. For 1.500 mol kg^{-1}, 1.625 mol kg^{-1} and 1.750 mol kg^{-1} NaCl fittings are also reported.

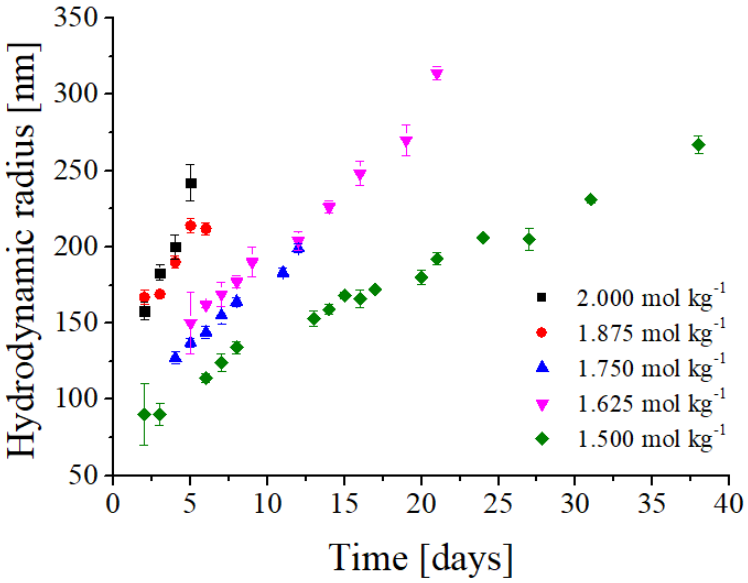

Figure 5.1.2.4 – Evolution of aggregate R_H (obtained from DLS measurements) over time at 5 different NaCl concentrations.

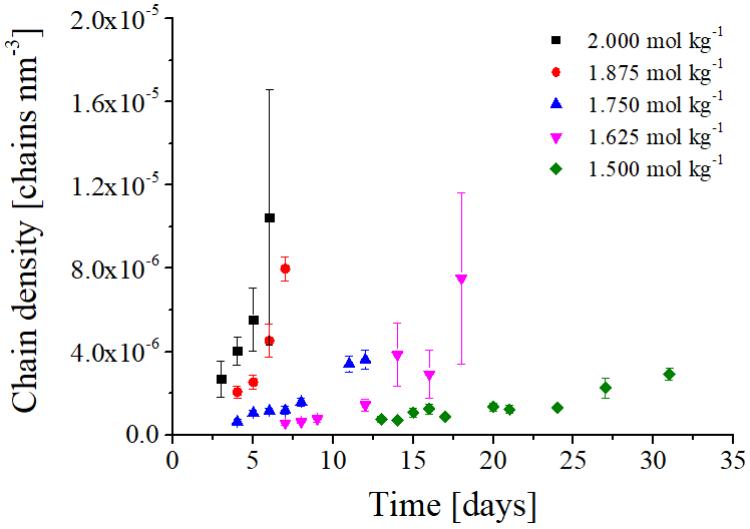

Figure 5.1.2.5 – Evolution of aggregate chain density over time at 5 different NaCl concentrations. These results were obtained by combining SLS and DLS data.

From the exponential dependence of M_w over time we can infer that the PVA aggregation occurs under a RLA (Reaction Limited Aggregation) mechanism[125]. In particular, the aggregation rate is given by the following expression:

$$k \gg n\exp(V_b / k_B T) \qquad \text{equation 5.1.2.1}$$

where V_b is the repulsive barrier between two approaching particles and v is the attempt frequency, that depends on the diffusive motion of the particles, as well as on their radius and concentration. When two particles approach each other closely on Brownian trajectories, the probability P of sticking increases with the aggregate mass. RLA typically occurs when $V_b \geq k_B T$, making k sufficiently small that there is a significant range of cluster size with $P << 1$, even though the attempt frequency, that depends on diffusion, remains high.[125] Once observed an exponential dependence of M_w on the aggregation time, experimental data reported in fig. 5.1.2.3 were fitted by using a modified version of an equation already reported in literature[125]:

$$M_w = A_0 + A\exp(t / t_m) \qquad \text{equation 5.1.2.2}$$

where A_0 is the intercept at time = 0, A is the pre-exponential factor and t_m is a sample-dependent constant which is related to the aggregation rate. Interpolation of the experimental data was possible only for the datasets at 1.500 mol kg^{-1}, 1.625 mol kg^{-1} and 1.750 mol kg^{-1} NaCl, since a minimum number of experimental points was required for the fitting. The obtained values of t_m are reported in tab. 5.1.2.1. We can observe a progressive decrease of this parameter with NaCl concentration, which indicates that the aggregation process is faster at higher NaCl concentrations.

Table 5.1.2.1 – Values of t_m obtained from fittings of the data reported in fig. 5.1.2.3.

	NaCl 1.500 mol kg^{-1}	**NaCl 1.625 mol kg^{-1}**	**NaCl 1.750 mol kg^{-1}**
t_m [days]	7.4 ± 0.5	3.2 ± 0.2	2.8 ± 0.2

As regards the evolution of the chain density (or packing degree) over time, it is possible to observe a general increase of this parameter with aggregation time for all NaCl concentrations. Moreover, at higher NaCl concentrations, the chain density increases faster. At the same time, if we compare the values of packing degree at different NaCl concentrations but at the same aggregation time (i.e. 5 days for 1.750 mol kg^{-1}, 1.875 mol kg^{-1} and 2.000 mol kg^{-1} NaCl) we can notice that this parameter is higher when salt concentration increases. This means that a higher salt concentrations leads to a more compact aggregate, as already observed for EVOH particles. Similar comparisons can be made for different datasets at distinct aggregation times.

The knowledge of the parameters derived from SLS measurements on PVA particle solutions allowed us to obtain further insights into the particle structure. In particular, the values of aggregate molar weight and gyration radius obtained from the Zimm plot analysis (whose examples are shown in fig. 5.1.2.2) at the same aggregation time were fitted for 3 different datasets (1.500 mol kg^{-1}, 1.625 mol kg^{-1}

and 1.750 mol kg^{-1} NaCl) by applying the following equation, that allows obtaining the value of the shape parameter α[126]:

$$R_g = BM_w^{\alpha} \qquad \text{equation 5.1.2.3}$$

where B is a pre-exponential factor.

This analysis was not carried out for 1.875 mol kg^{-1} and 2.000 mol kg^{-1} NaCl, due to the limited amount of available experimental points, that did not allow obtaining a reliable fitting. The couples (M_w, R_g) derived from Zimm plot analysis at specific aggregation times are reported in fig. 5.1.2.6, where also interpolations are shown. The values of α from the fittings are presented in tab. 5.1.2.2.

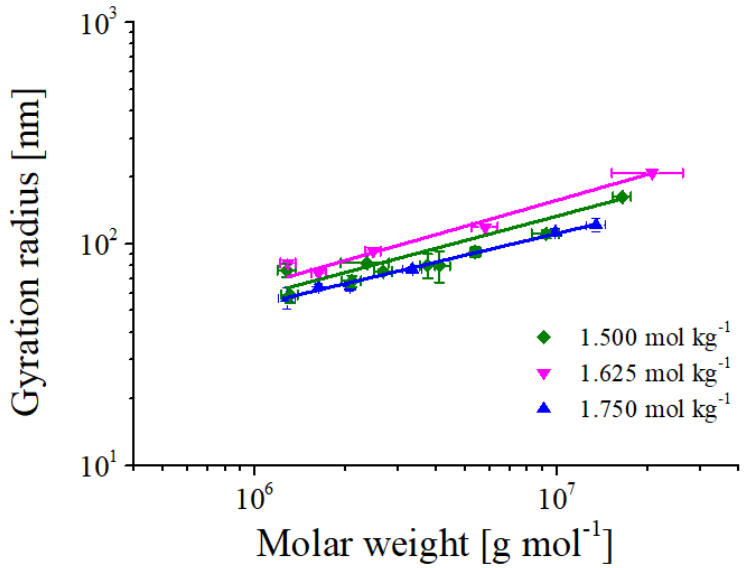

Figure 5.1.2.6 – Dependence of gyration radius on aggregate molar weight at 3 different NaCl concentrations. The couples (M_w, R_g) derived from Zimm plot analysis at specific aggregation times were considered.

Table 5.1.2.2 – Values of α obtained from fittings of the data reported in fig. 5.1.2.6.

	NaCl 1.500 mol kg^{-1}	**NaCl 1.625 mol kg^{-1}**	**NaCl 1.750 mol kg^{-1}**
α	0.36 ± 0.02	0.39 ± 0.02	0.32 ± 0.02

The parameter α gives information about the shape of the particle. The theoretical value for a spherical homogeneous particle is 0.33[127], thus we can infer that PVA aggregates show a shape similar to a sphere characterized by a homogeneous density. This finding is coherent with the TEM image previously shown. Moreover, since α does not substantially change with NaCl concentration, we can observe that salt concentration does not affect the shape of the particle.

5.2 – Investigation on mesoscopic length scales

5.2.1 – EVOH particles

EVOH samples in NaCl solutions were also analyzed by SANS, in order to obtain more detailed structural information. SANS measurements were performed in a mixed solvent, containing a D_2O/H_2O weight ratio of 80/20, which gave a good contrast between the polymer and the solvent. However, we are aware, from previous studies reported in literature[128,129], that the presence of D_2O influences the aggregation rate, since D_2O is a worse solvent than H_2O due to the isotopic effect of deuterium.

As an example, fig. 5.2.1.1 shows the comparison between the hydrodynamic radii distributions obtained after 3 days for an EVOH sample at 1% w/w at 0.65 mol kg^{-1} NaCl in the presence of pure H_2O and in the mixed solvent (D_2O/H_2O, 80/20). We can observe the presence of two main populations (free chains and aggregates) for the sample in pure H_2O and one main population of aggregates for the sample in the presence of D_2O. Therefore, it can be assumed that heavy water influences both the aggregation rate and the aggregate size. In particular, in the presence of D_2O, the conversion from free chains to aggregates is faster and the aggregate size is bigger if compared to the sample in pure H_2O.

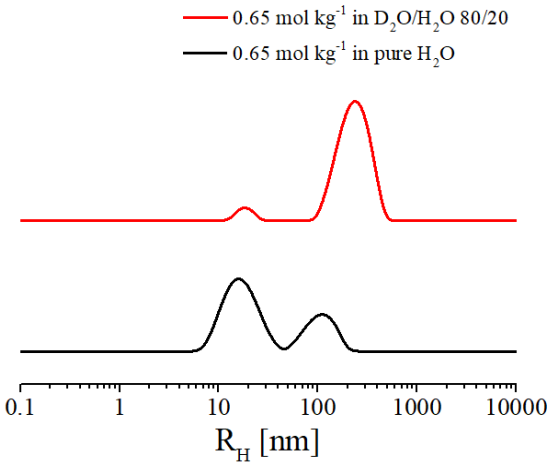

Figure 5.2.1.1 – Hydrodynamic radii distributions after 3 days from preparation for an EVOH 1% w/w sample in 0.65 mol kg^{-1} NaCl in water and at a weight D_2O/H_2O ratio of 80/20.

Nevertheless, since we were interested in a trend of the structural parameters at different NaCl concentrations, for SANS measurements we chose salt concentrations lower with respect to those used for SLS and DLS, in order to avoid a too fast aggregation process. In this way, we could obtain aggregation rates very similar to those ones obtained for the samples measured by SLS and DLS.

SANS experimental profiles were collected after 6 days from the preparation, in order to shed light on possible morphological changes at different NaCl concentrations, as already observed from SLS and DLS measurements. Data were analyzed through a double approach, by separating the scattering data at low *q*-values and at intermediate and high *q*-values, respectively. The information obtained from the low *q*-region is related to wider length scales, whereas the data at intermediate and high *q*-values give information at lower length scales, i.e. the microstructural properties. In particular, the intermediate and high *q*-region was analyzed by using a form factor, whereas the low *q*-region was analyzed through the Kratky plot. Fig. 5.2.1.2 shows the experimental profiles at intermediate and high *q*-values and the related fittings.

As regards the choice of the proper form factor, in all curves we could generally observe the presence of a slope value close to -2 at intermediate *q*-values and its slight increase with NaCl concentration: this indicates an increasing fractal dimension of the aggregates, i.e. a progressive growth of the degree of compactness of the polymer chains, as already shown from SLS measurements.

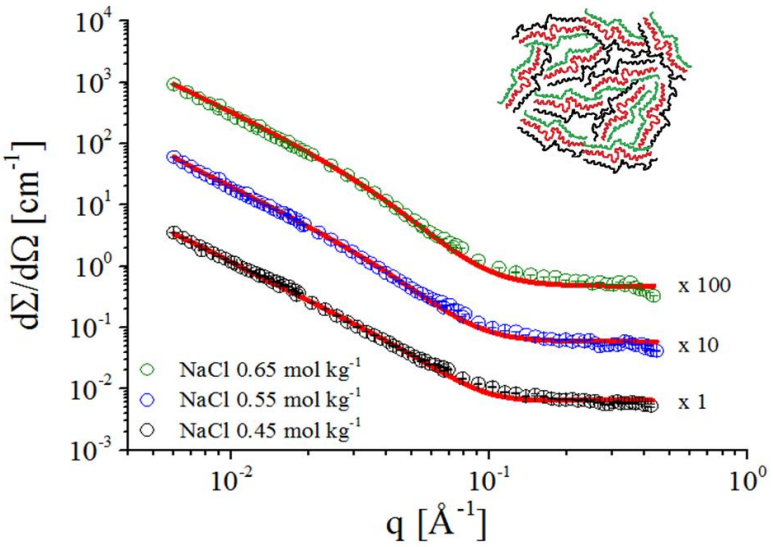

Figure 5.2.1.2 – SANS experimental profiles and related fittings at 1% w/w EVOH and 3 different NaCl concentrations. Curves were scaled for a better comparison as indicated in the graph. Inset: Sketch representing the hypothetical structure of the aggregates, formed by randomly oriented lamellae.

By considering the results from DLS measurements, it can be assumed that the aggregation process mainly involves free chains that form bigger particles. At the same time, from Cryo-TEM images we could observe the presence of primary particles of sizes ranging from 15 nm to 20 nm, compatible with the values of R_H measured by DLS. As a consequence, it was possible to consider that EVOH particles were formed by free chains as primary particles. Therefore, we tried to fit the experimental profile by using different shape-independent form factors like the mass fractal model[130], the surface fractal model[130] and their combination[131].

However, the first and the second model were not able to fit the experimental profiles, whereas the third model gave a value of surface fractal dimension[130] (about 3.5) which was not physically acceptable. Hence, we needed to explore different compatible models. A diagnostic feature of the scattering profile is the slope at intermediate *q*-values. In particular, a value of the slope close to -2 at can be related to the presence of bidimensional scattering objects. In our case, from Cryo-TEM measurements we know that polymer aggregates are present as spheres, so that both a vesicle model[132] and a spherical core shell form factor[132] were chosen. Also in this case both models were not appropriate to fit the experimental profiles. Finally, we tried to use a very simple and general model for bidimensional scattering objects, i.e. the lamellar form factor, which gave the best results from the fittings. Its equation is reported below:

$$P(q) = \frac{2\Delta\rho^2}{q^2}\left[1 - \cos(q\delta)\right] \qquad \text{equation 5.2.1.1}$$

where $\Delta\rho$ is the neutron contrast and δ is the lamellar thickness.

This model relates to the scattering intensity for a lyotropic lamellar phase where a uniform scattering length density and random distribution in solution are assumed[133,134]. Thickness polydispersity was also considered in the fitting by assuming a Schulz distribution.

By applying the lamellar form factor, we assumed that the aggregate is a spherical particle composed by small randomly oriented lamellae formed during the aggregation process. In particular, we could infer that the free chains in the presence of NaCl go through a conformational change from random coils to open linear chains. This is due to the aggregation process that favors the formation of hydrogen bonds among different polymer chains that assume a more locally ordered phase. At the same time, the addition of free chains to the aggregates is a process that can happen along any orientation, thus the lamellae are randomly oriented in the space and form a spherical aggregate (see inset/sketch in fig.

5.2.1.2). We focused on the evolution of the lamellar thickness at 3 different NaCl concentrations. The results obtained from the fittings are reported in tab. 5.2.1.1 and show that the thickness increases with salt concentration.

The region of the scattering profiles at low *q*-values was analyzed through the Kratky plot, in which $I(q)q^2$ is reported as a function of q.[135] In this type of plot, the *q*-value related to the maximum can be used to estimate the radius of gyration of the particles by applying the following equation:

$$R_g = \frac{2\pi}{q} \qquad \text{equation 5.2.1.2}$$

Kratky plots are shown in fig. 5.2.1.3 and the obtained values of R_g are reported in tab. 5.2.1.1. We could observe a progressive increase of the radii of gyration with NaCl concentration, matching with the results found by DLS. Even though the investigated concentrations are not the same, we could observe the same trend, indicating a good agreement among the results obtained from light and neutron scattering techniques.

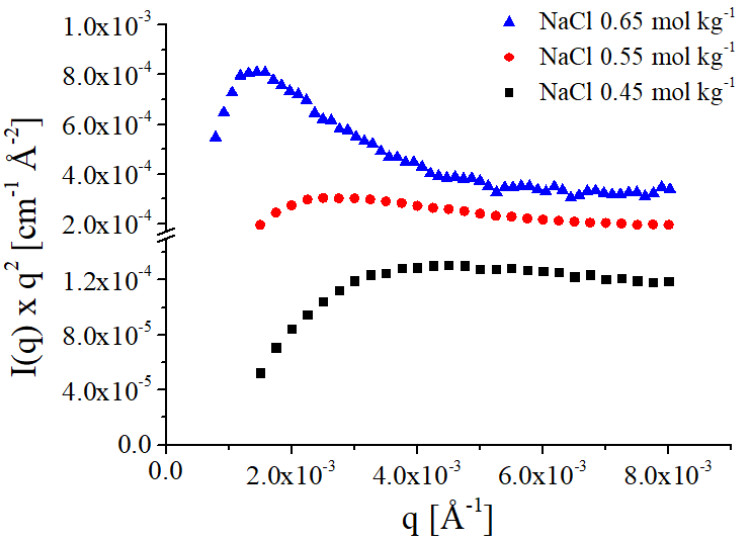

Figure 5.2.1.3 – Kratky plots at 3 different NaCl concentrations.

Table 5.2.1.1 – Comparison of the structural parameters (lamellar thickness and radius of gyration) obtained from SANS fittings and Kratky plot analysis. Errors on lamella thickness and related polydispersity are derived from the fitting, whereas the error on R_g was estimated by considering the standard deviation on this parameter calculated by considering a point adjacent to the maxima of the curves shown in fig. 5.2.1.3.

NaCl concentration [mol kg^{-1}]	**0.45**	**0.55**	**0.65**
Thickness [Å]	42.4 ± 0.1	48.3 ± 0.3	55.2 ± 0.1
polydispersity	0.24 ± 0.01	0.53 ± 0.01	0.54 ± 0.01
R_g [nm]	136 ± 5	240 ± 16	415 ± 25

5.2.2 – PVA particles

Also PVA samples in NaCl solutions were analyzed by SANS. In this case, the measurements were performed in D_2O, since such a solvent does not strongly affect PVA solubility. For all samples, we chose a lower PVA concentration (0.85% w/w) with respect to that one used for DLS measurements, in order to have comparable aggregation times. Moreover, the use of D_2O as a solvent allowed obtaining a sufficiently high contrast even though polymer concentration was lower. SANS measurements were repeated at 3 different times from preparation, in order to shed light on possible morphological changes. At the same time, we were able to compare the evolution of the structural parameters with NaCl concentration, by choosing identical times from preparation for the samples at 1.50 mol kg^{-1} and 1.75 mol kg^{-1} NaCl (8 days) and for those ones at 1.75 mol kg^{-1} and 2.00 mol kg^{-1} NaCl (4 and 6 days).

Fig. 5.2.2.1 shows the data and the related fittings. As already performed for EVOH samples, the intermediate and high *q*-region was analyzed by using a form factor, whereas the low *q*-region was analyzed through the Kratky plot.

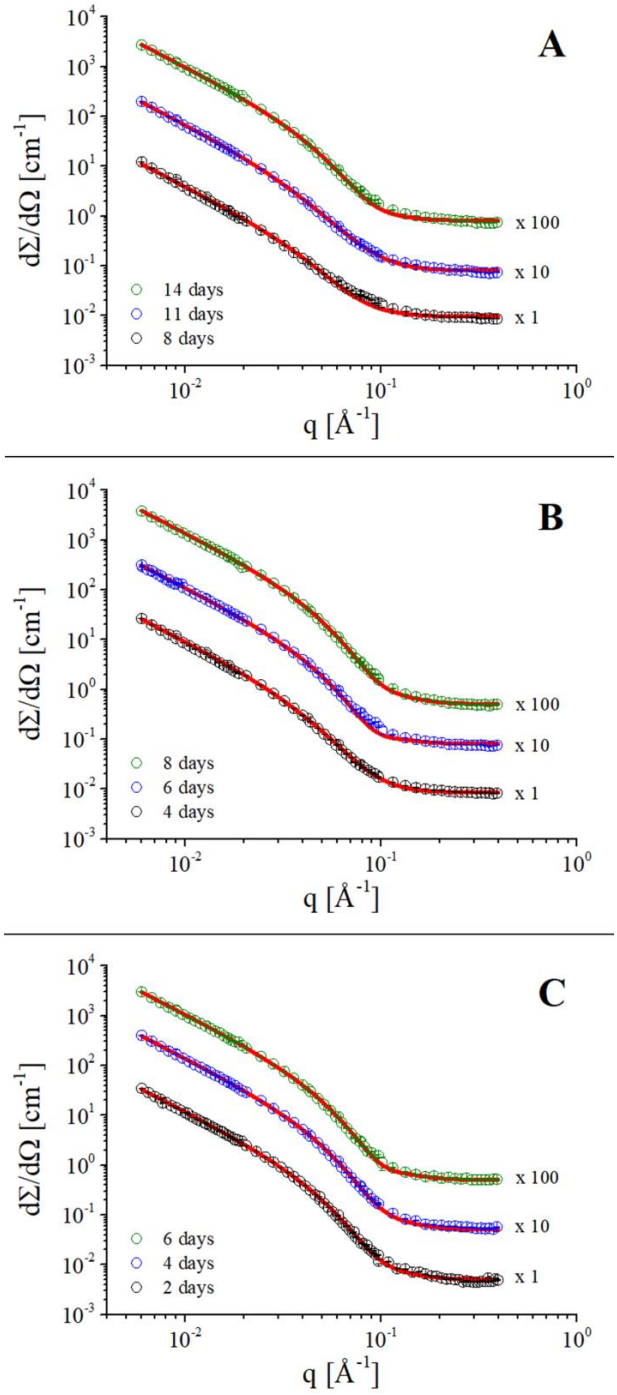

Figure 5.2.2.1 – SANS data and fittings at 0.85% w/w PVA and 1.50 mol kg^{-1}, 1.75 mol kg^{-1} and 2.00 mol kg^{-1} NaCl (panels A, B and C, respectively) and 3 different times from preparation. Curves were scaled for a better comparison.

Also in this case, the lamellar form factor, reported in equation 5.2.1.1, gave the best results from the fittings. By applying this model, we assumed that the PVA particles are formed according to the same mechanism described for EVOH. Since PVA aggregation occurs over a wider time scale, we were able to study the effect of both time from preparation and salt concentration on the lamellar thickness obtained from the fittings. The results are reported in tab. 5.2.2.1 and show that the thickness increases with time for the samples at 1.50 mol kg^{-1} NaCl, whereas for the samples at higher concentration such a trend is not observed. Thus, we could infer that for 1.75 mol kg^{-1} and 2.00 mol kg^{-1} NaCl, the maximum values of thickness are reached after 4 days and 2 days from preparation, respectively. As regards the effect of NaCl concentration at the same time from preparation, we could observe an increase of the thickness by comparing the samples at 1.50 mol kg^{-1} and at 1.75 mol kg^{-1} NaCl.

Table 5.2.2.1 – Structural parameters obtained from SANS fittings and Kratky plot analysis. Errors on lamella thickness and related polydispersity are derived from the fitting, whereas the error on R_g was estimated by considering the standard deviation on this parameter calculated by considering a point adjacent to the maxima of the curves whose examples are shown in fig. 5.2.2.2.

1.50 mol kg^{-1} NaCl	**8 days**	**11 days**	**14 days**
Thickness [Å]	49.4 ± 0.2	57.5 ± 0.3	61.4 ± 0.1
polydispersity	0.61 ± 0.03	0.57 ± 0.03	0.32 ± 0.02
R_g [nm]	228 ± 18	280 ± 27	314 ± 32
1.75 mol kg^{-1} NaCl	**4 days**	**6 days**	**8 days**
Thickness [Å]	59.9 ± 0.1	60.1 ± 0.2	61.6 ± 0.2
polydispersity	0.28 ± 0.02	0.44 ± 0.01	0.24 ± 0.03
R_g [nm]	278 ± 41	472 ± 39	-
2.00 mol kg^{-1} NaCl	**2 days**	**4 days**	**6 days**
Thickness [Å]	59.7 ± 0.3	58.7 ± 0.2	58.4 ± 0.3
polydispersity	0.31 ± 0.01	0.29 ± 0.02	0.25 ± 0.03

An example of the Kratky plot analysis for the dataset at 1.50 mol kg^{-1} NaCl is reported in fig. 5.2.1.2, and the results are shown in tab. 5.2.2.1. For some samples this analysis was not possible because the maxima of the curves were out of the investigated *q*-range. In general, we can observe a progressive increase of the radii of gyration with NaCl concentration and time.

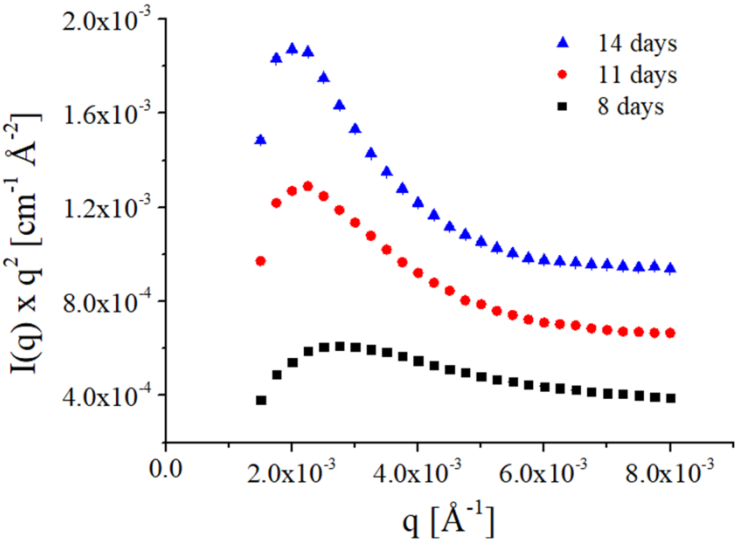

Figure 5.2.1.3 – Kratky plots at 1.50 mol kg^{-1} NaCl and 3 different times from preparation.

Chapter 6 – The effect of surfactants on polymer aggregation and structural properties: a model study

After studying the polymer aggregation process and the particle structural properties, we carried out a model study by using two mixtures of surfactants that are commonly used in liquid detergent formulations and that are present as main components in the laundry product used for the washing tests performed in this work: a mixture of non-ionic ethoxylated surfactants and sodium laureth sulfate. In particular, in this chapter we show the results regarding the effect of both surfactant mixtures on polymer aggregation and structural properties.

6.1 – Surfactant characterization in aqueous solutions

The structures of the investigated species are reported in fig. 6.1.1. Both surfactants are complex mixtures of different components, due to the polydispersity of the alkyl chains and the ethoxylated units.

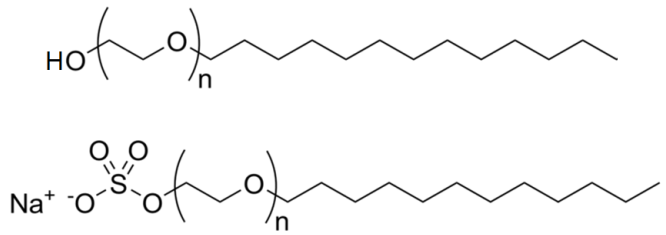

Figure 6.1.1 – Structures of the surfactants used in the present study. Top: C13 ethoxylated alcohol; bottom: SLES. For the non-ionic surfactant mixture, *n* (i.e. the number of the ethoxylated units) may change between 4 and 10, whereas for SLES *n* ranges between 2 and 3.

As a first step, we performed surface tension measurements at 25 °C in order to estimate the critical micellization concentration (cmc) of both mixtures of

surfactants. Such measurements were carried out on aqueous solutions of the single mixtures by increasing the surfactant concentration gradually through small additions of a stock surfactant solution. The values of surface tension were measured 3 times after each addition and the average values at each surfactant concentration were considered. As an example, fig. 6.1.2 reports the surface tension as a function of surfactant concentration for both mixtures of surfactants in water and the graphical method used for the determination of the cmc. In both curves, we could observe a dramatic change of the slope, which is related to the concentration value corresponding to the formation of surfactant micelles. In particular, the cmc was estimated by fitting the experimental data before and after the slope change and determining the graphical intersection of both linear fits.

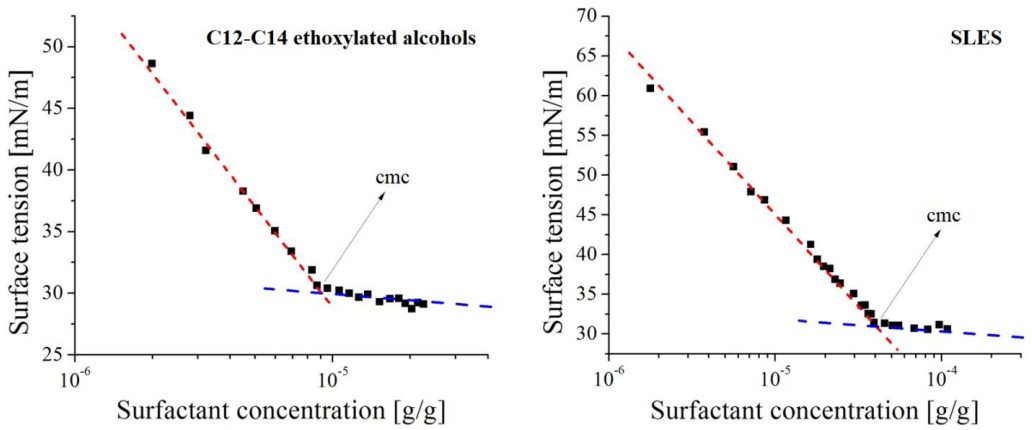

Figure 6.1.2 – Variation of the surface tension as a function of surfactant concentration for the mixture of ethoxylated surfactants (left) and for SLES (right). Dashed lines show the graphical method used for the determination of the cmc.

In order to investigate about a possible interaction among the surfactants and the polymers used in this study, we also determined the critical micellization concentration for both mixtures of surfactants in the presence of PVA and EVOH by keeping the polymer concentration constant at 1% w/w. Tab. 6.1.1 reports the values of cmc of all the investigated systems. In the absence of PVA and EVOH,

the cmc value that we found for SLES well agrees with that one from literature (0.12 mM, comparable with 0.095 mM, corresponding to $4.1 \cdot 10^{-5}$ g/g, estimated in our study)[136]. For C12-C14 ethoxylated alcohol a direct comparison with literature values is not simple, since the mixture of surfactants is particularly complex. However, we found a good agreement with the cmc value calculated and observed for a C13 8-ethoxylated alcohol ($C_{13}E_8$), which was found to be 0.027 mM (that corresponds to $1.5 \cdot 10^{-5}$ g/g)[137]. Moreover, the cmc in the absence and in the presence of both kinds of polymer changes slightly. This happens for both surfactant mixtures. Therefore, such evidence clearly indicates that interaction among components are quiet weak, due to the fact that both polymers are not charged.

Table 6.1.1 – Cmc values of C12-C14 ethoxylated alcohols and SLES at 25 °C in water, in the presence of 1% w/w EVOH and in the presence of 1% w/w PVA.

Surfactant	**Critical micellization concentration [g/g]**		
	H_2O	**EVOH solution**	**PVA solution**
C12-C14 ethoxylated alcohols	$9.0 \cdot 10^{-6}$	$1.8 \cdot 10^{-5}$	$1.0 \cdot 10^{-5}$
SLES	$4.1 \cdot 10^{-5}$	$2.6 \cdot 10^{-5}$	$3.5 \cdot 10^{-5}$

As a second step, we characterized the aggregation and the structural properties of the surfactant solutions by means of DLS and SANS. Fig. 6.1.3 reports the evolution of R_H for C12-C14 ethoxylated alcohols and SLES over time at a surfactant concentration of 3% w/w. The values of hydrodynamic radius for the mixture of non-ionic surfactants and SLES are 6 ± 1 nm and 2.7 ± 0.9 nm, respectively. No additional populations were observed over the 15 days of measurements. Thus, we can infer that aggregation does not occur over time for both systems. We also noticed that when changing surfactant concentration, no significant variation of R_H was observed.

Fig. 6.1.4 shows the neutron scattering profiles for a 5% w/w solution of C12-C14 ethoxylated alcohols in D_2O and for a 5% w/w solution of SLES. We chose higher concentrations with respect to those ones used for DLS measurements in order to have enough scattering intensity.

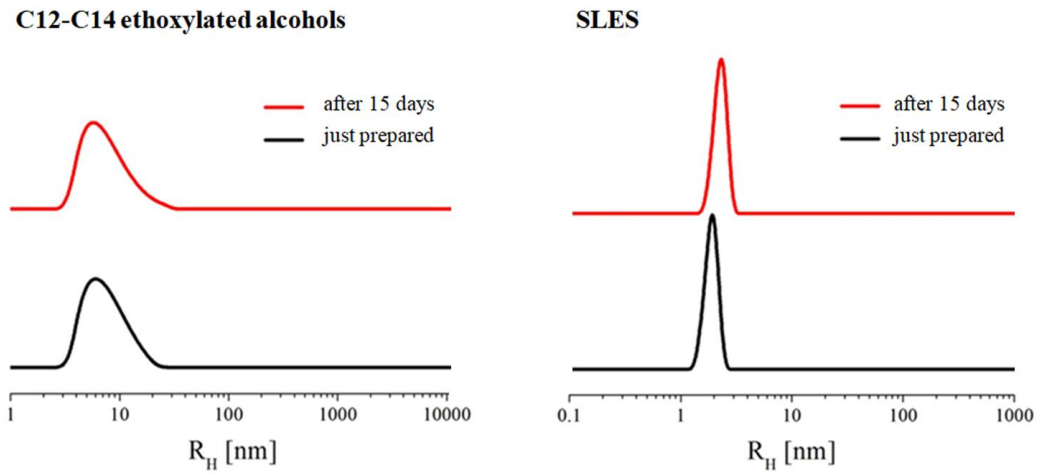

Figure 6.1.3 – Evolution of R_H over time for the non-ionic surfactant mixture (left) and SLES (right).

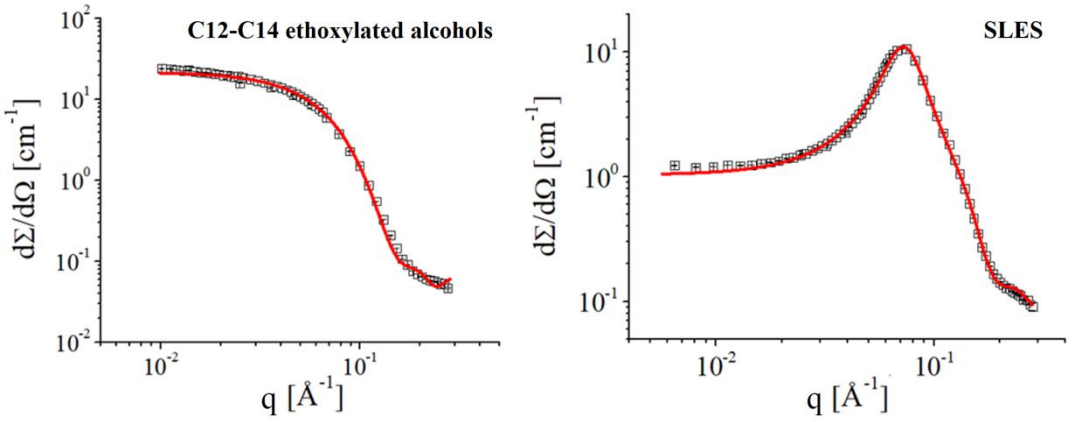

Figure 6.1.4 – Neutron scattering profiles and related fittings for the mixture of ethoxylated surfactants (left) and SLES (right).

Experimental data for the mixture of non-ionic surfactants were fitted by using a core-shell spherical form factor[132], where the core is composed by the hydrophobic alkyl chains and the shell by the hydrated ethoxylated groups. The equation of the model used for the fitting is reported below:

$$P(q) = \frac{scale}{V_s}\left\{\begin{array}{l} 3V_c(\rho_c - \rho_s)\dfrac{[\sin(qr_c) - qr_c\cos(qr_c)]}{(qr_c)^3} + \\ + 3V_s(\rho_s - \rho_{solv})\dfrac{[\sin(qr_s) - qr_s\cos(qr_s)]}{(qr_s)^3} \end{array}\right\}^2 + bkg \qquad \text{equation 6.1.1}$$

where *scale*, V_s, V_c, ρ_c, ρ_s, ρ_{solv}, r_c, r_s and *bkg* are the scale factor, the volume of the outer shell, the volume of the core, the scattering length density (SLD) of the core, the shell SLD, the solvent SLD, the core radius, the shell radius and the background, respectively. We obtained a hydrophobic core value of 2.01 ± 0.05 nm and a hydrophilic thickness value of 2.16 ± 0.03 nm. The obtained results well agree with those ones obtained from DLS, if we consider that the hydrodynamic radius is slightly larger due to the presence of the hydration water.

The scattering intensity profile obtained for SLES shows a well-pronounced peak at intermediate *q*-values. Therefore, we used an ellipsoid form factor together with a Hayter Penfold structure factor[138,139]. Such structure factor is used in case of charged, spheroidal objects in a dielectric medium and takes into account the interparticle interference effects due to screened coulomb repulsion between charged particles. The equation representing the ellipsoid form factor is shown below:

$$P(q,\alpha) = \frac{scale}{V} f^2(q) + bkg \qquad \text{equation 6.1.2}$$

where $f(q) = \dfrac{3\Delta\rho V[\sin(qr) - qr\cos(qr)]}{(qr)^3}$ and $r = (R_b^2\sin^2\alpha + R_a^2\cos^2\alpha)^{1/2}$.

In particular, *V*, $\Delta\rho$, R_a, R_b and α are the volume of the ellipsoid, the neutron contrast between the particle and the solvent, the ellipsoid radius along the rotational axis, the ellipsoid radius perpendicular to the rotational axis and the

angle between the rotational axis and the scattering vector, respectively. We used a simplified version of the model, which does not take into account the orientation of the ellipsoid axis and the *q*-vector, assuming a system of randomly oriented ellipsoids. We obtained R_a = 4.01 ± 0.01 nm , R_b = 2.15 ± 0.01 nm and a surface charge of 27 electrons. Polydispersity on R_a and R_b was also considered and the values were found to be 0.28 ± 0.01 and 0.13 ± 0.01, respectively. Also in this case, the dimensions are in good agreement with those ones found by DLS.

6.2 – Aggregation process in the presence of surfactants

6.2.1 – NaCl effect on critical micellization concentration

With the aim of characterizing the aggregation process of PVA and EVOH in the presence of surfactant micelles, we needed to define the surfactant concentration ranges within which to perform our study. Thus, we had to consider the effect of the salt on the surfactant aggregation properties. In particular, we are aware that the presence of NaCl may influence the cmc value, due to the salting-out effect exerted by the salt on the surfactants.[140,141,142] Therefore, we performed surface tension measurements in the presence of NaCl at the highest concentration used for our polymer aggregation studies (2 mol kg^{-1}). The obtained results are reported in tab. 6.2.1.1.

Table 6.2.1.1 – Cmc values of C12-C14 ethoxylated alcohols and SLES in an aqueous 2 mol kg^{-1} NaCl solution at 25 °C.

Surfactant	Critical micellization concentration [g/g]
C12-C14 ethoxylated alcohols	$1.3 \cdot 10^{-6}$
SLES	$9.5 \cdot 10^{-7}$

We observed that the presence of NaCl causes a cmc decrease of almost one order of magnitude for C12-C14 ethoxylated alcohols and of more than one order of magnitude for SLES with the respect to the cmc values obtained in pure water, shown in tab. 6.1.1. Such a result was quite expected, since the presence of a high concentration of ions coming from the salt results in a decrease of the hydration degree of the ethoxylated units, leading to an increase of the "effective" surfactant concentration. Such phenomenon was already shown in literature for non-ionic[143] and anionic[144] ethoxylated surfactants.

Therefore, in both cases the presence of NaCl lowers the cmc value. Since we have already shown that the presence of the polymer does not dramatically influence the surfactant cmc, we chose the cmc values of the surfactants in water as the threshold reference concentration at which surfactant micelles are present in solution.

6.2.2 – Aggregation properties of EVOH and PVA in the presence of surfactants

The characterization of the aggregation process of EVOH and PVA at 1% w/w in the presence of surfactants was performed by considering a surfactant concentration which was 5 times higher than the cmc value determined in water. As regards NaCl concentration, in order to monitor the aggregation process over a adequately long time, we chose 0.65 mol kg^{-1} and 1.50 mol kg^{-1} for EVOH and PVA, respectively. As a reference, we also prepared 2 solutions at the same polymer and salt concentrations without surfactants and the aggregation process was studied by DLS. Fig. 6.2.2.1 reports the trend of R_H as a function of time for all the investigated samples.

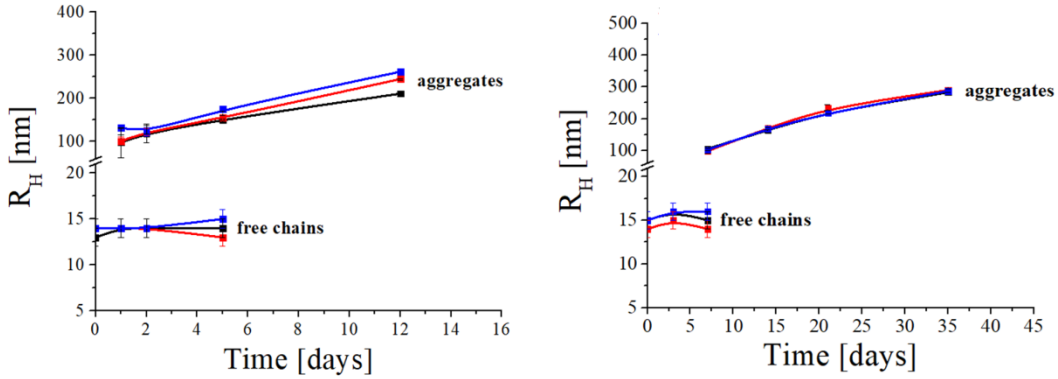

Figure 6.2.2.1 – Hydrodynamic radii of free chains and aggregates plotted ad a function of time for EVOH (left) and PVA (right) in NaCl solution (black curves), in a NaCl solution containing C12-C14 ethoxylated alcohols (red curves) and in a NaCl solution containing SLES (blue curves).

It can be clearly observed that aggregation occurs in the same way for the reference samples (without surfactants) and for the samples containing both kinds of surfactants. Therefore, the presence of surfactant micelles, at the investigated surfactant concentrations does not influence the aggregation process of both polymers.

6.3 – Aggregate structural properties in the presence of surfactants

The microstructural properties of EVOH and PVA aggregates in the presence of surfactants were studied through SANS at a surfactant concentration which was 5 times higher than the cmc value determined in water. EVOH samples were prepared at 0.45 mol kg^{-1} NaCl, whereas PVA samples at 1.50 mol kg^{-1} NaCl, which correspond to the lowest NaCl concentrations used for the SANS analysis carried out in the absence of surfactant. As already performed in the case of DLS measurements, we studied the effect of both C12-14 ethoxylated alcohols and SLES on the structural properties of EVOH and PVA particles.

We followed the same data analysis approach explained in detail in paragraph 5.2. Fig. 6.3.1 and fig. 6.3.2 report the SANS experimental profiles with related fittings and the Kratky plot analysis for EVOH aggregates. Results are summarized in tab. 6.3.1. As regards the values of lamellar thickness, no significant differences are found in the presence of surfactants. This means that the microstructural properties of the aggregates are not influenced by either C12-C14 ethoxylated alcohols or SLES. Concerning the values of R_g, we can observe an increase of this parameter in the presence of surfactants. However, we have to consider that whereas the surfactant-free sample was measured after 6 days from preparation, the experimental profiles of the samples in the presence of surfactants were collected after 8 days from preparation. Therefore, a slight effect of the time from preparation on the radius of gyration has to be considered.

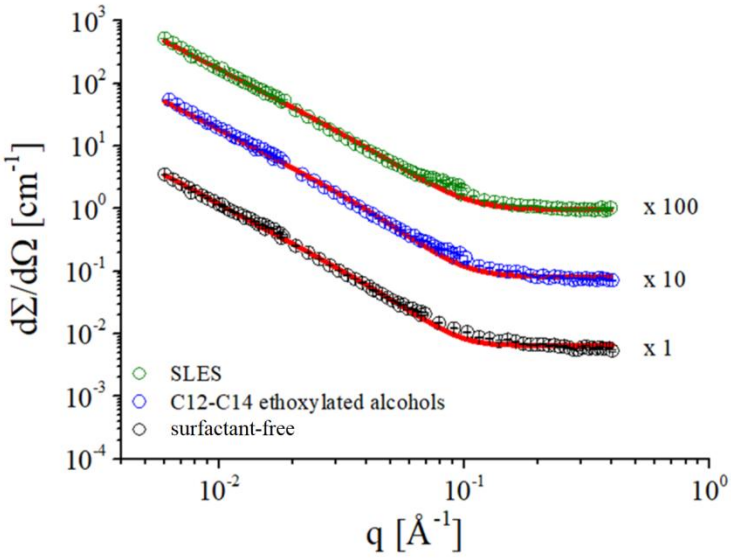

Figure 6.3.1 – SANS experimental profiles and related fittings at 1% w/w EVOH, 0.45 mol kg^{-1} NaCl in the presence and in the absence of surfactants. Curves were scaled for a better comparison as indicated in the graph.

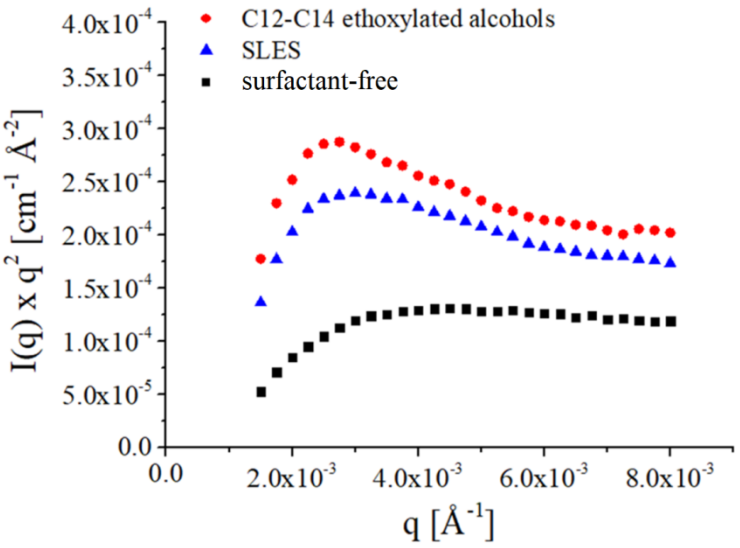

Figure 6.3.2 – Kratky plots for EVOH samples in the presence and in the absence of surfactants.

Table 6.3.1 – Comparison of the structural parameters (lamellar thickness and radius of gyration) obtained from SANS fittings and Kratky plot analysis. Errors on lamella thickness and related polydispersity are derived from the fitting, whereas the error on R_g was estimated by considering the standard deviation on this parameter calculated by considering a point adjacent to the maxima of the curves shown in fig. 6.3.2.

	surfactant-free	**C12-C14 ethoxylated alcohols**	**SLES**
Thickness [Å]	42.4 ± 0.1	40.6 ± 0.3	40.1 ± 0.2
polydispersity	0.24 ± 0.01	0.41 ± 0.03	0.32 ± 0.01
R_g [nm]	136 ± 5	212 ± 19	225 ± 16

Fig. 6.3.3 and fig. 6.3.4 report the SANS experimental profiles with related fittings and the Kratky plot analysis for PVA aggregates. Results are summarized in tab. 6.3.2. In this case, we cannot observe any significant difference among the structural parameters in the absence and in the presence of surfactants.

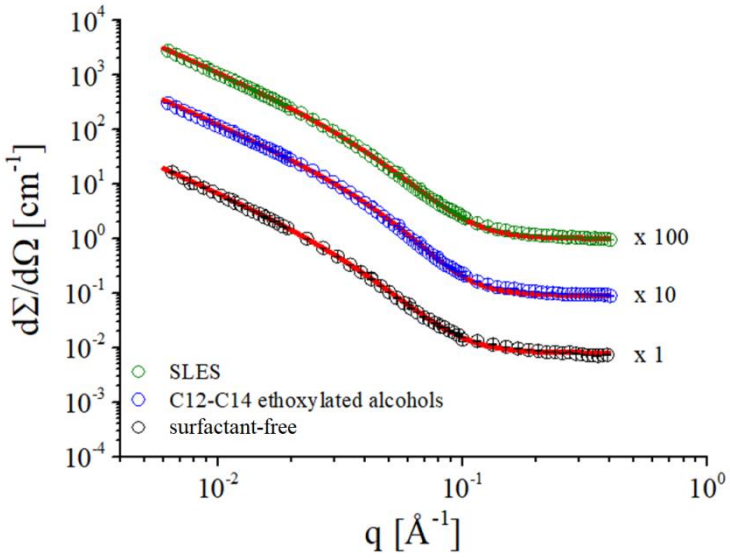

Figure 6.3.3 – SANS experimental profiles and related fittings at 0.85% w/w PVA, 1.50 mol kg^{-1} NaCl in the presence and in the absence of surfactants. Curves were scaled for a better comparison as indicated in the graph.

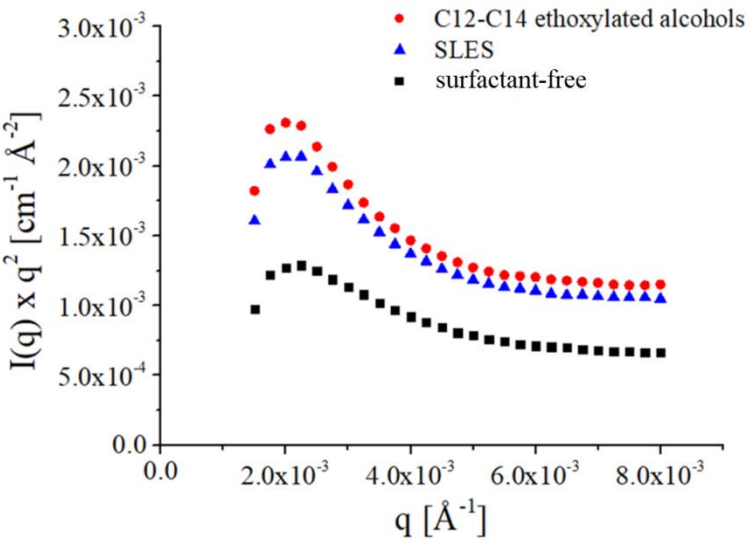

Figure 6.3.4 – Kratky plots for PVA samples in the presence and in the absence of surfactants.

Table 6.3.2 – Comparison of the structural parameters (lamellar thickness and radius of gyration) obtained from SANS fittings and Kratky plot analysis. Errors on lamella thickness and related polydispersity are derived from the fitting, whereas the error on R_g was estimated by considering the standard deviation on this parameter calculated by considering a point adjacent to the maxima of the curves shown in fig. 6.3.4.

	surfactant-free	**C12-C14 ethoxylated alcohols**	**SLES**
Thickness [Å]	57.5 ± 0.3	55.9 ± 0.2	55.3 ± 0.2
polydispersity	0.57 ± 0.03	0.40 ± 0.01	0.53 ± 0.01
R_g [nm]	280 ± 27	313 ± 32	278 ± 36

6.4 – General considerations

We observed that for both EVOH and PVA the presence of surfactant micelles does not influence the structure of the aggregates. At the same time, we are aware that higher surfactant concentrations may have a deep impact on both the aggregation and the structural properties of the particles. However, this model study, carried out at surfactant concentrations that are not comparable with the liquid detergent compositions, gave a first piece of information in terms of understanding the compatibility of the polymer particles with two common surfactants used in laundry products. All the synergic effects provided by the components of a complex mixture cannot be considered separately, thus a performance study, described later in chapter 8, is definitely more useful in order to understand the formulatability and the applicability of the investigated technology.

Chapter 7 – Fragrance segregation within the polymer particles

The polymer particles prepared through salting-out can be used as an effective carrier system for target molecules used in laundry products. In particular, additives like fragrances, which are present at low concentrations in the final product, can be segregated within the polymer particles present in solution. In this chapter, we report a detailed classification of the perfumes used for the segregation tests, as well as the characterization of the polymer aggregation in the presence of perfumes. Finally, the fragrance segregation efficiency of the tested polymer particles is evaluated.

7.1 – Perfume Raw Material classification

Perfume construction is a complicated process whose development strictly depends on the formulation type. Specifically, in the case of laundry detergents, there are three different categories of fragrances which are commonly employed: top notes, characterized by a high volatility; middle notes, whose presence is fundamental to give body and to fill out the perfume; base notes, i.e. species with a high boiling point that provide the perfume foundation and support top and middle notes. Because of their different purposes, fragrances employed in laundry formulations may belong to distinct functional classes (i.e. ethers, alcohols, esters), hence they are characterized by diverse chemico-physical properties. Boiling point and hydrophobicity (expressed as the logarithm of the partition coefficient in water and octanol, *LogP*) are the main parameters used to categorize them in the quadrant model (fig. 7.1.1, panel A).

We received from Procter and Gamble a prototype mixture of 10 critical Perfume Raw Materials (PRMs), since the most of them is easily lost during the washing

and the drying step. Every fragrance contained in the prototype mixture was classified according to boiling point and hydrophobicity, whose values were taken from the MSDS of each of them (fig. 7.1.1, panel B).

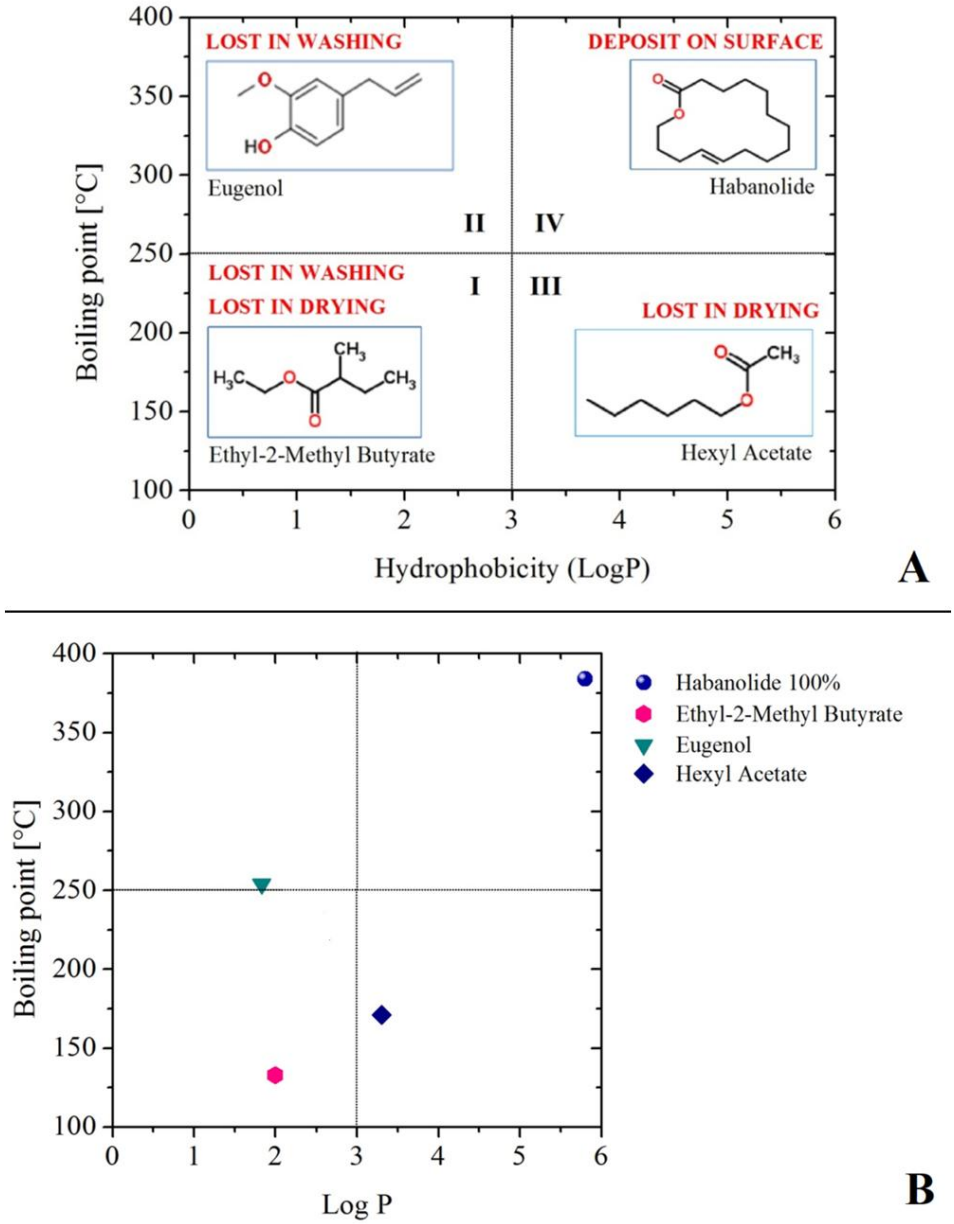

Figure 7.1.1 – Quadrant model including four examples of molecules characterized by different boiling point and hydrophobicity (panel A) and classification of four fragrances contained in the prototype mixture (panel B).

We chose Gas Chromatography with Flame Ionization Detector (GC-FID) for the identification of the perfumes, thanks to the high sensitivity of such technique and to the availability of the single fragrances composing the prototype mixture. In order to obtain a calibration curve for each perfume, three standard fragrance solutions were prepared by using a mixture 100:1 wt:wt of hexane (main component) and octane (chosen as internal standard) as a solvent. A temperature-programmed analysis was carried out and the retention times of each fragrance were determined. Then we analyzed the prototype mixture by using the same configuration setting for the single fragrances, so as to quantify the percentage of perfume oils through the calibration curves. The chromatogram of the prototype mixture where the fragrance peaks are identified is shown in fig. 7.1.2. It is worth noting that some of the fragrances contain impurities or isomers (in particular E-Z isomers for citral and eugenol), which cannot be isolated: the strong signal of such species indicates their relatively high concentration. Results are shown in tab. 7.1.1.

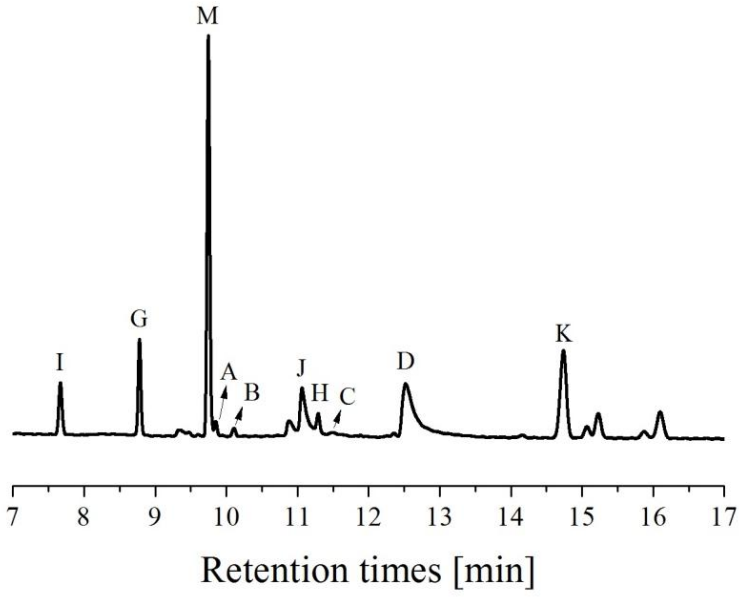

Figure 7.1.2 – Fragrance peaks in the prototype mixture. Hexane and octane peaks are not shown.

Table 7.1.1 – Results obtained from GD-FID measurements. Hexane (main solvent) and octane (internal standard) peaks have a retention time of 5.86 min and 6.20 min respectively. Data for PRM A are not shown due to confidentiality.

Fragrance	**Letter**	**Retention time [min, ± 0.05 min]**	**Composition in prototype mixture [%wt, ± 0.1 %wt]**
Decylaldheyde	A	9.82	0.6
p-Methylacetophenone	B	10.20	1.5
Methyl salicylate	C	11.45	0.8
Eugenol	D	12.56	13.5
Hexyl Acetate	G	8.74	7.1
Citral	H	11.25	2.6
Ethyl-2-Methyl Butyrate	I	7.61	4.8
Geraniol	J	11.08	12.1
Habanolide	K	14.74	10.1
PRM A	M	not shown	not shown
impurities, isomers			to 100

7.2 – Aggregation process in the presence of Perfume Raw Materials

7.2.1 – Solubilization tests

In order to study the effect of the Perfume Raw Materials on the polymer aggregation, we monitored the aggregation by means of DLS. However, we needed to find a proper solvent, which was able to solubilize the fragrances contained in the prototype mixture. Therefore, we decided to use a mixture of ethanol and water, since all the Perfume Raw Materials contained in the prototype mixture show a poor solubility in pure water.

Solubilization tests were carried out by choosing different ethanol/water ratios and different perfume concentrations. As an example, fig. 7.2.1.1 shows the appearance

of the solutions at the highest perfume concentration tested (1% w/w). For ethanol concentrations lower than 0.19 g/g phase separation occurs, since the amount of ethanol is not sufficient to obtain a homogeneous system. For ethanol concentrations higher than 0.29 g/g a single phase is obtained. At ethanol concentrations corresponding to 0.19 g/g and 0.29 g/g we observe the formation of an emulsion, which is stable for 24 hours in the first case and for 48 hours in the second case. The opalescence of these two solutions is due to the so-called Ouzo effect[145,146], which is related to the presence of a microemulsion.

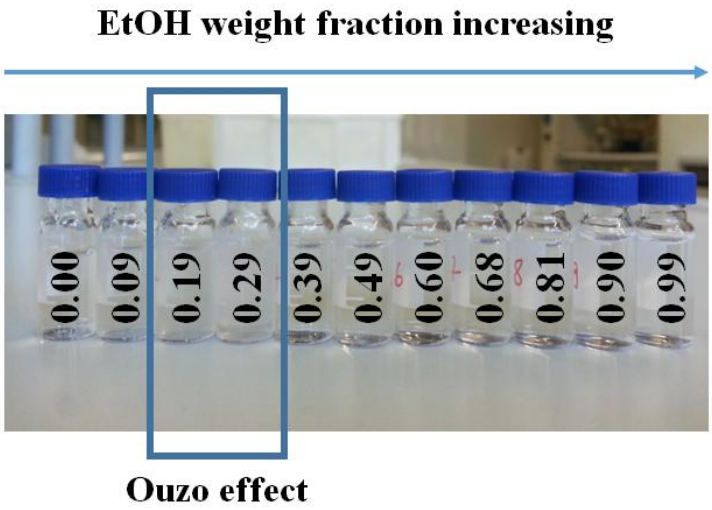

Figure 7.2.1.1 – Image showing the appearance of 11 different solutions containing the prototype fragrance mixture at a concentration of 1% w/w and different ethanol contents (indicated in the picture). The opalescence of the solutions containing 0.19 g/g and 0.29 g/g ethanol is due to the Ouzo effect.

From the obtained results, an ethanol concentration of about 0.40 g/g should be sufficient to obtain a homogeneous system. However, we were aware that ethanol might have a strong impact on the polymer aggregation.[147,148] In fact, at this ethanol concentration, precipitation of both EVOH and PVA was observed. Therefore, for our study we reduced the fragrance concentration to 0.5% w/w. At this fragrance

concentrations we obtained a homogeneous system already at ethanol concentrations of 0.30 g/g. Consequently, we studied the aggregation process at these conditions.

7.2.2 – Characterization of the aggregation process in the absence of NaCl

We monitored the aggregation behavior of both polymers, EVOH and PVA, at a concentration of 1% w/w in the presence of 0.5% w/w fragrance solubilized in ethanol/water 30/70 w/w. DLS measurements were carried out over almost 3 weeks and the results are shown in fig. 7.2.2.1.

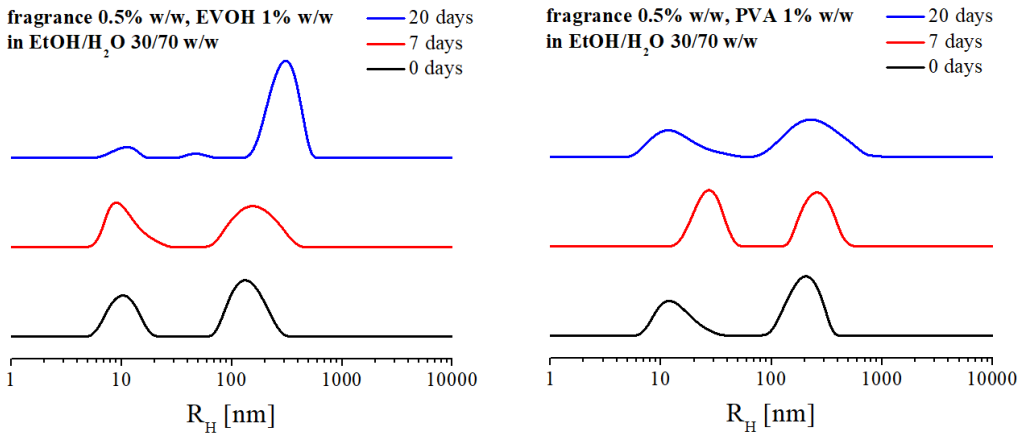

Figure 7.2.2.1 – Evolution of hydrodynamic radii for the samples in the presence of 0.5% w/w fragrance solubilized in a mixed ethanol/water solvent 30/70 w/w in the case of EVOH (left part) and PVA (right part).

At time = 0 from the preparation we can observe the presence of two populations of distinct hydrodynamic radii in the case of both polymers. For EVOH the first one is centered at about 12 nm, whereas the second one is at about 150 nm. For PVA the first population is centred at about 15 nm, whilst the second one is at about 200 nm. For both polymers the second population grows over time until reaching a radius of about 300 nm. Therefore, we observed that the presence of the PRMs in the mixed

solvent causes a partial polymer aggregation. This process is paricularly fast, since already at time = 0 a significant aggregate population is present. For both polymers the evolution to bigger sizes is very slow and no polymer precipitation over time was observed. However, from the obtained results we are not able to discriminate between the contribution to the aggregation given by the mixed solvent and by the fragrances, since an ethanol/water solvent is necessary in order to obtain a homogeneous system. Nevertheless, we were able to study the effect of the mixed solvent on the polymer aggregation in the absence of fragrances and for the most water-soluble fragrances (p-Methylacetophenone and Eugenol) we studied the aggregation process in water, by introducing an amount of PRM which was 0.5 times the solubility limit in water. Finally, we could observe that the contribution given by ethanol is definitely stronger than the one given by the PRMs, even though the effect of the fragrances is not negligible.

The characterization of the aggregation process in the system in the presence of polymer, fragrance, ethanol, water and NaCl was performed in a second step, once optimized the polymer and salt concentrations for the industrial application. The results related to this study will be shown in the next chapter.

7.3 – Perfume Raw Material segregation

7.3.1 – GC-FID measurements

As already discussed above, one of the peculiar features of the fragrance carrier system to develop is the high stability in liquid detergent formulations and, of course, a high efficiency of fragrance segregation. Therefore, we set up a method aimed at segregating a selection of Perfume Raw Materials and estimating the amount of fragrances lodged in the polymer aggregates. The method consists in adding a solution containing the PRMs to a solution containing the polymer

particles prepared through salting-out. Since the most of the PRMs is insoluble in water, their solubility was increased by using ethanol as solvent for the PRM solution. Aggregates with sizes above the filter cut off (0.20 µm) were removed through filtration and the residual fragrances present in the filtered solution were extracted by using hexane. The organic phase was analyzed by GC-FID. As a reference, we used a standard mixture of fragrances, containing a comparable concentration of PRMs. For this solution, we followed the same protocol described for the sample containing polymer particles. In these preliminary segregation tests, we were able to estimate the amount of some PRMs segregated by the polymer aggregates. We prepared both EVOH and PVA aggregates, in order to check and compare the segregation efficiency of both polymers. Results are summarized in tab. 7.3.1.1. Segregation efficiency *SE* was calculated through the following equation:

$$SE = \left[1 - \left(\frac{\frac{A_P}{m_{PRM,P}/m_{HEX,P}}}{\frac{A_R}{m_{PRM,R}/m_{HEX,R}}} \right) \right] \cdot 100\% \qquad \text{equation 7.3.1.1}$$

where A_P, A_R $m_{PRM,P}$, $m_{PRM,R}$, $m_{HEX,P}$ and $m_{HEX,R}$ are the areas from the chromatograms for the particle and the reference solution, the masses of PRM used for the preparation of the particle and the reference solution and the masses of hexane used for the extraction for the particle and the reference solution, respectively.

This parameter ranges between ~20% and ~75% and is generally higher for PVA. Less hydrophobic components are segregated better than the most hydrophobic ones (PRM C), probably due to their completely different structure. Such results represent a first proof of concept that encourages the use of such systems for the development of innovative fragrance carriers, which have to protect the target molecule from the emulsification process carried out by the surfactants contained in liquid detergent formulations.

Table 7.3.1.1 – Results obtained from some preliminary segregation tests performed by using both EVOH and PVA. Names are not disclosed for confidentiality.

PRM name	*SE* (EVOH)	*SE* (PVA)
PRM C	~20%	~50%
PRM D	~60%	~45%
PRM E	~25%	~70%
PRM A	~75%	~75%

7.3.2 – GC-MS measurements

The results presented in the previous paragraph show that PRM A is the component which is segregated better than the other ones contained in the prototype mixture. Therefore, we decided to focus our attention on this PRM and we repeated the segregation tests by following the same preparation protocol described above and using Mass Spectrometry as detection method.

Firstly, we prepared a solution containing PRM A in ethanol and a solution of polymer particles containing EVOH or PVA, water and NaCl. Both solutions were mixed. As a reference, we prepared a solution containing PRM A, NaCl, ethanol and water at the same concentrations. Secondly, with the aim of separating the polymer aggregates, both solutions (the one containing polymer particles and the reference sample) were filtered by using filters with a 0.20 µm cut off. Finally, the fragrance was extracted from the filtered solutions with hexane for 30 minutes through the use of an ultrasonic bath. In order to check the PRM A extraction efficiency, three different sets of samples at distinct fragrance concentrations (0.09% w/w, 0.12% w/w and 0.15% w/w) were prepared. For the solutions containing the polymer, the amount of polymer was also changed so as to have the same PRM A/polymer ratio. The organic phase was injected into a GC column

with equipped with a MS detector. By applying the same formula shown in the previous paragraph, we calculated the segregation efficiency. The results are shown in tab. 7.3.2.1.

Table 7.3.2.1 – Results obtained from the segregation tests performed by using both EVOH and PVA followed by GC-MS analysis at three different concentrations of PRM A and polymer.

PRM A concentration [% w/w]	**Polymer concentration [% w/w]**	***SE* (EVOH)**	***SE* (PVA)**
0.09	0.51	55 ÷ 58%	56 ÷ 59%
0.12	0.68	55 ÷ 57%	55 ÷ 59%
0.15	0.85	54 ÷ 59%	55 ÷ 60%

The percentage of segregation calculated by using the GC-MS method is lower with the respect of the value obtained by the GC-FID method. However, the results obtained from GC-MS measurements are definitely more accurate, thanks to the high sensitivity of the detection technique. Moreover, by GC-MS it is possible to repeat the analysis by using more sample replicates and, as a consequence, to define a confidence interval. The obtained results clearly show that the amount of PRM A segregated by the polymer particles is the same for EVOH and PVA (ranging between 54% and 60%). At the same time, the percentage of PRM A segregated by the particles is also independent on the PRM A concentration: this is probably due to the fact that the PRM A/polymer ratio was kept constant. Moreover, this result demonstrates that the extraction efficiency is the same within the interval of PRM A concentration tested.

Chapter 8 – Washing tests: evaluating the technology efficiency

From the results shown in the previous chapter we observe that polymer particles are able to segregate the PRMs. One important step that allows understanding the applicability of such systems from an industrial viewpoint consists in performing washing tests by reproducing conditions that are close to the real washing process. In this chapter we present the modification of the preparation protocol of polymer particles containing perfume, by taking into account the industrial timing, which obviously requires speeding up the aggregation process. Moreover, we show the results of the washing tests in order to evaluate the efficiency of the designed technology.

8.1 – Modification of the preparation protocol

8.1.1 – Speeding up the preparation protocol and the aggregation process

From the results shown in chapter 4 we could observe that the time needed for a complete conversion from free chains to aggregates is strictly dependent on NaCl concentration. In particular, we found that at 0.85 mol kg^{-1} NaCl and at 2.00 mol kg^{-1} NaCl a full conversion to aggregates is achieved for EVOH and PVA respectively after 3 days from the preparation. However, we know that such a time is not compatible with the industrial timing, hence a modification of the preparation protocol was fundamental in order to speed up the aggregation process.

Firstly, the sample preparation procedure was modified by applying the so-called mass-to-volume conversion. Instead of preparing each sample by weighing the stock solutions individually, the solutions were prepared by adding calculated volumes of each stock solution under stirring. This first modification allowed reducing the preparation time for a single solution from 5 minutes to 1 minute.

Secondly, the aggregation time was reduced by modifying the salt/polymer ratio. In order to achieve this purpose, we kept the salt concentration constant and we varied the polymer concentration.

8.1.2 – Comparison between two preparation protocols

The first preparation protocol that we tested is the so-called 5 steps in a row protocol. We needed to define the mixing steps to follow in order to prepare the final technology (polymer particles + fragrance) solution, so as to avoid polymer precipitation during the preparation. Therefore, 5 distinct stock solutions and solvents were added according to the following order:

1) Polymer stock solution;
2) Water (if needed);
3) Ethanol (if needed);
4) PRM stock solution in ethanol;
5) NaCl stock solution in water.

The second preparation protocol tested is the so-called 5 steps in 2 parts protocol. Also in this case we defined the mixing steps to follow in order to prepare the technology solution and to avoid polymer precipitation at the same time. Stock solutions and solvents were added according to the following order:

FIRST PART

1) Polymer stock solution;
2) Water (if needed);
3) NaCl stock solution in water;

SECOND PART (after complete conversion from free chains to aggregates)

4) Ethanol (if needed);
5) PRM stock solution in ethanol.

For both protocols we tested two PRMs, PRM A and PRM B, which are characterized by very different boiling point and hydrophobicity. The exact values of these parameters cannot be disclosed.

By comparing both preparation protocols, we observe that the mixing order is different. In the first case, all solutions or solvents are added at the same time and the NaCl stock solution is the last one added, whereas in the second case two solutions and water are added in a first step and then the other stock solution and ethanol are added in a second step. In the latter case, the time between the addition of ethanol and the PRM stock solution to the solution containing polymer, water and NaCl is strictly dependent on the time needed for achieving a complete conversion from free chains to aggregates. As clearly shown below, this time depends on the amount of polymer added during the first step.

Even though the final polymer, NaCl, PRM and ethanol concentrations are the same for both protocols, we wanted to check by means of DLS whether the mixing order affects the aggregation process. At the same time, we tested three different polymer concentrations and we kept the final NaCl concentration constant (2.00 mol kg^{-1} and 0.85 mol kg^{-1} for PVA and EVOH respectively).

As an example, fig. 8.1.2.1 shows the evolution of the hydrodynamic radii over time for the sample containing PVA at the highest polymer and PRM A concentrations tested (0.85% w/w and 0.15% w/w, respectively), which correspond to a technology concentration of 1% w/w. Panel A and panel B report the distribution curves related to the 5 steps in a row protocol and to the 5 steps in 2 parts protocol, respectively.

In the first case we observe the presence of two distinct populations: one centered at about 15 nm and another one at about 150 nm. After 7 days the second populations grows slightly, but free chains are still present in solution. By comparing the distribution curves collected at 7 days and 12 days from the preparation, no significant change in hydrodynamic radii can be noticed.

In the second case, after the addition of the polymer stock solution, water and NaCl stock solution, we can observe two populations at about 17 nm and about 100 nm after 30 minutes from the preparation. After 110 minutes the conversion from free chains to aggregates is almost complete and the aggregate population is bigger. Then, after 180 minutes the conversion from free chains to aggregates is complete and the hydrodynamic radius of the single aggregate population is about 280 nm. At this point, upon addition of ethanol and the PRM A solution, the aggregate population grows until reaching a stable value of about 320 nm after 6 days from the preparation. No polymer precipitation was observed over time. By considering all the collected data, the time needed for obtaining a monomodal distribution of aggregates is strictly dependent on the polymer concentration. In the case of PVA the time needed is 3 hours at a final polymer concentration of 0.85% w/w, 4 hours and 30 minutes at 0.68% w/w and 6 hours at 0.51% w/w. In the case of EVOH a complete conversion is achieved after 6 hours at a final polymer concentration of 0.85% w/w, after 8 hours at 0.68% w/w and after 10 hours at 0.51% w/w. As an example. Fig. 8.1.2.2 shows a picture of 3 PVA solutions and their reference samples at the 3 different polymer concentrations tested.

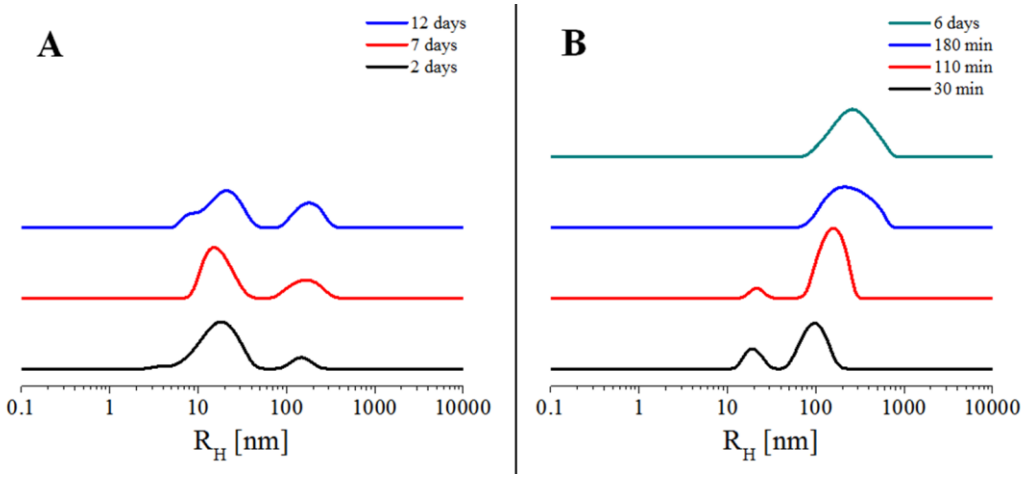

Figure 8.1.2.1 – Evolution of hydrodynamic radii for the samples prepared through the 5 steps in a row protocol (panel A) and the 5 steps in two parts protocol (panel B).

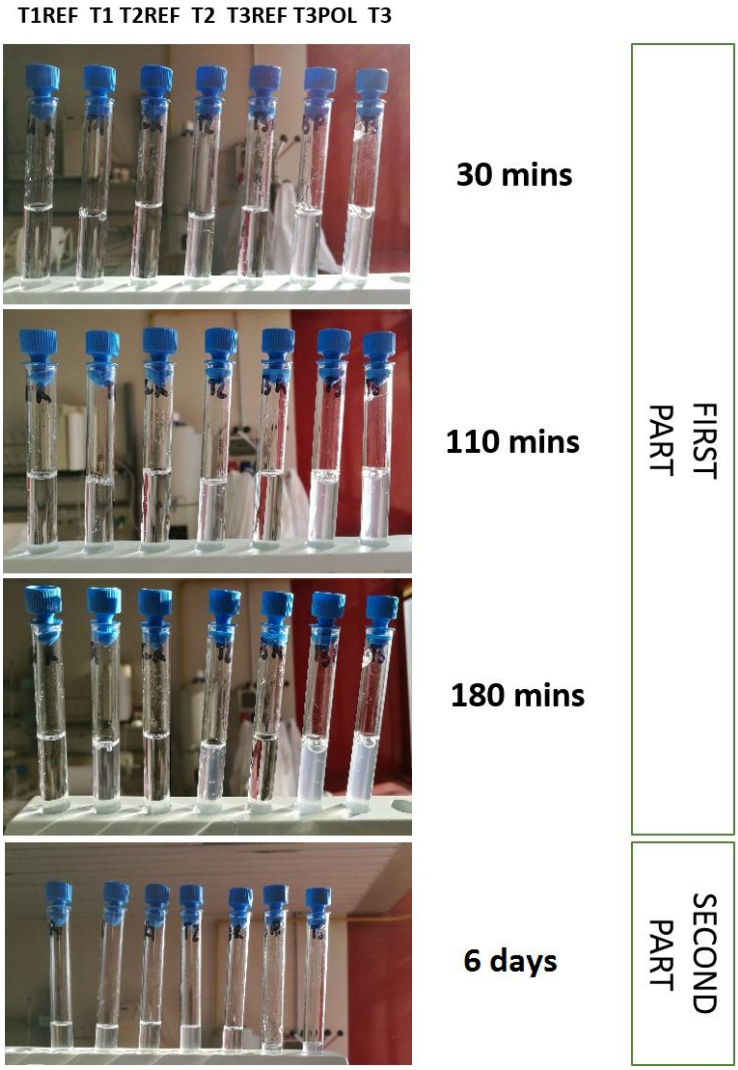

Figure 8.1.2.2 – Evolution of sample appearance over time for the analyzed PVA and NaCl solutions and their related references. T1REF, T2REF and T3REF = NaCl solutions containing PRM A at 0.09% w/w, 0.12% w/w and 0.15% w/w, respectively; T3POL = PVA and NaCl solution at a final salt concentration of 2.00 mol kg^{-1} and final PVA concentration of 0.85% w/w; T1, T2 and T3 = PVA and NaCl solutions at a final salt concentration of 2.00 mol kg^{-1} and final PVA concentrations of 0.51% w/w, 0.68% w/w and 0.85% w/w, respectively and containing PRM A at 0.09% w/w, 0.12% w/w and 0.15% w/w, respectively.

From the results shown above it is clear that the different order of adding the stock solutions and the solvents affects the aggregation process. For the 5 steps in a row protocol all components are added at the same time, thus the salt and the polymer concentrations are lower. Moreover, the presence of ethanol dramatically changes the dielectric constant of the solvent[149], leading to a different aggregation behavior. In particular, no further aggregation after 7 days is observed if ethanol is introduced at time = 0. For the 5 steps in two parts protocol polymer and NaCl are added before ethanol and the fragrance, thus the temporary concentrations of both components are higher. This leads to a very fast aggregation process. Upon addition of ethanol and the PRM solution in ethanol the aggregation is stopped due to the presence of ethanol. This is a key role of such a solvent, since it allows obtaining an aggregate solution which is stable over time. Indeed, in the absence of ethanol, polymer precipitation would have been observed, as already discussed in chapter 4.

These findings clearly show that the 5 steps in 2 parts protocol is more suitable than the 5 steps in a row protocol to obtain a complete conversion from free chains to aggregates and a stable aggregate suspension.

8.2 – Evaluation of the technology efficiency

8.2.1 – An overview of the tests

Technology efficiency was evaluated by performing middle scale tests through the use of a Launder-o-Meter. We tested two different types of fabric: cotton and polyester. We carried out two kinds of test: a first one aimed at evaluating the amount of PRM deposited on fabrics and a second one aimed at evaluating the amount of PRM released by the fabrics at three different touch points: wet, dry and rebloom. The wet touch point represents the stage corresponding to the wet fabric coming from the washing machine. In this condition the most volatile and

hydrophilic fragrances are easily detected and the perfume level is particularly high since a significant amount of water is absorbed on the fabric. In particular, due to the higher hydrophilicity of cotton, the perfume intensity is higher than for polyester. In our experiments the dry touch point corresponds to the fabric spontaneously dried overnight (about 15 hours) without the use of a drying machine. In this condition the less volatile fragrances are detected, since a significant amount of volatile component is lost during the drying process. Finally, the rebloom touch point represents the stage corresponding to a rebloomed fabric, i.e. a fabric which is rewetted by spraying a certain amount of water. At this stage the most volatile and hydrophilic fragrances which are still adsorbed on the fabrics can be released.

The technology efficiency was evaluated for the following technologies: PVA particles containing PRM A; PVA particles containing PRM B; EVOH particles containing PRM A; EVOH particles containing PRM B.

8.2.2 – Washing procedure and analysis approach

The washing tests in Launder-o-Meter were performed by scaling down the typical amounts of water and detergent used for washing. Normally, in European conditions the washing is performed using 13 L of water and about 66 g of liquid detergent. By considering the volume of water used in the Lauder-o-Meter (200 mL), the amount of detergent to be used is about 1 g. During the washing tests, a solution containing the technology (polymer particles + fragrance) was added on top, i.e. by adding a certain amount of solution into the Launder-o-Meter jars containing the fabric, water and detergent. In order to test the efficiency of the technology tested, we always used an internal reference, i.e. a solution containing free perfume, which is a fragrance solution without polymer particles. In this way, the fabrics washed with the technology and the fabrics washed with the reference solution were treated under the same conditions. It was not possible to use a

technology already in use as a reference for both business reasons and for the different preparation protocols needed, that could have introduced a significant variable to consider when evaluating the results. A detailed description of the washing procedure is given in chapter 2. After washing, the fabrics were analyzed in order to check the efficiency of the technology.

Deposition tests were carried out by using dry fabrics. After washing, the fabrics were spontaneously dried overnight (about 15 hours) without using a drying machine. Then, the residual fragrance was extracted by using ethanol. The extracts from the samples containing the technology and from the reference samples were analyzed by head-space GC-MS. Release tests were performed by analyzing the fabrics at wet, dry and rebloom touch points by head-space GC-MS. The experiments in wet conditions were carried out just after the washing step, whereas the dry release tests were carried out after drying the fabrics overnight. Finally, the rebloom release experiments were performed after rewetting the dry fabrics. A detailed description of both kinds of test is given in chapter 2.

8.2.3 – Deposition tests

The GC-MS head-space analysis performed to check the deposition efficiency was carried out by measuring directly the concentration of the fragrance in the head-space from ethanol extracts. Each sample was replicated twice (external replicates) and the average values of the correlation area obtained from the analysis were considered. The correlation areas were calculated by extracting the specific ion chromatogram for each sample. For PRM A, we used the characteristic *m/z* value of 121. After obtaining the extracted chromatogram, the signals at retention times corresponding to 5.68 min and 5.72 min were integrated and the sum of the correlation areas obtained from the integration was related to the PRM concentration in the head-space. For PRM B, we chose m/z = 228 and retention times corresponding to 9.30, 9.35, 9.58 and 9.63 min. Moreover, 3 standard

solutions containing the target PRM were prepared and a calibration curve for each experiment was built by correlating the results obtained from the integration to the PRM concentration, already known and previously calculated. The slope of the straight line used to fit the experimental data was used to estimate the fragrance concentration for each sample. Then, the concentration was normalized by the mass of fabric (after washing) and the mass of technology or perfume-free solution used for the washing step. The normalized concentration value obtained for the reference sample (without technology) and the main sample (with technology) were compared through a comparison factor *CF*, whose formula is reported below:

$$CF = \left(1 - \frac{C_{ref}}{C_{sample}}\right) \cdot 100\% \qquad \text{equation 8.2.3.1}$$

where C_{ref} and C_{sample} are the normalized head-space concentrations of the target fragrance in the ethanol extracts coming from the reference fabric and the fabric washed with the technology solution, respectively. However, since all experiments were performed by using an internal reference sample, the comparison factor could have been also calculated directly from the normalized correlation areas giving the same value. The values of *CF* were calculated for each technology by repeating the same experiment three times and by considering an average value. The results are reported in tab. 8.2.3.1

For every technology the value of comparison factor is positive. In particular, the best results were found for PVA particles containing PRM A, which lead to a very high increase of deposition on cotton and for PVA particles containing PRM B, that give a significant benefit on polyester. If we consider the hydrophobicity of both molecules, we can notice that the particles containing PRM A are less hydrophobic than the particles containing PRM B due to the different *LogP* of the PRMs used, thus a higher amount is deposited on the more hydrophilic cotton rather than on polyester. The opposite happens for PVA particles containing PRM B, which are deposited better on the more hydrophobic polyester.

Table 8.2.3.1 – Average values of comparison factor obtained from deposition tests for 4 different technologies.

Technology	Comparison factor	
	Cotton	**Polyester**
EVOH particles + PRM A	+15% ± 7%	+10% ± 6%
EVOH particles + PRM B	+8% ± 3%	+5% ± 3%
PVA particles + PRM A	+38% ± 13%	+8% ± 5%
PVA particles + PRM B	+5% ± 2%	+20% ± 5%

8.2.4 – Release tests

The GC-MS head-space analysis performed to check the release efficiency was carried out by measuring directly the concentration of the fragrance in the headspace from the fabrics. In this case, each measurement was replicated 3 times (internal replicate) and the average values of the correlation area were considered. In order to calculate the correlation areas, we followed the same approach described for the deposition tests, with the only exception that the comparison factor was calculated by considering directly the normalized correlation areas, i.e. the values obtained from the chromatograms normalized by the fabric mass (after washing) and the mass of technology or perfume-free solution used for the washing step. The formula used is reported below:

$$CF = \left(1 - \frac{A_{ref}}{A_{sample}}\right) \cdot 100\% \qquad \text{equation 8.2.4.1}$$

where A_{ref} and A_{sample} are the normalized correlation areas of the target fragrance for the reference fabric and the fabric washed with the technology solution, respectively.

Also in this case, the values of *CF* were calculated for each technology by repeating the same experiment three times and by considering an average value. The results are reported in the tab. 8.2.4.1

Table 8.2.4.1 – Average values of comparison factor obtained from release tests for 4 different technologies (CK = knitted cotton; PE = polyester).

Technology	Comparison factor					
	wet		dry		rebloom	
	CK	PE	CK	PE	CK	PE
EVOH particles + PRM A	+8% ± 1%	+7% ± 1%	+12% ± 5%	+7% ± 2%	+20% ± 6%	+2.5% ± 0.5%
EVOH particles + PRM B	+10.4% ± 0.4%	+16% ± 1%	-10% ± 6%	+7% ± 3%	-3% ± 1%	+3% ± 2%
PVA particles + PRM A	+13% ± 1%	+4% ± 1%	-16% ± 4%	+2.8% ± 0.9%	-5% ± 3%	+8% ± 1%
PVA particles + PRM B	+3.0% ± 0.6%	+17% ± 2%	+4% ± 2%	+17.4% ± 0.2%	+2.5% ± 0.5%	+3.7% ± 0.6%

In most of the cases, the value of comparison factor is positive and the best results are found at wet touch point for both kinds of fabrics. At this stage the values of comparison factor are always positive, i.e. all technologies deliver a benefit. As already observed from the deposition tests, particles containing PRM A lead to a higher value of comparison factor for cotton, whereas particles containing PRM B give more benefit on polyester. This clearly indicates that the PRM hydrophobicity significantly influences the deposition and the release efficiency.

In some cases, the comparison factors obtained from the dry release tests are negative. This could suggest a discrepancy between deposition and dry release tests

since both kinds of test are performed with dried fabrics. However, it is worth noting that in deposition tests the PRM extraction is forced by using a solvent, whereas in dry release no solvents are used. Therefore, a negative release value does not necessarily mean that less perfume is deposited on the fabric, since the presence of the technology may reduce the PRM volatility. The positive values of comparison factor from wet release tests for particles containing PRM A are very encouraging because PRM A represents one of the most used top notes in the perfume accords, with concentrations up to 20% w/w. A technology which favors the deposition and the release of such components is highly desirable, due to the high cost of the perfume components used in liquid detergent formulations.

As regards PRM B, the positive results obtained in the most of rebloom tests for both EVOH and PVA particles are particularly attractive, since this PRM is used as a malodor blocking component. Due to the fact that bad smell usually comes out when the fabrics are rewetted, a higher release of PRM B may reduce the perception of malodor from fabrics, especially in the case of polyester.

8.2.5 – Product aging

We also evaluated the aging effect on the technology efficiency. In particular, we decided to draw our attention on the technology that worked better (PVA particles + PRM A). The solution containing the technology was mixed with liquid detergent and the product was left at room temperature (20 °C) for 10 days. We followed the same procedure for the reference product (without technology and containing free perfume). The washing step was carried out by using the aged products and wet release test was performed. Data were analyzed as described in the previous paragraphs. We still obtained positive comparison factors: +10% ± 0.1% for cotton and +3% ± 1% for polyester. Therefore, storing PVA particles containing PRM A with liquid detergent does not affect the technology efficiency negatively.

Chapter 9 – Conclusions

In this chapter the main conclusions derived from the experimental results previously shown are summarized. Final remarks and future perspectives are also reported.

9.1 – An easy, fast and cheap protocol for the preparation of vinyl alcohol-based particles

In this project, we have shown that vinyl alcohol-based copolymers are suitable candidates for the preparation of polymer particles able to segregate perfume ingredients. Differently from the preparation protocols commonly used in literature and at industrial level, salting-out is an easy, fast and cheap method for preparing polymer particles. Indeed, such a protocol does not require the use of chemical cross-linkers and allows preserving the biocompatibility and the biodegradability of the polymers used for the preparation, since the chemical structure of the polymer is not altered due to the absence of covalent bonds among polymer chains. At the same time, the particles show a compact structure, thanks to the presence of hydrogen bonds among the hydroxyl side groups composing the repeating units.

9.2 – Tunable aggregation and structural properties

The aggregation time can be easily tuned by varying both polymer and salt concentration within an optimized range. We have shown that it is possible to speed-up the aggregation process by increasing both the salt and the polymer concentration up to threshold values above which massive precipitation of the polymer is observed. Polymer and salt concentrations also affect the structural parameters of the polymer particles, like the hydrodynamic radius, whose value

increases at higher concentrations and same aggregation times. Moreover, salt concentration directly affects the microstructural properties of the aggregates. Both the packing degree and the lamellar thickness of the particles tend to increase when NaCl content is higher. The knowledge acquired through a deep study of the thermodynamic properties of polymer solutions in the presence of NaCl has allowed us to optimize the salting-out preparation protocol, obtaining very short aggregation times, compatible with the industrial timing.

9.3 – Surfactant-resistant polymer particles

The model study performed on solutions containing polymer particles in the presence of two common surfactants used in liquid detergent formulations has shown that, when surfactant micelles are present in solution, neither the aggregation process or the structural properties are dramatically influenced. Even though the composition of the final product is extremely different from the simplified mixture here characterized, such a result is a useful proof of concept that encourages the use of these polymer particles for laundry applications.

9.4 – High segregation efficiency and fragrance deposition/release

Both EVOH and PVA particles are able to segregate the fragrances. In particular, we have found a perfume segregation efficiency of about 60%. Such a high segregation efficiency allows reducing the amount of technology needed for achieving the desired benefit for the consumers. This implies the use of a lower amount of perfume which reduces the formulation costs.

At the same time, we have observed that the presence of the here presented technology allows obtaining both a higher fragrance deposition on fabric and a higher perfume release with the respect to the washing product containing free (i.e.

not segregated) perfume. Such a benefit is particularly evident for fragrance release from wet fabrics. The achieved result is extremely encouraging, since the effective release in wet conditions represents an important step for consumers' acceptance.

9.5 – Final remarks and future perspectives

The technology presented in this work may represent a suitable alternative to the current carrier systems used in laundry products, i.e. the polymer capsules. Indeed, the main drawback of this technology is the perfume leakage that can easily happen due to the breakage of the capsule walls caused by mechanical stress. The use of a soft particle-based technology like the one designed in this project may avoid the performance reduction caused by leakage.

At the same time, we are aware that still many fundamental steps forward have to be made. Firstly, the formulatability in liquid detergent composition has to be studied, in order to avoid a too high water content in the final laundry product. Secondly, the product stability over time has to be tested: we have already observed that no polymer precipitation occurs over time, but local aggregation phenomena within the complex matrix may take place over longer time scales and they are not easy to detect due to the high number of the product components. Finally, the perfume diffusion out of the polymer particles has to be studied in the final matrix, since the presence of surfactants may reduce the segregation efficiency of the technology. However, the encouraging results obtained after product aging have shown that the designed technology present a good compatibility with the other matrix components.

Appendices

In the following appendices we report the data analysis approach followed for the collected Light Scattering data.

A.1 – SLS data analysis

In SLS experiments the time-averaged scattering intensity is related to the molecular properties of the systems, i.e. solute-solvent interaction, reflected in the second virial coefficient, molecular weight, shape and size of the scattering objects. The relation between the scattering intensity, concentration of the scattering objects and scattering angle is the following[150]:

$$\frac{Kc}{R_\theta} = \frac{1}{M_w}\left[1 + \frac{q^2\left\langle R_g^2\right\rangle}{3} + 2A_2M_wc\right] \qquad \text{equation A.1.1}$$

where c is the concentration of the scattering objects and $K = \frac{1}{N_A}\left(\frac{2\pi n}{\lambda^2}\frac{dn}{dc}\right)^2$ is a constant that depends on the incident wavelength λ, the Avogadro number N_A, the solvent refractive index n and the variation of the solution refractive index with the polymer concentration dn/dc. When samples are highly diluted, it can be assumed that dn/dc does not change with the wavelength.

The parameter $q = 4\pi n \sin(\theta/2)/\lambda$ is the modulus of the scattering vector, where θ represents the scattering angle. M_w, R_g and A_2 are the mass average molecular weight, the radius of gyration and the second virial coefficient for the scattering objects, respectively, that are the structural and the thermodynamic parameters that can be derived from SLS measurements. Finally, R_Θ is the Rayleigh ratio and represents the term of the equation where the scattering intensity appears.

Its expression is:

$$R_\theta = \frac{(I_S - I_0)}{I_R}\frac{n_0^2}{n_R^2}R_{\theta,R} \qquad \text{equation A.1.2}$$

where I_S, I_0 and I_R are the scattering intensities of the sample, the solvent and the reference (toluene), respectively, n_0 is the refractive index of the solvent and n_R is the refractive index of the reference. $R_{\Theta,R}$ is the Rayleigh ratio of the reference at the same incident wavelength, calculated by applying the following relation[151]:

$$R_{\theta,R} = \frac{2\cdot(4.90\cdot 10^6)\lambda^{-4.17}}{(1+\rho_u)} \qquad \text{equation A.1.3}$$

where λ is the incident wavelength and ρ_u is the depolarization factor for non-polarized light, which was calculated by considering an average value from those already reported in the literature for different wavelengths[151].

In the case of small particles, typically with dimension $d < \lambda/10$, it is possible to neglect the angular contribution to the scattering intensity, i.e. the scattering object can be represented as a point and, therefore, the constructive/destructive interference arising from the optical path difference can be considered null.[150] Therefore, equation A.1.1 can be modified in:

$$\frac{Kc}{R_\theta} = \frac{1}{M_w} + 2A_2c \qquad \text{equation A.1.4}$$

In this case, it is sufficient to perform a linear fit of the experimental data at different concentrations in order to obtain information about the molecular weight (from the intercept) and the second virial coefficient (from the slope).

In the presence of bigger particles, this approximation is not longer valid and the scattering intensity dependence on both concentration and scattering angle has to be taken into account. Therefore, the values of $\frac{Kc}{R_\theta}$ have to be plotted as a function of two independent variables, c and q, in order to obtain the so-called Zimm plot[152].

By extrapolating the values of $\frac{Kc}{R_\theta}$ at both null concentration and null angle (i.e. null scattering vector), it is possible to obtain two datasets that, once fitted, give the molecular weight, the second virial coefficient and the radius of gyration, as shown in the equations below:

$$\frac{Kc}{R_\theta} = \frac{1}{M_w} + 2A_2c \quad \text{for } \theta = 0 \qquad \text{equation A.1.5}$$

$$\frac{Kc}{R_\theta} = \frac{1}{M_w}\left[1 + \frac{\left\langle R_g^2 \right\rangle}{3} q^2\right] \quad \text{for } c = 0 \qquad \text{equation A.1.6}$$

A.2 – DLS data analysis

In DLS measurements the intensity autocorrelation function, $g^{(2)}(t)$, is related to the electric field autocorrelation function, $g^{(1)}(t)$, shown in equation A.2.1 as the inverse Laplace transform of the distribution of the relaxation rate Γ, which allows calculating the translational diffusion coefficient $D = \Gamma/q^2$ [153]:

$$g^{(1)}(t) = \int_{-\infty}^{+\infty} \tau A(\tau) \exp(-t/\tau) d \ln \tau \qquad \text{equation A.2.1}$$

where $\tau = 1/\Gamma$ and q is the modulus of the scattering vector. A modified version of the CONTIN algorithm incorporated in the Precision Deconvolve software[154] can be used in order to perform the inverse Laplace transform. In the case of spherical objects, continuous medium and infinite dilution, the diffusion coefficient can be easily related to the hydrodynamic radius R_H through the Stokes-Einstein equation:

$$R_H = \frac{k_B T}{6\pi\eta D} \qquad \text{equation A.2.2}$$

where k_B is the Boltzmann constant, T is the absolute temperature and η is the solvent viscosity. For non-spherical particles, R_H represents the radius of a spherical aggregate with the same measured diffusion coefficient. In this

hypothesis, equation A.2.2 can be reasonably used to estimate the averaged hydrodynamic radius of the particles.[118,153] From the diffusion coefficients it is possible to determine also other parameters. In a given solvent, the diffusion coefficient can be expressed as a function of the concentration of the scattering objects[108]:

$$D = D(0) + Sc \qquad \text{equation A.2.3}$$

where D is the diffusion coefficient at a specific concentration, $D(0)$ is the diffusion coefficient at infinite dilution and S represents the slope of the linear fitting obtained by plotting D as function of c. S and $D(0)$ are related to the interaction concentration coefficient k_D[108], through the following expression:

$$k_D \frac{N_A V_H}{M_w} = \frac{S}{D(0)} \qquad \text{equation A.2.4}$$

where V_H is the hydrodynamic volume. Lower values of the interaction coefficient indicate a stronger tendency to the aggregation, i.e. the interaction among solute molecules or particles is favored. By combining equation A.2.2 and equation A.2.4 it is possible to obtain the equation below:

$$k_D = \frac{SM_w}{D(0)N_A \frac{4\pi}{3}\left[\frac{k_B T}{6\pi\eta D(0)}\right]^3} \qquad \text{equation A.2.5}$$

where the hydrodynamic volume of the sphere is made explicit by introducing the hydrodynamic radius obtained from the Stokes-Einstein equation.

References

1. Allouche, J., *Nanomaterials: A Danger or a Promise? - Chapter 2 - Synthesis of Organic and Bioorganic Nanoparticles: An Overview of the Preparation Methods*. Springer-Verlag London 2013: 2013.

2. Crucho, C. I. C., Barros, M. T. Polymeric nanoparticles: A study on the preparation variables and characterization methods. *Materials Science and Engineering C* **2017,** 80, 771–784.

3. Li, X., Anton, N., Arpagaus, C., Belleteix, F., Vandamme, T. F. Nanoparticles by spray drying using innovative new technology: the Büchi Nano spray dryer B-90. *J. Controlled Release* **2010,** 147, 304-310.

4. Lee, S. H., Heng, D., Ng, W. K., Chan, H. K., Tan, R. B. H. Nano spray drying: a novel method for preparing protein nanoparticles for protein therapy. *Int. J. Pharm.* **2011,** 403, 192–200.

5. York, P. Strategies for particle design using supercritical fluid technologies. *Pharm. Sci. Technol. Today* **1999,** 2, 430–440.

6. Shariati, A., Peters, C. J. Recent developments in particle design using supercritical fluids. *Curr. Opin. Solid State Mater Sci.* **2003,** 7, 371–383.

7. Wright, I. K., Higginbotham, A., Baker, S. M., Donnelly, T. D. Generation of nanoparticles of controlled size using ultrasonic piezoelectric oscillators in solution. *ACS Appl. Mater. Interfaces* **2010,** 2, 2360–2364.

8. Becher, P., *Emulsions: theory and practice*. Reinhold Pub Corp, New York: 1965.

9. Becher, P., *Encyclopedia of emulsion technology*. Marcel Dekker Inc, New York: 1985.

10. Mittal, K. L., Lindman, B., *Surfactants in solution*. Plenum, New York: 1984.

11. Ruschak, K. J., Miller, C. A. Spontaneous emulsification in ternary systems with mass transfer. *Ind. Eng. Chem. Fundam.* **1972,** 11, 534–540.

12. Miller, C. A. Spontaneous emulsification produced by diffusion—a review. *Colloids Surf.* **1988,** 29, 89–102.

13. Bouchemal, K., Briançon, S., Perrier, E., Fessi, H. Nano-emulsion formulation using spontaneous emulsification: solvent, oil and surfactant optimization. *Int. J. Pharm.* **2004,** 280, 241-251.

14. Usón, N., Garcia, M. J., Solans, C. Formation of water-in-oil (W/O) nano-emulsions in a water/mixed non-ionic surfactant/oil systems prepared by a low-energy emulsification method. *Colloids Surf. A* **2004,** 250, 415-421.

15. Izquierdo, P., Esquena, J., Tadros, T. F., Dederen, C., Garcia, M. J., Azemar, N., Solans, C. Formation and stability of nano-emulsions prepared using the phase inversion temperature method. *Langmuir : the ACS journal of surfaces and colloids* **2002,** 18, 26-30.

16. Lizarraga, M. S., Pan, L. G., Anon, M. C., Santiago, L. G. Stability of concentrated emulsions measured by optical and rheological methods. Effect of processing conditions-I. Whey protein concentrate. *Food Hydrocoll.* **2008,** 22, 868–878.

17. Corzo-Martinez, M., Soria, A. C., Villamiel, M., Olano, A., Harte, F. M., Moreno, F. J. Effect of glycation on sodium caseinate-stabilized emulsions obtained by ultrasound. *J. Dairy Sci.* **2011,** 94, 51–58.

18. Mongenot, N., Charrier, S., Chalier, P. Effect of ultrasound emulsification on cheese aroma encapsulation by carbohydrates. *J. Agric. Food Chem.* **2000,** 48, 861–867.

19. Zhao, C.-X., Middelberg, A. P. J. Two-phase microfluidic flows. *Chem. Eng. Sci.* **2011,** 66, 1394-1411.

20. Engl, W., Backov, R., Panizza, P. Controlled production of emulsions and particles by milli- and microfluidic techniques. *Curr. Opin. Colloid Interface Sci.* **2008,** 13, 206-216.

21. Lee, W.-K., Park, J-Y., Jung, S., Chul, W. Y., Kim, W-U., Kim, H-Y., Park, J-H., Park, J-S. Preparation and characterization of biodegradable nanoparticles entrapping immunodominant peptide conjugated with PEG for oral tolerance induction. *J. Controlled Release* **2005,** 105, 77-88.

22. Zambaux, M. F., Bonneaux, F., Gref, R., Maincent, P., Dellacherie, E., Alonso, M. J., Labrude, P., Vigneron, C. Influence of experimental parameters on the characteristics of poly(lactic acid) nanoparticles prepared by a double emulsion method. *J. Controlled Release* **1998,** 50, 31-40.

23. Choonara, Y. E., Pillay, V., Ndesendo, V. M. K., duToit, L. C., Kumar, P., Khan, R. A., Murphy, C. S., Jarvis, D-L. Polymeric emulsion and crosslink-mediated synthesis of super-stable nanoparticles as sustained-release anti-tuberculosis drug carriers. *Colloids Surf. B* **2011,** 87, 243-254.

24. Trimaille, T., Pichot, C., Ela, A., Fessi, H., Briançon, S., Delair, T. Poly(D,L-lactic acid) nanoparticle preparation and colloidal characterization. *Colloid Polym. Sci.* **2003,** 281, 1184-1190.

25. Choi, S.-W., Kwon, H-Y., Kim, W-S., Kim, J-H. Thermodynamic parameters on poly(d,l-lactide-co-glycolide) particle size in emulsification-diffusion process. *Colloids Surf. A* **2002,** 201, 283-289.

26. Yan, C., Chen, D., Gu, J., Qin, J. Nanoparticles of 5-fluorouracil (5-FU) loaded N-succinyl-chitosan (Suc-Chi) for cancer chemotherapy: preparation, characterization-in vitro drug release and anti-tumour activity. *J. Pharm. Pharmacol.* **2006,** 58, 1177-1181.

27. Nguyen, C. A., Allémann, E., Schwach, G., Doelker, E., Gurny, R. Synthesis of a novel fluorescent poly(D,L-lactide) end-capped with 1-pyrenebutanol used for the preparation of nanoparticles. *Eur. J. Pham. Sci.* **2003,** 20, 217-222.

28. Zweers, M. L. T., , Engbers, G. H. M., Grijpma, D. W., Feijen, J. In vitro degradation of nanoparticles prepared from polymers based on DL-lactide, glycolide and poly(ethylene oxide). *J. Controlled Release* **2004,** 100, 347-356.

29. Perugini, P., Simeoni, S., Scalia, S., Genta, I., Modena, T., Conti, B., Pavanetto, F. Effect of nanoparticle encapsulation on the photostability of the sunscreen agent, 2-ethylhexyl-pmethoxycinnamate. *Int. J. Pharm.* **2002,** 246, 37-45.

30. Allemann, E., Gurny, R., Doelker, E. Preparation of aqueous polymeric nanodispersions by a reversible salting-out process: Influence of process parameters on particle size. *Int. J. Pharm 87* **1992,** 87, 247-253.

31. Wang, N., Wu, X. S. Preparation and characterization of agarose hydrogel nanoparticles for protein and peptide drug delivery. *Pharm. Dev. Technol.* **1997,** 2, 135-142.

32. Reis, C. P., Neufeld, R. J., Ribeiro, A. J., Veiga, F. Design of insulin-loaded alginate nanoparticles: influence of the calcium ion on polymer gel matrix properties. *Chem. Ind. Chem. Eng. Q* **2006,** 12, 47-52.

33. Costa, C., Santos, A. F., Fortuny, M., Araújo, P. H. H., Sayer, C. Kinetic advantages of using microwaves in the emulsion polymerization of MMA. *Mater. Sci. Eng. C* **2009,** 29, 415-419.

34. Muñoz-Bonilla, A., Van Herk, A. M., Heuts, J. P.A. Preparation of hairy particles and antifouling films using brush-type amphiphilic block copolymer surfactants in emulsion polymerization. *Macromolecules* **2010,** 43, 2721-2731.

35. Akgöl, S., Öztürk, N., Denizli, A. New generation polymeric nanospheres for lysozyme adsorption. *J. Appl. Polym. Sci.* **2010,** 115, 1608-1615.

36. Liu, G., Liu, P. Synthesis of monodispersed crosslinked nanoparticles decorated with surface carboxyl groups via soapless emulsion polymerization. *Colloids Surf. A* **2010,** 354, 377-381.

37. Baruch-Sharon, S., Margel, S. Synthesis and characterization of polychloromethylstyrene nanoparticles of narrow size distribution by emulsion and miniemulsion polymerization processes. *Colloid Polym. Sci.* **2010,** 288, 869-877.

38. Jiang, X., Dausend, J., Hafner, M., Musyanovych, A., Röcker, C., Landfester, K., Mailänder, V., Ulrich Nienhaus, G. Specific effects of surface amines on polystyrene nanoparticles in their interactions with mesenchymal stem cells. *Biomacromolecules* **2010,** 11, 748-753.

39. Choi, J. W., Han, M. G., Kim, S. Y., Oh, S. G., Im, S. S. Poly(3,4-ethylenedioxythiophene) nanoparticles prepared in aqueous DBSA solutions. *Synth. Met.* **2004,** 141, 293-299.

40. Jang, J., Oh, J. H., Stucky, G. D. Fabrication of ultrafine conducting polymer and graphite nanoparticles. *Angew. Chem. Int. Ed.* **2002,** 41, 4016-4019.

41. Jang, J., Bae, J., Park, E. Selective fabrication of poly(3,4-ethylenedioxythiophene) nanocapsules and mesocellular foams using surfactant-mediated interfacial polymerization. *Adv. Mater.* **2006,** 18, 354-358.

42. Min, K., Gao, H., Yoon, J. A., Wu, W., Kowalewski, T., Matyjaszewski, K. One-pot synthesis of hairy nanoparticles by emulsion ATRP. *Macromolecules* **2009,** 42, 1597-1603.

43. Limayem Blouza, I., Charcosset, C., Sfar, S., Fessi, H. Preparation and characterization of spironolactone-loaded nanocapsules for paediatric use. *Int. J. Pharm.* **2006,** 325, 124-131.

44. Legrand, P., Lesieur, S., Bochot, A., Gref, R., Raatjes, W., Barratt, G., Vauthier, C. Influence of polymer behaviour in organic solution on the production of polylactide nanoparticles by nanoprecipitation. *Int. J. Pharm.* **2007,** 344, 33-43.

45. Lannibois, H., Hasmy, A., Botet, R., Chariol, O. A., Cabane, B. Surfactant limited aggregation of hydrophobic molecules in water. *J. Phys. I* **1997,** 7, 319-342.

46. Chronopoulou, L., Fratoddi, I., Palocci, C., Venditti, I., Russo, M. V. Osmosis based method drives the self-assembly of polymeric chains into micro-and nanostructures. *Langmuir : the ACS journal of surfaces and colloids* **2009,** 25, 11940-11946.

47. Weber, C., Coester, C., Kreuter, J., Langer, K. Desolvation process and surface characterisation of protein nanoparticles. *Int. J. Pharm.* **2000,** 194, 91-102.

48. De Martimprey, H., Vauthier, C., Malvy, C., Couvreur, P. Polymer nanocarriers for the delivery of small fragments of nucleic acids: oligonucleotides and siRNA. *Eur. J. Pharm. Biopharm.* **2009,** 71, 490-504.

49. Rajaonarivony, M., Vauthier, C., Couarraze, G., Puisieux, F., Couvreur, P. Development of a new drug carrier made from alginate. *J. Pharm. Sci.* **1993,** 82, 912-917.

50. Drogoz, A., David, L., Rochas, C., Domard, A., Delair, T. Polyelectrolyte complexes from polysaccharides: formation and stoichiometry monitoring. *Langmuir : the ACS journal of surfaces and colloids* **2007,** 23, 10950-10958.

51. Aguadisch, L., Berthod, D. P. M., Van Buuren, G., Donker, C. B., Lenoble, B., Renauld, F. Detergent composition comprising fragance particle. 2004.

52. Boeckh, D., Nörenberg, R., Hildebrandt, S., Mohr, B., Schöpke, H., Leyrer, R. J., Huff, J. Use of cationically modified, particulate, hydrophobic polymers as an additive for rinsing, cleaning and impregnating agents for hard surfaces 2003.

53. Warkotsch, N., Middelhauve, B., Schiedel, M-S., Hilsmann, J. Fixating fragrances originating from detergents and cleaning agents on hard and soft surfaces. 2008.

54. Dasque, B. M., Davidson, N. E., Burckett-St.Laurent, J. C. T. R., De Buzzaccarini, F., Denome, F. W. Detergent product. 2007.

55. Aussant, E. J. L. C., Ranade, V. S. Perfume composition. 2007.

56. Guerin, G., Morvan, M., Joubert, D. Water-dispersible granules comprising a fragrance in a water-soluble or water-dispersible matrix, and process for their preparation. 2003.

57. Schudel, M., Quellet, C., Taschi, M., Bouwmeesters, J. Fragrance compositions. 2002.

58. De Belder, G., Metrot, V. S., Papadaki, M., Rogers, N., Ronn, K., P., Tomarchio, V., Reynen, M. J. A lavatory bowl rim-block providing a combination of ongoing perfume delivery with a perfume boost upon flushing 2014.

59. Cross, T., Buehler T. A., Druckrey, A. K. Particles. 2016.

60. Nogaito, E., Takashima, H., Yokoya, H., Iwakiri, R., Matsushita, M., Kawaguchi, M., Yamaura, N., Adachi, H., Inoue, R., Hirai, Y., Umetani, Y., Isaka, Y., Sato, Y., Takemura, M., Komoto, S., Harada, A., Ara, H., Kashih, A. Material in gel state. 2006.

61. Popplewell, M., Zhen, Y., Bryant, C. M., Pluyter, J. G. L. Particulate fragrance deposition on surfaces and malodour elimination from surfaces. 2009.

62. Dufton, D. J., Howe, S. Process for making a water-soluble foam component 2003.

63. Whyte, D. D. Perfumed particles and detergent composition containing same. 1980.

64. Gupta, G., Lammert, M., McDermott, K. Fragrance containing cleaning product 2003.

65. Popplewell, L. M., Helft-Brummer, G. A., Russo, R. V., Pringgosusanto F. A., Gennler, C. Method for imparting substantive fragrance and, optionally, anti-static properties to fabrics during washing and/or drying procedure. 2008.

66. Jordan, G. T. I., Kluesener, B. W., Sivik, M. R., Santamarina, V., Dykstra, R. R., Lebedev, N., Gallon, L. S., Baker, E. S., Amrhein, P., Boeckh, D., Frenzel, S., Jahns, E., Scwendemann, V. Perfume polymeric particles. 2009.

67. Jun-Seok, H., Jin-Nam, K., Young-Jung, W., Jong-Sun, Y., Hong-Gi, J., Sun-Ho, K., Hwa-Won, R. Preparation and characterization of melamine-formaldehyde resin microcapsules containing fragrant oil. *Biotechnology and Bioprocess Engineering* **2006,** 11, 332-336.

68. Peña, B., Panisello, C., Aresté, G., Garcia-Valls, R., Gumí, T. Preparation and characterization of polysulfone microcapsules for perfume release. *Chemical Engineering Journal* **2012,** 179, 394-403.

69. Hofmeister, I., Landfester, K., Taden, A. pH-Sensitive Nanocapsules with Barrier Properties: Fragrance Encapsulation and Controlled Release. *Macromolecules* **2014,** 47, 5768-5773.

70. Sansukcharearnpon, A., Wanichwecharungruang, S., Leepipatpaiboon, N., Kerdcharoen, T., Arayachukeat, S. High loading fragrance encapsulation based on a polymer-blend: Preparation and release behavior. *International journal of pharmaceutics* **2010,** 391, 267-273.

71. Lee, H., Choi, C-H., Abbaspourrad, A., Wesner, C., Caggioni, M., Zhu, T., Weitz, D. A. Encapsulation and Enhanced Retention of Fragrance in Polymer Microcapsules. *ACS Appl. Mater. Interfaces* **2016,** 8, 4007-4013.

72. Li, J. K., Wanga, N., Wuab, X. S. Poly(vinyl alcohol) nanoparticles prepared by freezing–thawing process for protein/peptide drug delivery. *Journal of Controlled Release* **1998,** 56, 117-126.

73. Wang, A., Xu, C., Zhang, C., Gan, Y., Wang, B. Experimental Investigation of the Properties of Electrospun Nanofibers for Potential Medical Application. *Journal of Nanomaterials* **2015,** 2015, 1-8.

74. Bourke, S. L., Al-Khalili, M., Briggs, T., Michniak, B. B., Kohn, J., Poole-Warren, L. A. A Photo-Crosslinked Poly(vinyl Alcohol) Hydrogel Growth Factor Release Vehicle for Wound Healing Applications. *AAPS Pharm. Sci.* **2003,** 5, 1-11.

75. Fei, L., Lili, Y., Lin, Y., Jingshu, Z. Preparation of Micron-sized Crosslinked Poly(vinyl alcohol) Microspheres via Inverse Suspension-chemical Crosslinking Method. *Journal of Applied Science* **2013,** 13, 2676-2681.

76. Xu, D., Zhu, K., Zheng, X., Xiao, R. Poly(ethylene-co-vinyl alcohol) Functional Nanofiber Membranes for the Removal of Cr(VI) from Water. *Ind. Eng. Chem. Res.* **2015,** 54, 6836-6844.

77. Min, C., Min, X., Yixin, L., Yuezhong, M. Novel in situ preparation of crosslinked ethylene-vinyl alcohol copolymer foams with propylene carbonate. *Materials Letters* **2006,** 60, 3286-3291.

78. Hofmeister, F. Zur Lehre von der Wirkung der Salze. *Arch Exp Pathol Pharmakol* **1888,** 25, 1-30.

79. Jungwirth, P., Cremer, P. S. Beyond Hofmeister. *Nat Chem.* **2014,** 6, 261-263.

80. Thormann, E. On understanding of the Hofmeister effect: how addition of salt alters the stability of temperature responsive polymers in aqueous solutions. *RSC Adv.* **2012,** 2, 8297-8305.

81. Bauduin, P., Renoncourt, A., Touraud, D., Kunz, W., Ninham, B. W. Hofmeister effect on enzymatic catalysis and colloidal structures. *Curr. Opin. Colloid Interface Sci.* **2004,** 9, 43-47.

82. Lo Nostro, P., Ninham, B. W. Hofmeister phenomena: an update on ion specificity in biology. *Chemical reviews* **2012,** 112, 2286-322.

83. Heyda, J., Dzubiella, J. Thermodynamic Description of Hofmeister Effects on the LCST of Thermosensitive Polymers. *J. Phys. Chem. B* **2014,** 118, 10979–10988.

84. Deyerle, B. A., Zhang, Y. Effects of Hofmeister Anions on the Aggregation Behavior of PEO–PPO–PEO Triblock Copolymers. *Langmuir : the ACS journal of surfaces and colloids* **2011,** 27, 9203-9210.

85. Salis, A. P., M. C.; Bilaničová, D.; Monduzzi, M.; Lo Nostro, P.; Ninham, B. W. Specific Anion Effects on Glass Electrode pH Measurements of Buffer Solutions: Bulk and Surface Phenomena. *J. Phys. Chem. B* **2006,** 110, 2949-1956.

86. Collins, K. D. Ions from the Hofmeister series and osmolytes: effects on proteins in solution and in the crystallization process. *Methods* **2004,** 34, 300-311.

87. Varhač., R. T., N.; Fabián, M.; Sedlák, E. Kinetics of cyanide binding as a probe of local stability/flexibility of cytochrome c. *Biophys. Chem.* **2009,** 144, 21-26.

88. Pinna, M. C. S., A.; Monduzzi, M.; Ninham, B. W. Hofmeister Series: The Hydrolytic Activity of Aspergillus niger Lipase Depends on Specific Anion Effects. *J. Phys. Chem. B* **2005,** 109, 5406-5408.

89. Rossi, S. L. N., P.; Lagi, M.; Ninham, B. W.; Baglioni, P. Specific Anion Effects on the Optical Rotation of α-Amino Acids. *J. Phys. Chem. B* **2007,** 111, 10510-10519.

90. Ivanov, I. B. S., R. I.; Basheva, E. S.; Sidzhakova, D.; Karakashev, S. I. Hofmeister effect on micellization, thin films and emulsion stability. *Adv. Colloid Interface Sci.* **2011,** 168, 93-104.

91. Okazaki , Y. I., K.; Kawauchi, S.; Satoh, M.; Komiyama, J. Ion-Specific Swelling and Deswelling Behaviors of Ampholytic Polymer Gels. *Macromolecules* **1996,** 29, 8391-8397.

92. Zhang, Y. F., S.; Bergbreiter, D. E.; Cremer, P. S. Specific Ion Effects on the Water Solubility of Macromolecules: PNIPAM and the Hofmeister Series. *J. Am. Chem. Soc.* **2005,** 127, 14505-14510.

93. Salis, A., Ninham, B. W. Models and mechanisms of Hofmeister effects in electrolyte solutions, and colloid and protein systems revisited. *Chem. Soc. Rev.* **2014,** 43, 7358-7377.

94. Adamson, A. W., *A Textbook of Physical Chemistry*. Academic Press, New York: 1979.

95. Jones, G., Dole, M. The viscosity of aqueous solutions of strong electrolytes with special reference to barium chloride. *JACS* **1929,** 51, 2950-2964.

96. Collins, K. D., Washabaugh, M. W. The Hofmeister effect and the behaviour of water at interfaces. *Q. Rev. Biophys.* **1985,** 18, 323-422.

97. Ries-Kautt, M. M., Ducruix, A. F. Relative effectiveness of various ions on the solubility and crystal growth of lysozyme. *J. Biol. Chem.* **1989,** 264, 745-748.

98. Schwierz, N., Horinek, D., Sivan, U., Netz, R. R. Reversed Hofmeister series—The rule rather than the exception. *Current Opinion in Colloid & Interface Science* **2016,** 23, 10-18.

99. Green, A. A. Studies in the physical chemistry of the proteins: X. The solubility of hemoglobin in solutions of chlorides and sulfates of varying concentration. *J. Biol. Chem.* **1932,** 95, 47-66.

100. Medda, L., Carucci, C., Parsons, D. F., Ninham, B. W., Monduzzi, M., Salis, A. Specific Cation Effects on Hemoglobin Aggregation below and at Physiological Salt Concentration. *Langmuir : the ACS journal of surfaces and colloids* **2013,** 29, 15350-15358.

101. Omta, A. W., Kropman, M. F., Woutersen, S., Bakker, H. J. Negligible effect of ions on the hydrogen-bond structure in liquid water. *Science* **2003,** 301, 347-349.

102. Song, J., Kang, T. H., Kim, M. W., Han, S. Ion specific effects: decoupling ion-ion and ion-water interactions. *Phys. Chem. Chem. Phys.* **2015,** 17, 8306-8322.

103. Zajforoushan Moghaddam, S., Thormann, E. Hofmeister effect of salt mixtures on thermo-responsive poly(propylene oxide). *Physical chemistry chemical physics : PCCP* **2015,** 17, 6359-66.

104. Sadeghi, R., Jahani, F. Salting-in and salting-out of water-soluble polymers in aqueous salt solutions. *The journal of physical chemistry. B* **2012,** 116, 5234-41.

105. Shi, S., Uchida, M., Cheung, J., Antochshuk, V., Shameem, M. Method qualification and application of diffusion interaction parameter and virial coefficient. *Int. Journ. Bio. Macro.* **2013,** 62, 487-493.

106. Khougaz, K., Astafieva, I., Eisenberg, A. Micellization in Block Polyelectrolyte Solutions. 3. Static Light Scattering Characterization. *Macromolecules* **1995,** 28, 7135–7147.

107. Weatherly, G. T., Pielak, G. J. Second virial coefficients as a measure of protein–osmolyte interactions. *Protein Sci* **2001,** 10, 12-16.

108. Han, C. C., Ziya Akcasu, A. Concentration dependence of diffusion coefficient at various molecular weights and temperatures. *Polymer* **1981,** 22, 1165-1168.

109. Lin, M. Y., Lindsay, H. M., Weitz, D. A., Ball, R. C., Klein, R., Meakin, P. Universal diffusion-limited colloid aggregation. *J. Phys. Condens. Matter* **1990,** 2, 3093-3113.

110. Lin, M. Y., Lindsay, H. M., Weitz, D. A., Ball, R. C., Klein, R., Meakin, P. Universal reaction-limited colloid aggregation. *Physical Review A* **1990,** 41, 2005-2020.

111. Cohen, R. J., Benedek, G. B. Equilibrium and kinetic theory of polymerization and the sol-gel transition. *J. Phys. Chem.* **1982,** 86, 3696-3714.

112. Wu, H., Morbidelli, M. Gelation of polymeric nanoparticles. *Particuology* **2014,** 14, 1-11.

113. Zhang, Y.; Cremer, P. S. Interactions between macromolecules and ions: The Hofmeister series. *Current opinion in chemical biology* **2006,** 10 (6), 658-63 DOI: 10.1016/j.cbpa.2006.09.020.

114. Okur, H. I., Hladílkova, J., Rembert, K. B., Cho, Y., Heyda, J., Dzubiella, J., Cremer, P. S., Jungwirth, P. Beyond the Hofmeister Series: Ion-Specific Effects on Proteins and Their Biological Functions. *J. Phys. Chem. B* **2017,** 121, 1997−2014.

115. Baldwin, R. L. How Hofmeister Ion Interactions Affect Protein Stability. *Biophysical journal* **1996,** 71, 2056-2063.

116. Paradossi, G., Cavalieri, F., Chiessi. E., Spagnoli, C., Cowman, M. K. Poly(vinylalcohol) as versatile biomaterial for potential biomedical applications. *Journal of Materials Science: Materials in Medicine* **2003,** 14, 687-691.

117. Xu, D., Zhu, K., Zheng, X., Xiao, R. Poly(ethylene-co-vinyl alcohol) Functional Nanofiber Membranes for the Removal of Cr(VI) from Water. *Ind. Eng. Chem. Res* **2015,** 54, 6836–6844.

118. Higgins, J. S., Benoit, H. C., *Polymers and Neutron Scattering*. Clarendon Press: 1997.

119. Hammouda, B., Worcester, D. The Denaturation Transition of DNA in Mixed Solvents. *Biophys J.* **2006,** 91, 2237–2242.

120. McAfee, M. S., Annunziata, O. Cross-diffusion in a colloid–polymer aqueous system. *Fluid Phase Equilibria* **2013,** 356, 46-55.

121. Dai, S., Tam, K. C., Jenkins, R. D. Aggregation behavior of methacrylic acid/ethyl acrylate copolymer in dilute solutions. *European Polymer Journal* **2000,** 36, 2671-2677.

122. Chen, S., Huang, J. S., Tartaglia, P., *Structure and Dynamics of Strongly Interacting Colloids and Supramolecular Aggregates in Solution*. Springer: 1992.

123. Kastelica, M., Kalyuzhnyib, Y. V., Hribar-Leea, B., Dillc, K. A., Vlachy, V. Protein aggregation in salt solutions. *PNAS* **2015,** 112, 6766-6770.

124. Quigley, A., Williams, D. R. The second virial coefficient as a predictor of protein aggregation propensity: A self-interaction chromatography study. *European Journal of Pharmaceutics and Biopharmaceutics* **2015,** 96, 282–290.

125. Ball, R. C., Weitz, D. A., Witten, T. A., Leyvraz, F. Universal Kinetics in Reaction-Limited Aggregation. *Physical review letters* **1987,** 58, 274-277.

126. Fourmaux-Demange, V., Boué, F., Brûlet, A., Keller, P., Cotton, J. P. Effect of the Molecular Weight on the Whole Conformation of a Liquid Crystalline Comb-like Polymer in Its Melt. *Macromolecules* **1998,** 31, 801-806.

127. Villegas, J. A., Cervantes, J. Unusual Behavior of Poly(methylhexylsiloxane) Short Chain Molecules in Solution. *J Inorg Organomet Polym* **2011,** 21, 157-164.

128. Liu, P., Xiang, L., Tan, Q., Tanga, H., Zhang, H. Steric hindrance effect on thermoresponsive behaviors of pyrrolidone-based polymers. *Polym. Chem.* **2013,** 4, 1068-1076.

129. Gripon, C., Rosenman, I., Vidal, O., Robert, M. C., Boué, F. Lysozyme solubility in H2O and D2O solutions: a simple relationship. *Journal of Crystal Growth* **1997,** 177, 238-247.

130. Mildner, D., Hall, P. Small-angle scattering from porous solids with fractal geometry. *J. Phys. D: Appl. Phys.* **1986,** 19, 1535-1545.

131. Schmidt, P. W. Small-angle scattering studies of disordered, porous and fractal systems. *J. Appl. Cryst.* **1991,** 24, 414-435.

132. Guinier, A., Fournet, G., *Small-Angle Scattering of X-Rays*. John Wiley and Sons, New York: 1955.

133. Nallet, F., Laversanne, R., Roux, D. Modelling X-ray or neutron scattering spectra of lyotropic lamellar phases : interplay between form and structure factors. *J. Phys. II France* **1993,** 3, 487-502.

134. Berghausen, J., Zipfel, J., Lindner, P., Richtering, W. Influence of Water-Soluble Polymers on the Shear-Induced Structure Formation in Lyotropic Lamellar Phases. *J. Phys. Chem. B* **2001,** 105, 11081-11088.

135. Burchard, W. Particle Scattering Factors of Some Branched Polymers *Macromolecules* **1977,** 10, 919-927.

136. Cócera, M., López, O., Estelrich, J.,Parr, J. L., de la Maza, A. Adsorption of Sodium Lauryl Ether Sulfate on Liposomes by Means of a Fluorescent Probe: Effect of the Ethylene Oxide Groups. *Langmuir : the ACS journal of surfaces and colloids* **2002,** 18, 8250–8254.

137. Huibers, P. D. T., Lobanov, V. S., Katritzky, A. R., Shah, D. O., Karelson, M. Prediction of Critical Micelle Concentration Using a Quantitative Structure−Property Relationship Approach. 1. Nonionic Surfactants. *Langmuir : the ACS journal of surfaces and colloids* **1996,** 12, 1462-1470.

138. Hayter, J. B., Penfold, J. An analytic structure factor for macroion solutions. *Molecular Physics* **1981,** 42, 109-118.

139. Hansen, J., Hayter, J. B. A rescaled MSA structure factor for dilute charged colloidal dispersions. *Molecular Physics* **1982,** 46, 651-656.

140. Maiti, K., Mitra, D., Guha, S., Moulik, S. P. Salt effect on self-aggregation of sodium dodecylsulfate (SDS) and tetradecyltrimethylammonium bromide (TTAB): Physicochemical correlation and assessment in the light of Hofmeister (lyotropic) effect. *Journal of Molecular Liquids* **2009,** 146, 44–51.

141. Hayashi, S., Ikeda, S. Micelle Size and Shape of Sodium Dodecyl Sulfate in Concentrated NaCl Solutions. *J. Phys. Chem.* **1980,** 84, 744-751.

142. Schott, H., Royce, A. E., Kyu Han, S. Effect of inorganic additives on solutions of nonionic surfactants: VII. Cloud point shift values of individual ions. *Journal of colloid and interface science* **1984,** 98, 196-201.

143. Imperatore, R., Vitiello, G., Ciccarelli, D., D'Errico, G. Effects of Salts on the Micellization of a Short-Tailed Nonionic Ethoxylated Surfactant: An Intradiffusion Study. *Journal of Solution Chemistry* **2014,** 43, 227–239.

144. Dahanayake, M., Cohen, A. W., Rosen, M. J. Relationship of structure to properties of surfactants. 13. Surface and thermodynamic properties of some oxyethylenated sulfates and sulfonates. *J. Phys. Chem.* **1986,** 90, 2413-2418.

145. Aschenbrenner, E., Bley, K., Koynov, K., Makowski, M., Kappl, M., Landfester, K., Weiss, C. K. Using the Polymeric Ouzo Effect for the Preparation of Polysaccharide-Based Nanoparticles. *Langmuir : the ACS journal of surfaces and colloids* **2013,** 29, 8845−8855.

146. Ganachaud, F., Katz, J. L. Nanoparticles and Nanocapsules Created Using the Ouzo Effect: Spontaneous Emulsification as an Alternative to Ultrasonic and High-Shear Devices. *Chemphyschem : a European journal of chemical physics and physical chemistry* **2005,** 6, 209-216.

147. Hoogenboom, R., Thijs, H. M. L., Wouters, D., Hoeppener, S., Schubert, U. S. Tuning solution polymer properties by binary water–ethanol solvent mixtures. *Soft matter* **2008,** 4, 103-107.

148. Traiphol, R., Charoenthai, N., Srikhirin, T., Kerdcharoen, T., Osotchan, T., Maturos, T. Chain organization and photophysics of conjugated polymer in poor solvents: Aggregates, agglomerates and collapsed coils. *Polymer* **2017,** 48, 813-826.

149. Wyman, J. The dielectric constant of mixtures of ethyl alcohol and water from -5 to 40°. *JACS* **1931,** 53, 3292–3301.

150. Johnson, C. S., Gabriel, D. A., *Laser Light Scattering*. Dover Publications: 1995.

151. Wu, H. Correlations between the Rayleigh ratio and the wavelength for toluene and benzene. *Chemical Physics* **2010,** 367, 44-47.

152. Zimm, B. H. The Scattering of Light and the Radial Distribution Function of High Polymer Solutions. *J. Chem. Phys.* **1948,** 16, 1093-1098.

153. Berne, B. J., Pecora, R., *Dynamic Light Scattering: With Applications to Chemistry, Biology*. Couvire Dover Publications: 2003.

154. Lomakin, A., Teplow, D., Benedek, G., *Amyloid Proteins*. E. Sigurdsson, Humana Press: 2005.

Ph. D. Course Activity Summary

Candidate: Marco Perfetti **Tutors:** Luigi Paduano, Gerardino D'Errico, Giulia Bianchetti

1) **Attended Courses (6 minimum, 8 hours each):**

- Metodi di struttura elettronica per materiali allo stato solido;
- Tecniche di estrazione solido-liquido impiegate nella preparazione del campione per l'analisi chimica e nella produzione di estratti per usi industriali;
- Inelastic neutron scattering;
- Small Angle Neutron Scattering and Reflectometry for soft matter;
- Glicoscienze;
- JCNS Neutron Laboratory Course 2015 – Theoretical part.

2) **Attended Seminars:**

Title	Speaker	Date	Place
European large scale facilities: neutron and synchroton sources	Serge Perez	06/05/2015	Naples
Non-conventional techniques for the modification of carbon nanoforms	Ester Vazquez	28/04/2015	Naples
Biosensing and bioelectronics based on organic electrochemical devices: from monitoring drug dynamics to hybrid bio-organic memristive devices	Salvatore Iannotta	11/06/2015	Naples
Bleaching systems in domestic laundry detergents	Giulia Bianchetti	29/10/2015	Naples

Multimodal approaches for preclinical molecular imaging	Luca Menichetti Mario Chiariello	05/02/2016	Naples
The study of organic materials in art and archaeological object	Ilaria Bonaduce	13/06/2016	Naples
The versatility of mesoscopic solar cells	Anders Hagfeldt	14/04/2016	Naples
Development of the fluid FM and its applications for 2D patterning as well as 3D microprinting	Tomaso Zambelli	17/10/2016	Naples

3) Attended Integration Exams (for candidates not graduated in Chemical Science):

Title	Professor	Date
-	-	-

4) Visiting periods in Institutions different from University of Naples "Federico II":

Host Institution	Country	Start Date	End Date
Procter & Gamble Services nv	Belgium	02/11/2016	30/09/2017

5) Publications (include submitted and in preparation):

- Sannino, F., Pernice, P., Imparato, C., Aronne, A., D'Errico, G., Minieri, L., Perfetti, M., Pirozzi, D., *Hybrid TiO_2-Acetylacetonate Amorphous Gel-Derived Material with Stably Adsorbed Superoxide Radical Active in Oxidative Degradation of Organic Pollutants*. RSC Adv., **2015**, 5, 93831;

- Panzella, L., Melone, L., Pezzella, A., Rossi, B., Pastori, N., Perfetti, M., D'Errico, G., Punta, C., d'Ischia, M. *Surface-Functionalization of Nanostructured Cellulose Aerogels by Solid State Eumelanin Coating.* Biomacromolecules, **2016**, 17, 564;
- Iacomino, M. G., Mancebo-Aracil, J., Guardingo Melian, M., Martín, R., D'Errico, G., Perfetti, M., Manini, P., Crescenzi, O., Busqué, F., Napolitano, A., d'Ischia, M., Sedó, J., Ruiz-Molina, D., *Replacing Nitrogen by Sulfur: From Structurally Disordered Eumelanins to Regioregular Thiomelanin Polymers.* Int. J. Mol. Sci., **2017**, 18, 2169;
- Perfetti, M., Russo Krauss, I., Radulescu, A., Ruocco, G., D'Errico, G., Bianchetti, G. O., Paduano, L., *Poly-ethylene-vinyl alcohol microgels prepared through salting out: rationalizing the aggregation process and tuning the microstructural properties*. ARTICLE ACCEPTED by Polymer; https://doi.org/10.1016/j.polymer.2018.01.018
- Perfetti, M., et al., *Perfume delivery aggregates*. SUBMITTED PATENT;
- *Revealing the aggregation mechanism and the structural properties of polyvinyl alcohol microgels prepared through salting out.* ARTICLE IN PREPARATION;
- *Influence of salts belonging to Hofmeister series on properties and structure of DTAB-C8E5 aqueous aggregates.* ARTICLE IN PREPARATION;
- *Rationalizing the Antioxidant Activity of Bioinspired Phenolic Polymers: an Insight into (the Role of Extended) π-Conjugation Features by EPR and UV-vis Analysis.* ARTICLE IN PREPARATION.

6) Attended congresses/workshops/summer schools:

- XXVI Congresso Annuale della Società Italiana di Spettroscopia Neutronica (1^{st}-3^{rd} July 2015, Rome and Frascati) – ORAL PRESENTATION: *PVA-based microgels as carrier systems for industrial applications*;
- XXVII Congresso Annuale della Società Italiana di Spettroscopia Neutronica (29^{th} June-1^{st} July 2016, Ancona and Senigallia);
- ECIS 2016 – 30^{th} Conference of the European Colloid and Interface Society (4^{th}-9^{th} September 2016, Rome) – POSTER PRESENTATION: *Poly-vinyl alcohol-based microgels prepared through salting out: Rationalizing the aggregation process*;
- 6^{th} EuCheMS Chemistry Congress (11^{th}-15^{th} September 2016, Seville) – POSTER PRESENTATION: *Phase behavior and structural properties of poly(ethylene-co-vinyl alcohol)-based microgels prepared through salting out*;
- XLIV Congresso Nazionale di Chimica Fisica (20^{th}-23^{rd} September 2016, Naples) – ORAL PRESENTATION: *Poly(ethylene-co-vinyl alcohol)-based microgels prepared through salting out: Phase behavior and structural properties*;
- P&G – CSGI 1^{st} Workshop on Complex Fluids and Interfaces, 28^{th} and 29^{th} September 2016, CSGI, Sesto Fiorentino, Italy – ORAL PRESENTATION: *Fragrance stabilization and increase of deposition efficiency in liquid detergents*;
- JCNS Neutron Laboratory Course 2015 – Exercises;
- JCNS Neutron Laboratory Course 2015 – Experimental part.

7) Other Activities:

- 11 months of research activity spent at Procter & Gamble Brussels Innovation Center located in Strombeek-Bever, Belgium (Erasmus + Program for 3rd level students);
- 1 beam time at ISIS Neutron Source, located at Rutherford Appleton Laboratory, UK;
- 3 beam times at FRM-II Neutron Source, located at Garching, Germany.